

AFRL-AFOSR-JP-TR-2022-0051

Fore-Wake Excitations from Orbiting Space Debris: Signature and Significance for Space Situational Awareness

Abhijit Sen
INSTITUTE FOR PLASMA RESEARCH
NEAR INDIRA BRIDGE,
GANDHINAGAR, GUJARAT, 382428
IND

06/12/2022
Final Technical Report

DISTRIBUTION A: Distribution approved for public release.

Air Force Research Laboratory
Air Force Office of Scientific Research
Asian Office of Aerospace Research and Development
Unit 45002, APO AP 96338-5002

REPORT DOCUMENTATION PAGE

PLEASE DO NOT RETURN YOUR FORM TO THE ABOVE ORGANIZATION.

1. REPORT DATE	2. REPORT TYPE	3. DATES COVERED	
20220612	Final	START DATE 20180928	END DATE 20220327

4. TITLE AND SUBTITLE
Fore-Wake Excitations from Orbiting Space Debris: Signature and Significance for Space Situational Awareness

5a. CONTRACT NUMBER	5b. GRANT NUMBER	5c. PROGRAM ELEMENT NUMBER
	FA2386-18-1-4022	61102F
5d. PROJECT NUMBER	**5e. TASK NUMBER**	**5f. WORK UNIT NUMBER**

6. AUTHOR(S)
Abhijit Sen

7. PERFORMING ORGANIZATION NAME(S) AND ADDRESS(ES)
INSTITUTE FOR PLASMA RESEARCH
NEAR INDIRA BRIDGE,
GANDHINAGAR, GUJARAT 382428
IND

8. PERFORMING ORGANIZATION REPORT NUMBER

9. SPONSORING/MONITORING AGENCY NAME(S) AND ADDRESS(ES)	10. SPONSOR/MONITOR'S ACRONYM(S)	11. SPONSOR/MONITOR'S REPORT NUMBER(S)
AOARD UNIT 45002 APO AP 96338-5002	AFRL/AFOSR IOA	AFRL-AFOSR-JP-TR-2022-0051

12. DISTRIBUTION/AVAILABILITY STATEMENT
A Distribution Unlimited: PB Public Release

13. SUPPLEMENTARY NOTES

14. ABSTRACT
The primary focus of this study has been on the investigation of nonlinear wave excitations from a charged body moving at a high speed in a plasma. The motivation has been to model the excitations that can occur in the ionosphere due the passage of charged debris objects and explore the feasibility of exploiting them for Space Situational Awareness (SSA) purposes. The excitations, that can be either electrostatic or electromagnetic in nature, can arise because the debris objects constitute a perturbing charge source as well as a perturbing current source. The nonlinear saturated state of such perturbations can take the form of solitons. Multiple soliton emissions can then create a cloud of plasma irregularity that can be easier to detect from earth and act as a tracking aid for the debris. To this end we have carried out a series of theoretical and experimental investigations to characterize the nature of these excitations and assess their dependence on various properties of the charged object. A novel feature of the study has been the exploration of electromagnetic solitons using both fluid and particle-in-cell (PIC) simulations. Our PIC simulations, in particular, have provided the first theoretical
evidence of electromagnetic precursors in the form of magneto-sonic solitons. Electromagnetic excitations offer several potential advantages over electrostatic structures for SSA studies. They can be much longer lived than electrostatic waves as the latter can suffer strong Landau damping under the ionospheric conditions of the LEO region. The electromagnetic solitons also have a larger spatial extent that can contribute towards a wider dimension of the irregularity cloud. While electrostatic fore-wakes consisting of nearly one
dimensional (planar) solitons have been experimentally observed, our present theoretical results can stimulate similar experimental investigations towards detecting electromagnetic solitons in a laboratory setting.

15. SUBJECT TERMS

16. SECURITY CLASSIFICATION OF:			17. LIMITATION OF ABSTRACT	18. NUMBER OF PAGES
a. REPORT U	b. ABSTRACT U	c. THIS PAGE U	SAR	75

19a. NAME OF RESPONSIBLE PERSON	19b. PHONE NUMBER *(Include area code)*
TONY KIM	315-227-7008

Final Performance Report for AOARD Grant FA2386-18-1-4022

June 8, 2022

Project Title: *Fore-Wake Excitations from Orbiting Space Debris: Signature and Significance for Space Situational Awareness*

Principal Investigator: Prof. Abhijit Sen

Affiliation: Institute for Plasma Research

Mailing Address: Near Indira Bridge, Bhat, Gandhinagar 382428, India

Telephone: +919825051578

Fax: +917923969016

Email: senabhijit@gmail.com

Period of Performance: 09/28/2018 – 03/ 27/2022

DISTRIBUTION A: Distribution approved for public release. Distribution unlimited

Abstract

The primary focus of this study has been on the investigation of nonlinear wave excitations from a charged body moving at a high speed in a plasma. The motivation has been to model the excitations that can occur in the ionosphere due the passage of charged debris objects and explore the feasibility of exploiting them for Space Situational Awareness (SSA) purposes. The excitations, that can be either electrostatic or electromagnetic in nature, can arise because the debris objects constitute a perturbing charge source as well as a perturbing current source. The nonlinear saturated state of such perturbations can take the form of solitons. Multiple soliton emissions can then create a cloud of plasma irregularity that can be easier to detect from earth and act as a tracking aid for the debris. To this end we have carried out a series of theoretical and experimental investigations to characterize the nature of these excitations and assess their dependence on various properties of the charged object. A novel feature of the study has been the exploration of electromagnetic solitons using both fluid and particle-in-cell (PIC) simulations. Our PIC simulations, in particular, have provided the first theoretical evidence of electromagnetic precursors in the form of magneto-sonic solitons. Electromagnetic excitations offer several potential advantages over electrostatic structures for SSA studies. They can be much longer lived than electrostatic waves as the latter can suffer strong Landau damping under the ionospheric conditions of the LEO region. The electromagnetic solitons also have a larger spatial extent that can contribute towards a wider dimension of the irregularity cloud. While electrostatic fore-wakes consisting of nearly one dimensional (planar) solitons have been experimentally observed, our present theoretical results can stimulate similar experimental investigations towards detecting electromagnetic solitons in a laboratory setting.

DISTRIBUTION A: Distribution approved for public release. Distribution unlimited

Work Done Report

In pursuance of the main objectives of the proposal we have accomplished the following:

(i) Made a detailed experimental and theoretical study of the effect of size and shape of a charged object on the nature of the electrostatic fore-wake structures.

(ii) Made the first experimental observation of `pinned' solitons and elucidated the conditions for their excitation and provided a theoretical model calculation in support of the experimental observations.

(iii) Provided the first theoretical evidence of precursor electromagnetic solitons using detailed PIC simulations.

(iv) Used PIC simulations to further characterize the nature of electromagnetic precursors as a function of the source parameters and to also identify signatures depicting the subsequent interactions of these precursors with the ambient plasma.

(v) Made a detailed analytic and numerical study (using a fluid model) to investigate the nature of pinned solitons and the feasibility of using them to detect small sized space debris objects in the ionosphere.

For details about (i) please refer to the publication:

Garima Arora, P. Bandyopadhyay, M. G. Hariprasad, and A. Sen, ``*Effect of size and shape of a moving charged object on the propagation characteristics of precursor solitons'',* Physics of Plasmas **26**, 093701 (2019); doi: 10.1063/1.5115313
(attached as Annexure I)

For details on (ii) please refer to the publication:

Garima Arora, P. Bandyopadhyay, M.G. Hariprasad and A. Sen*,* `` *Experimental observation of pinned solitons in a flowing dusty plasma'',* Physical Review E **103** (2021) 013201
(attached as Annexure II)

For details on (iii) please refer to the publication:

Atul Kumar and Abhijit Sen*,* ``*Precursor magneto-sonic solitons in a plasma from a moving charge bunch'',* New J. Phys. **22** (2020) 073057
(attached as Annexure III)

For details on (iv) please refer to the preprint:

Vikram Dharodi, Atul Kumar and Abhijit Sen, "*Signatures of an energetic charged body moving in a plasma*", submitted to New Journal of Physics.
(attached as Annexure IV)

DISTRIBUTION A: Distribution approved for public release. Distribution unlimited

For details on (v) please refer to the preprint:

> Abhijit Sen, Rupak Mukherjee, Sharad K. Yadav, Chris Crabtree, and Gurudas Ganguli, "*Electromagnetic Pinned Solitons for Space Debris Detection*" submitted to Physics of Plasmas.
> (attached as Annexure V)

DISTRIBUTION A: Distribution approved for public release. Distribution unlimited

List of Publications and Significant Collaborations that resulted from the AOARD supported project

a) Papers published in peer-reviewed journals

(i) Garima Arora, P. Bandyopadhyay, M. G. Hariprasad, and A. Sen, ``*Effect of size and shape of a moving charged object on the propagation characteristics of precursor solitons'',* Physics of Plasmas **26**, 093701 (2019); doi: 10.1063/1.5115313

(ii) Abhijit Sen*, ``Nonlinear Precursor Waves from a Moving Charged Object in a Plasma'',* Radio Science Bulletin **371** (2019) 17

(iii) Atul Kumar and Abhijit Sen*, ``Precursor magneto-sonic solitons in a plasma from a moving charge bunch'',* New J. Phys. **22** (2020) 073057

(iv) Garima Arora, P. Bandyopadhyay, M.G. Hariprasad and A. Sen*, `` Experimental observation of pinned solitons in a flowing dusty plasma'',* Physical Review E **103** (2021) 013201

b) Papers published in peer-reviewed conference proceedings,

Nil

c) Papers published in non-peer-reviewed journals and conference proceedings,

Nil

d) Conference presentations without papers,

i) *Oral Presentation* : "**Electromagnetic precursor excitations from a moving charged object",** Abhijit Sen, Gurudas Ganguli and Chris Crabtree, at the *2nd Asia-Pacific Conference on Plasma Physics, 12-17,11.2018, Kanazawa, Japan.*

ii) *Keynote Lecture*: **"Nonlinear Precursor Waves from a Moving Charged Object in a Plasma'',** Abhijit Sen, Gurudas Ganguli and Chris Crabtree at the *URSI AP- RASC 2019, New Delhi, India 09 – 15 March 2019.*

iii) *Invited Talk:* **"Stimulated Fore-wake Excitations from Moving Charged Objects in the Ionosphere",** A. Sen, S. K. Yadav, G. Ganguli and C. Crabtree , at the *ICEAA APWC 2019, Granada, Spain 09 - 14 September 2019.*

iv) *Invited Talk*: "Characteristics and applications of nonlinear fore-wake excitations from moving charged objects in space plasmas"
at the Asia Pacific Plasma Conference, 17-22 Nov.2019, Kuching, Malaysia

*v) Oral presentation: "***Excitation of pinned structures in flowing complex plasma",** Garima Arora*, P. Bandyopadhyay, M. G. Hariprasad and A. Sen, *at the Plasma Science Society of India Annual Conference, Chennai (Dec. 3-6, 2019)*

DISTRIBUTION A: Distribution approved for public release. Distribution unlimited

vi) Invited talk: **"Precursor Magneto-sonic solitons in a plasma from a movinobject",** Atul Kumar and Abhijit Sen, at the *Conference on Plasma Simulations, Institute for Plasma Research, Gandhinagar (*Jan.23-24, 2020*)*

vii) Keynote Lecture: "**Nonlinear Fore-wake Excitations in Plasmas",** Abhijit Sen, at the *3rd National Seminar on Nonlinear and Complex Phenomena (NCP20) on February 18,2020 at Kolkata.*

*ix) Invited Talk: "***Nonlinear Fore-wake excitations in Space and Laboratory Plasmas**" delivered online at the Frontiers in Astrophysics and Fluid Mechanics, May 6, 2021, Mumbai

*x) Invited Talk: "***Precursor Magneto-sonic solitons from moving charged objects in the Ionosphere**", delivered online at the ICEAA APWC 2021, August 9-13,2021, Hawaii, U.S.A.

e) *Manuscripts submitted but not yet published*,

(i) Vikram Dharodi, Atul Kumar and Abhijit Sen, "*Signatures of an energetic charged body moving in a plasma*", submitted to New Journal of Physics.

(ii) Abhijit Sen, Rupak Mukherjee, Sharad K. Yadav, Chris Crabtree, and Gurudas Ganguli, "*Electromagnetic Pinned Solitons for Space Debris Detection*" submitted to Physics of Plasmas.

(iii) P. Bandyopadhyay and Abhijit Sen, "Driven Nonlinear Structures in Flowing Dusty Plasmas", submitted to Reviews of Modern Plasma Physics.

f) *List any interactions with industry or with Air Force Research Laboratory scientists or significant collaborations that resulted from this work.*

Scientific Collaboration with:

(i) Dr. Gurudas Ganguli,
Naval Research Laboratory
Plasma Physics Division, Code 6709,
Washington, DC 20375, U.S.A.

(ii) Dr. Chris Crabtree,
Naval Research Laboratory
Plasma Physics Division, Code 6709,
Washington, DC 20375, U.S.A.

(iii) Dr. Rupak Mukherjee
Princeton Plasma Physics Laboratory,
Princeton, NJ, U.S.A.

DISTRIBUTION A: Distribution approved for public release. Distribution unlimited

Physics of Plasmas

Effect of size and shape of a moving charged object on the propagation characteristics of precursor solitons

Cite as: Phys. Plasmas **26**, 093701 (2019); https://doi.org/10.1063/1.5115313
Submitted: 17 June 2019 . Accepted: 13 August 2019 . Published Online: 06 September 2019

Garima Arora, P. Bandyopadhyay, M. G. Hariprasad, and A. Sen

View Online Export Citation CrossMark



© 2019 Author(s).

DISTRIBUTION A: Distribution approved for public release. Distribution unlimited

Physics of Plasmas ARTICLE scitation.org/journal/php

Effect of size and shape of a moving charged object on the propagation characteristics of precursor solitons

Cite as: Phys. Plasmas **26**, 093701 (2019); doi: 10.1063/1.5115313
Submitted: 17 June 2019 · Accepted: 13 August 2019 ·
Published Online: 6 September 2019

View Online Export Citation CrossMark

Garima Arora,[a] P. Bandyopadhyay, M. G. Hariprasad, and A. Sen

AFFILIATIONS

Institute for Plasma Research, HBNI, Bhat, Gandhinagar, Gujarat 382428, India

[a]Electronic mail: garimagarora@gmail.com

ABSTRACT

We report on experimental observations of the modifications in the propagation characteristics of precursor solitons due to the different shapes and sizes of the object over which the dust fluid flows. The experiments have been performed in a Π shaped Dusty Plasma Experimental device where dusty plasma is created in a DC glow discharge Ar plasma using kaolin particles. A floating copper wire installed radially on the cathode acts as a charged object in the plasma environment. The flow on the dust fluid is initiated by suddenly lowering the potential of the charged object from grounded potential to close to floating potential. The size (height and width) of the potential hill is then varied by drawing current from the wire through a variable resistance. With a decrease in the height of the potential hill, the amplitude, velocity, and number of excited precursor solitons are found to decrease, whereas the widths of the solitons are seen to increase. It is found that below a threshold value, these solitary waves are not excited, and the dust fluid simply flows over the hill. To examine the effect due to the shape of the potential profiles, the wire is replaced by a triangular object. Only trailing wakes are seen to be excited when the dust fluid faces the linearly increasing slope of the potential profile, whereas both solitons and wakes get excited when the object is placed with the sharp edge facing the flow. All the experimental findings qualitatively agree with numerical solutions obtained with different source terms in the forced-Korteweg–de Vries model equation.

Published under license by AIP Publishing. https://doi.org/10.1063/1.5115313

I. INTRODUCTION

The simultaneous excitation of precursor solitons ahead of a fast moving object with wakes behind it is a phenomenon that has been widely studied in hydrodynamics particularly in the context of disturbances created by ships and boats close to the coast.[1–3] These earlier studies have also provided model descriptions of this fascinating nonlinear phenomenon by employing a forced Korteweg–de Vries equation or a forced generalized Boussinesq equation.[4] Controlled laboratory experiments using model ships moving in a channel were carried out by Huang[5] and Sun.[6] It was found that as long as the speed of the object moving through the fluid (water) was below a critical value (in this case, the phase velocity of the surface water waves), the movement only created the customary trailing waves (wakes) in the downstream direction. A dramatic change occurred when the object speed was transcritical. Then, in addition to the trailing wakes, the object also created a steady stream of solitons ahead of it in the upstream direction. These solitons with a speed higher than the object moved away as precursors. The phenomenon was Galilean invariant[4]—it could be reproduced by keeping the object stationary and moving the fluid over it.

Fluid concepts have often been successfully translated and exploited to understand collective phenomena in plasmas. A prime example is the extensive past study of linear waves and nonlinear structures in a dusty (or complex) plasma medium. Such a medium, consisting of heavy dust grains immersed in a plasma of electrons and ions, displays a host of collective excitations on a slow time scale due to the low charge to mass ratio of the dust particles and can be understood from a fluid model of the dusty plasma. There is rich literature on the study of linear waves, e.g., Dust Acoustic Waves (DAWs),[7,8] Dust Ion Acoustic Waves (DIWs),[9] and Dust Lattice (DL) Waves,[10] and nonlinear waves like Dust Acoustic Solitary Waves (DASw),[11,12] Shock Waves,[13,14] dust voids,[15–17] Vortices,[18–20] etc.,[21] consisting of both theoretical and experimental investigations. As in a hydrodynamic fluid, there have also been observations of wake structures in laboratory dusty plasmas.[19,22,23] These wakes (sometimes termed as Mach cones[24–28]) are generated when a dust particle moves through a

Published under license by AIP Publishing

DISTRIBUTION A: Distribution approved for public release. Distribution unlimited

stationary dusty plasma medium. The topic of fore-wake excitations (precursor waves) has, however, received very limited attention until now. The first experimental demonstration of the generation of a precursor soliton in a flowing dusty plasma was reported in 2016 by Jaiswal *et al.*[29] In their study, they observed the spontaneous excitation of precursor solitons when a supersonically (with respect to the dust acoustic speed) moving dusty plasma fluid was made to flow over an electrostatic potential structure. The physical mechanism underlying this phenomenon can be understood in terms of the fluid concept used to explain hydrodynamic precursors. An object moving in a fluid always creates a pileup of matter in front of it. If its speed is subcritical, then the matter in front can disperse away at the linear phase velocity, leading to the creation of a wake structure. However, if the object speed is supercritical, then the matter in front cannot disperse away fast enough and continues to build up. At a certain stage, nonlinear effects become important, and this can lead to the formation of solitons or other nonlinear structures. These nonlinear structures can move at a higher speed and can therefore separate from the object and move away as precursors. These first ever observations of precursor solitons in a plasma have been well characterized by detailed experimental measurements of their propagation features and qualitative comparisons with results from theoretical models. The existence of such precursor excitations has also been confirmed from full scale fluid simulations[30] and molecular dynamic simulations.[31]

The objective of our present study is to further consolidate and extend the previous experimental study[29] by carrying out a detailed investigation of the propagation characteristics of the precursors under varying excitation conditions. In particular, we look at the effects of varying the size and shape of the potential hill on the fore-wake phenomenon. We find that there is a systematic dependence of the amplitude, velocity, and number of excited precursors on the size of the potential hill and the existence of a threshold value of the potential height, below which no precursors are excited. There is also a very interesting dependence on the shape of the potential hill that highlights the role of sharp gradients in the excitation of precursors.

This paper is organized as follows: in Sec. II, we describe the experimental setup and procedure for excitation of precursor solitons and wakes. The experimental results of precursor solitons and wakes are discussed in Sec. III A. The excitation of these forced solitary waves over different sizes of the potential profile of the charged object is described in Sec. III B, and the results on the influence of the shape of the potential profile are described in Sec. III C. A brief summary of all the results and some concluding remarks are given in Sec. IV.

II. EXPERIMENTAL SETUP AND PROCEDURE

The experiments are performed in a Π shaped Dusty Plasma Experimental (DPEx) device, and its schematic diagram is shown in Fig. 1. A detailed description of the experimental setup and its associated diagnostics are available in Ref. 32. The DPEx device is basically an inverted Π shaped glass chamber which has a number of axial and radial ports used for different purposes. A rotary pump is connected to one of the arms of the DPEx device for evacuating the vacuum vessel, whereas a mass flow controller is attached to the gas port to feed argon gas into the chamber. A disk shaped anode and a tray shaped cathode are used for plasma generation. The tray type configuration of the cathode is chosen for providing radial confinement to the dust particles. In addition to that, two metal strips are also placed at the ends

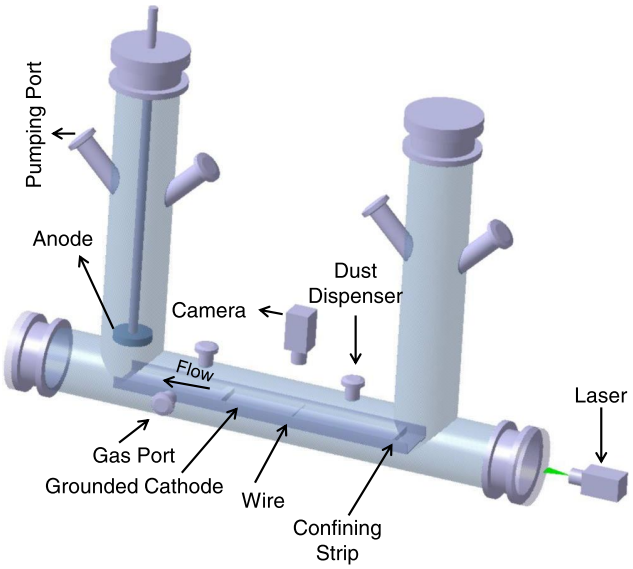


FIG. 1. A schematic diagram of the dusty plasma experimental (DPEx) setup.

of the cathode to confine the particles axially. For the experiments to study the effect of the obstacle height on the solitons, a copper wire of diameter 1 mm and length 50 mm is mounted at a height of 10 mm from the base of the cathode. The wire acts as a charged object for the excitation of solitary waves as reported in Ref. 29. This wire is connected to the grounded potential through a switch, and it can also be kept at various potentials by connecting a variable resistance ranging from 10 kΩ to 10 MΩ in between the wire and the switch. Micrometer-sized kaolin particles (2–5 μm) are sprinkled on the cathode in between the wire and the right strip before closing the chamber for creating a dusty plasma. These dust particles get negatively charged in the presence of the background plasma and levitate in the cathode sheath region where the sheath electrostatic force acting on the particle balances the gravitational force. The mass of the levitated dust particles is $m_d \sim 8.9 \times 10^{-14}$ kg for a radius of $r = 2\ \mu$m. These levitated micro particles are then illuminated by a green laser light, and their dynamics are captured using a fast CCD camera for further analysis.

To start with, the chamber is pumped down to a base pressure of 0.1 Pa, and then, argon gas is injected into the device to set the working pressure at 9–15 Pa. In this condition, the gate valve attached with the pump is opened at 20%, whereas the mass flow controller is opened at 5% to maintain the equilibrium pressure in the chamber. An argon plasma is produced between the anode and the grounded cathode by applying a voltage in the range of 280–320 V using a DC power supply. The plasma parameters such as plasma density (n_i) and electron temperature (T_e) are measured using a single Langmuir probe, and they come out to be $n_i \sim 0.5$–$3 \times 10^{15}/\text{m}^3$ and $T_e \sim 2$–5 eV for the range of discharge conditions as discussed in detail in Ref. 32. To create a dusty plasma, first the plasma is formed at a higher voltage and left for a few minutes. Later, the discharge voltage is reduced and set accordingly so that a highly dense dust cloud is formed. To repeat the earlier observations of Jaiswal *et al.*,[29] the wire is kept at ground potential (negative

Published under license by AIP Publishing

DISTRIBUTION A: Distribution approved for public release. Distribution unlimited

compared to the plasma potential), which acts as a barrier for these negatively charged dust particles, and as a result, the particles remain confined between the wire and the right potential strip as shown in Fig. 2(a) and exhibit only thermal motion. For the present set of experiments, the discharge condition is kept in such a way that there is no spontaneous excitation of waves in dust cloud due to ion streaming. For a specific discharge condition, $V_d = 320$ V and p = 11 Pa, and the average charge of these micrometer sized dust particles comes out to be $Q_d \sim 8.43 \times 10^3 e$ which is estimated from a Collision Enhanced plasma Collection (CEC) model.[33,34] The other dust parameters such as dust density $n_d \sim 10^{11}/m^3$ and dust temperature $T_d \sim 0.6$–1.2 eV are estimated with the help of an IDL based super Particle Identification Tracking (sPIT) code.[35,36] Based on the above parameters, the phase velocity of the Dust Acoustic Wave (DAW) turns out to be $C_{da} \sim 20$ mm/s. To compare the theoretical estimation, a separate experiment is also carried out to excite DAW for the above discharge condition by applying a sinusoidal signal to the wire. It is found that the measured C_{da} comes out to be ~25 mm/s, which is in good agreement with the estimated value.

For the excitation of forced solitary waves and the wake structure, the dust particles are made to flow over the wire. The flow of the dust cloud is generated by suddenly lowering the height of the negative potential hill created by the charged object. When the wire is switched to near floating potential, the potential hill is lowered, and the dust particles flow from right to left over the wire as shown in Fig. 2(b). During the flow, the dust particles attain a constant velocity due to neutral drag force[37,38] and excite solitary waves along with wakes depending on the flow velocity of dust fluid. The flow velocity of dust fluid is measured by tracking the individual particles at the tail of the cloud using the Particle Image Velocimetry (PIV) technique.[39] The velocity of the dust fluid is changed from subsonic (~15–18 mm/s) to supersonic (~25–32 mm/s) values by varying the discharge parameters. To study the propagation characteristics of the excited structures, the size (both the height and the width) of the potential hill created by the charged object is altered by changing the resistance connected to the wire, whereas the shape of the potential profile is modified by using objects of different shapes. These studies are discussed in the Secs. III B and III C.

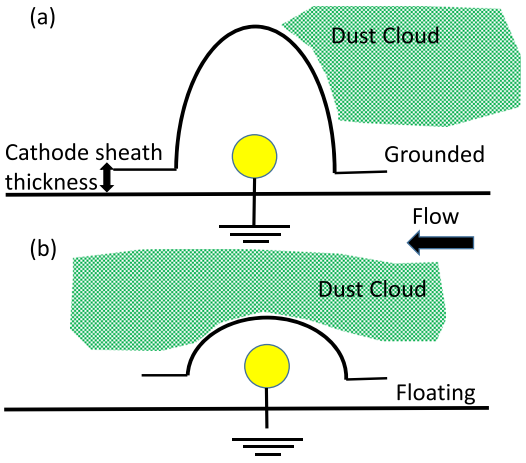


FIG. 2. (a) Equilibrium configuration of dust cloud before generating the flow. (b) Dust flow initiated by lowering the potential hill suddenly by making it floating. The yellow circle represents the location of the charged object, and flow is generated from right to left.

III. RESULTS AND DISCUSSION

A. Excitation of precursor solitons and wakes

Before investigating the dependence of the shape and size of the potential hill on the propagation characteristics of precursor solitons, the experiments of Jaiswal *et al.*[29] were repeated to serve as a benchmark. The results are briefly summarized here. As in Ref. 29, for a subsonic flow, only wake structures were observed in the downstream direction, whereas supersonic flows created precursor solitons propagating in the upstream direction ahead of the object and wakes in the downstream direction. Figure 3(a) depicts such a scenario for a supersonic flow of dust fluid, with Fig. 3(b) showing the normalized amplitudes of solitary and wake structures extracted from Fig. 3(a).

These nonlinear precursor structures were confirmed to be solitons by checking the constancy of the quantity amplitude × width^2. The following f-KdV[40] model equation was also solved as part of the benchmark exercise to obtain a qualitative account of the phenomenon:

$$\frac{\partial n_{d1}}{\partial t} + A n_{d1} \frac{\partial n_{d1}}{\partial \xi} + \frac{1}{2} \frac{\partial^3 n_{d1}}{\partial \xi^3} = \frac{1}{2} \frac{\partial S_2}{\partial \xi}, \quad (1)$$

where the source term (S_2) represents the charged object, n_{d1} is the perturbed density normalized to the equilibrium density n_{d0}, and $\xi(t)$ is the coordinate in the wave frame moving at the phase velocity u_{ph} normalized to the dust acoustic speed. The coefficient "A" associated with Eq. (1) depends upon the electron and ion temperatures and the plasma density. A detailed description of the f-KdV model equation and its solution can be found in Ref. 40. The source function S_2, as shown in Fig. 4(a), is chosen as a Gaussian with amplitude A_s and width G. Figure 4(b) shows the spatial variation of density perturbation which is obtained by solving the f-KdV equation [Eq. (1)] numerically. In this simulation, the Gaussian source function is made to move from left to right either subsonically or supersonically to replicate the relative velocity between the wire and the dust flow in our experiments, and the coefficient A is chosen to be 4 for our

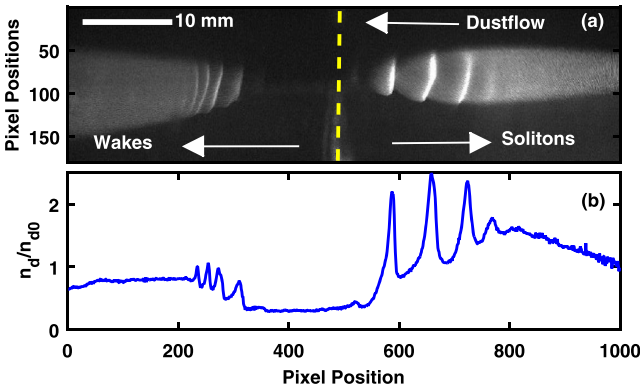


FIG. 3. (a) Propagation of solitons against the direction of flow (in the upstream direction) and wakes in the direction of flow (in the downstream direction) for the case of supersonic flow. The position of wire is represented by the yellow dashed line. (b) The intensity profile of the solitons and wakes.

Published under license by AIP Publishing

DISTRIBUTION A: Distribution approved for public release. Distribution unlimited

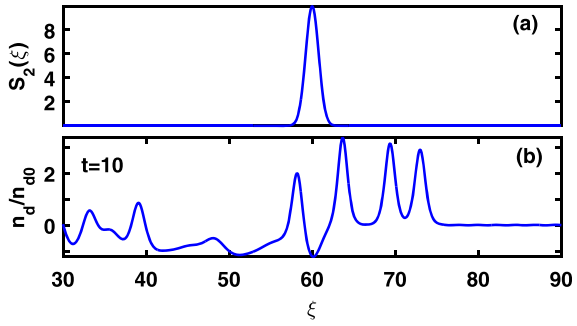


FIG. 4. (a) Source function. (b) Precursor solitons and wakes obtained from the numerical solution of the f-KdV equation.

experimental parameters. As shown in Fig. 4(b), just like the experimental observation, the numerical solution of the f-KdV equation yields the excitation of precursor solitons which propagate in the upstream direction, whereas the wakes move in the downstream direction. The f-Kdv equation will be further used to model the present set of experiments exploring the effect of the size and shape of the obstacle on the solitonic excitations.

B. Excitation of precursor solitons for flow over objects of different sizes

The benchmark experiments were executed by changing the height of the potential hill from its maximum value (grounded potential) to its minimum value (floating potential) to excite the precursor solitons. To investigate the effect of the size (height and width) of the potential hill on the phenomenon, a systematic set of experiments were performed by connecting a variable resistance in series with the wire to change the size of the potential hill. The size of the potential hill of the charged object is adjusted by drawing a current through various resistance values ranging from 10 kΩ to 10 MΩ and measuring the voltage across the resistance (V_{wg}). To begin with, the height and width of the potential hill are measured using dust particles as dynamic microprobes as discussed in Ref. 41. In this technique, these tracer particles are made to flow over the potential hill, and tracking of the individual particle trajectories yields their positions and velocities over the time. The potential of the electrostatic hill just above the wire is then directly estimated by using the energy conservation arguments. The height and the width of the potential hill are measured for a wide range of V_{wg} and plotted in Fig. 5. Figure 5(a) shows the variation of the height (represented by "o") and the width (represented by "⋆") of the potential hill created by the charged object with voltage measured (V_{wg}) across the different resistances connected with the wire in series. It can be seen that the height of the hill decreases and width increases with the increase in V_{wg}. The height of the potential hill is maximum when V_{wg} becomes close to the grounded potential which is negative with respect to the plasma potential, and it decreases when the voltage drop across the variable resistance moves toward the plasma potential which is ∼300 V for this specific set of experiments. The variation of the height (h) with width (w) of the potential hill created by the wire is plotted in Fig. 5(b), and it is seen that the width decreases with an increase in the height of the potential hill. The solid line represents the power law relationship ($h \sim w^{-3.13}$) between the width and the height. Further experiments are performed with a similar range of V_{wg} to examine the effect of the size of the potential hill on the excitation of forced solitary waves.

Figures 6(a)–6(c) show typical images of fully developed forced solitary structures. It visually shows how the number, amplitude, and width of solitons changes with the wire potential, V_{wg}. Figure 6(a) shows the solitary waves at $p = 11$ Pa and $V = 320$ V when V_{wg} is kept at 5 V which is approximately at grounded potential. The dotted line in this figure represents the location of the wire. For $V_{wg} = 5$ V, five prominent solitary waves get excited which are found to propagate in the upstream direction from the frame of fluid. When the resistance connected to the wire is increased such that $V_{wg} \sim 75$ V, the number of prominent solitary structures decreases to four as shown in Fig. 6(b). The number further decreases to two when V_{wg} is increased to 132 V as shown in Fig. 6(c). If the potential of the wire is increased further toward the floating potential, the height of the source object decreases, and it is not sufficient to excite any forced solitary structures. We have also found the threshold value, $V_{wg} = 135$ V, beyond which the particles simply flow and do not excite any wave structures. It is also found that the amplitude decreases, whereas the width of the fully developed solitons increases with the increase in V_{wg}, but the

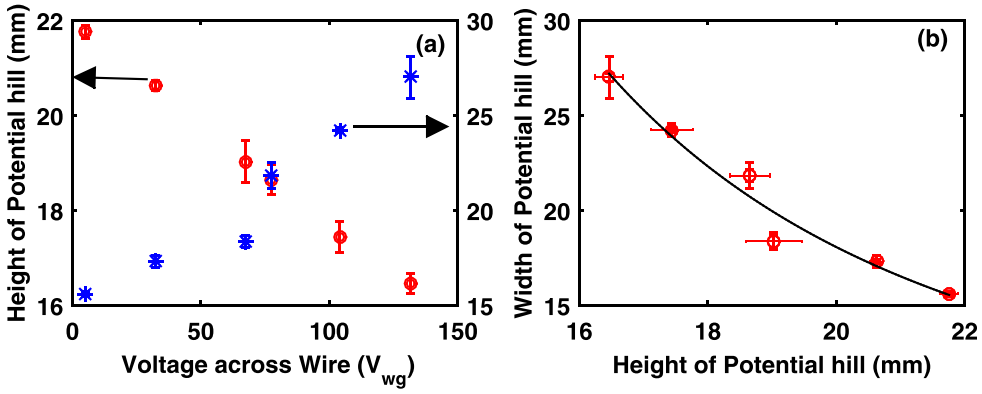


FIG. 5. (a) Variation of height (represented by red open circles) and width (represented by blue stars) of the potential hill with V_{wg}. (b) Power law fit on the height and width of the electrostatic potential created by the charged wire.

Published under license by AIP Publishing

DISTRIBUTION A: Distribution approved for public release. Distribution unlimited

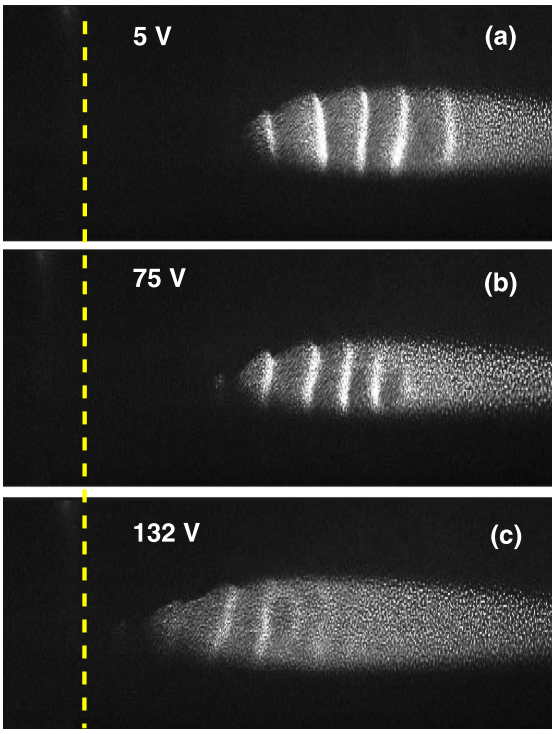


FIG. 6. Excitation of precursor solitons for (a) 5 V, (b) 75 V, and (c) 132 V by varying the voltage across the hill created by the charged wire.

change is not visually appreciable. A more quantitative discussion of the variation of amplitude, width, and velocity with V_{wg} is given later in this section. In all these experiments [Figs. 6(a)–6(c)], the dust velocity is measured using PIV analysis to make sure that the dust fluid moves supersonically over the wire.

Figure 6 qualitatively shows that the amplitude of the solitary structures decreases, whereas the width increases with the increase in V_{wg}. For a quantitative analysis of the amplitude (n_d/n_{d0}) of solitary waves, the maximum intensities are extracted from the images later normalized by the equilibrium intensity of dust density. Figure 7(a) shows the variation of this amplitude of forced dust acoustic solitary waves (f-DASw) with V_{wg}. It shows that the amplitude of these excited solitary waves decreases, whereas the width increases with the increase in V_{wg}. It can also be seen in Fig. 5(a) that the height of the potential hill decreases, whereas the width increases with the increase in V_{wg}. It essentially indicates that the amplitude of the solitary structures strongly depends on the size of the potential hill. In addition to that, the velocity of the forced dust acoustic solitary wave also decreases with the increase in V_{wg} as shown in Fig. 7(b). Hence, in our experiments, the solitary wave having higher amplitude propagates with higher velocity, which is one of the important properties of KdV type solitons. Therefore, it can be concluded that the size of the potential hill plays a salient role in the propagation characteristics of a solitary wave.

To model these experimental findings, we have again solved numerically the f-KdV equation [Eq. (1)] for different values of the amplitude (A_s) and width (G) of the Gaussian source function by choosing the values from the power law relationship derived from the experiments and measured the mean value of the amplitude of solitary structures. Figure 8 depicts the variation of amplitude of forced solitary waves obtained from the numerical solution of f-KdV with the height and width of the source function. For the present set of numerical simulations, the amplitudes and widths are chosen from the experiments as shown in Fig. 5(b). In Fig. 8(a), one can see that the amplitude of the excited forced solitary waves decreases with the decrease in amplitude of the source function, while it decreases with the increase in the width of the source function as shown in Fig. 8(b). The first point of Fig. 8(a) and the last point of Fig. 8(b) correspond to a single soliton solution of the equation, which is also the threshold condition for the creation of f-KdV solitons. A further decrease in A and an increase in G cause only the excitation of wake structures instead of the creation of solitons. Therefore, the findings from the numerical analysis qualitatively support our experimental observations, and there is indeed a threshold for the generation of solitons in the f-KdV simulation similar to the experiments.

C. Forced solitary waves over different shapes of the charged object

All the above experiments were performed by flowing the dust fluid supersonically over the wire of different sizes (height and width) of the potential hill. The potential profile around the wire[41] is indeed a

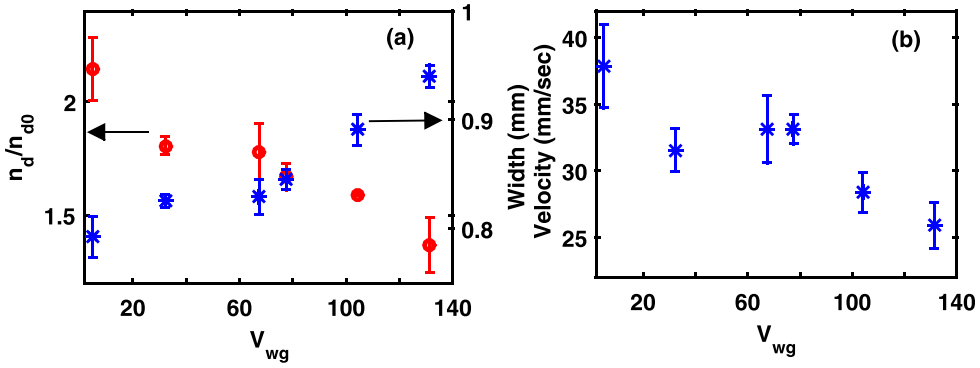


FIG. 7. Variation of (a) amplitude (represented by red open circles), width (represented by blue stars), and (b) velocity of the excited precursor solitons for the case of supersonic fluid flow with the voltage drop V_{wg} across the resistance.

Published under license by AIP Publishing

DISTRIBUTION A: Distribution approved for public release. Distribution unlimited

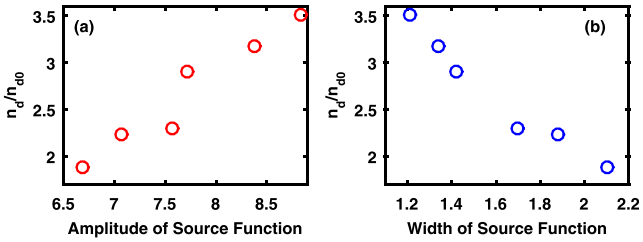


FIG. 8. Variation of amplitude of solitons with (a) amplitude of the source and (b) width of the source numerically obtained from the solution of f-KdV.

Gaussian where the fall of the sheath profile is symmetric and sharp around the object. Next, to investigate the effect of the shape of the potential profile on the propagation characteristics of forced solitary waves, a triangular shaped object was used in two different configurations as shown in Figs. 9(a) and 9(b). The supersonic flow in the dust fluid was again generated by switching the object from grounded potential to floating potential as described in Fig. 2. In the first case [see, Fig. 9(a)], the dust fluid flows over the rising slope of the potential profile created by the triangular charged object, whereas in another configuration, dust fluid flows over a steep charged object [see, Fig. 9(b)] first and then flows over the falling slope.

Figure 10(a) shows a typical image of the excited structures when the dust fluid supersonically flows over the charged object as shown in Fig. 9(a). Interestingly, in this configuration, no structures are found to propagate in the upstream direction dissimilar to the case when the object is purely Gaussian [see Fig. 3(a)]. Instead, a series of crests are found to propagate in the downstream direction. The perturbed dust density profiles [extracted from Fig. 10(a)] are plotted in Fig. 10(b) to explore the properties of these structures. These smaller amplitude crests propagate in the downstream direction with respect to the frame of fluid as wakes. These experimental findings are also compared with numerical solutions of the forced-KdV equation [see Eq. (1)] in which the source function is taken as a half Gaussian with a rising slope as shown in Fig. 11(a). In the case of the triangular object with flat hypotenuse [Figs. 11(a) and 13(a)], the object is replicated by a half Gaussian with a width $\left(\frac{W}{2} \sim 6\right)$ that is larger than the source function with a full Gaussian. The choice of the width of the source term is dictated by the size of the sheath that forms around the obstacle. For p = 11 Pa and V= 320 V, the sheath around the grounded wire of

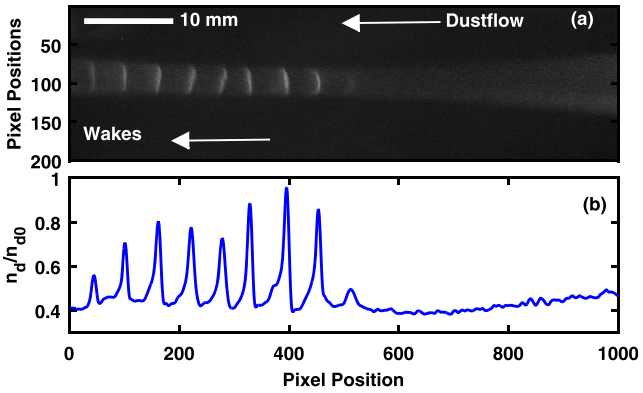


FIG. 10. (a) Generation of nonlinear wakes in the direction of flow when the flow is initiated and facing rising slope of the potential hill. (b) Intensity profile of Fig. 10(a).

1 mm diameter is ∼15.5 mm [see first "⋆" of Fig. 5(a)]. For the same discharge condition, the sheath around the triangular charged object (of hypotenuse 65 mm) is ∼80.5 mm. Hence, $\frac{W}{2}$ for the half Gaussian source function is chosen to be 6, which is approximately 5 times higher compared to the full Gaussian. Figure 11(b) displays the perturbed dust density profile for a given time when the object moves with supersonic velocity similar to our experimental situation. The solution of the f-KdV equation shows only the excitation of wake structures, which propagate in the downstream direction as observed in the experiments.

To investigate further the influence of shapes, the same triangular object is used in the reverse configuration as shown in Fig. 9(b). In this configuration, the dust fluid first faces a sharp rise of the potential and then it goes through a monotonic fall in the potential. When the fluid flows supersonically over this object, it excites both precursor solitons in the upstream direction and wakes in the downstream direction as shown in Fig. 12(a). The perturbed dust density extracted from Fig. 12(a) is shown in Fig. 12(b). To mimic the experimental observations, the f-KdV equation is again solved numerically by using a half Gaussian object like Fig. 11(a) but in the reverse direction as shown in Fig. 13(a). The solution of f-KdV also shows the excitation of solitary waves in the upstream direction and wakes in the downstream direction. Hence, it can be concluded further that the shape of the charged object is also an important parameter which decides the excitation of

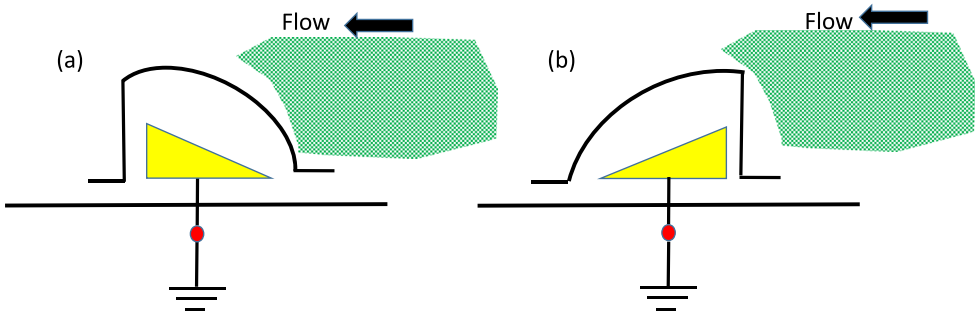


FIG. 9. Equilibrium configuration of dust cloud before generating the flow for two different shapes of the charged object.

Published under license by AIP Publishing

DISTRIBUTION A: Distribution approved for public release. Distribution unlimited

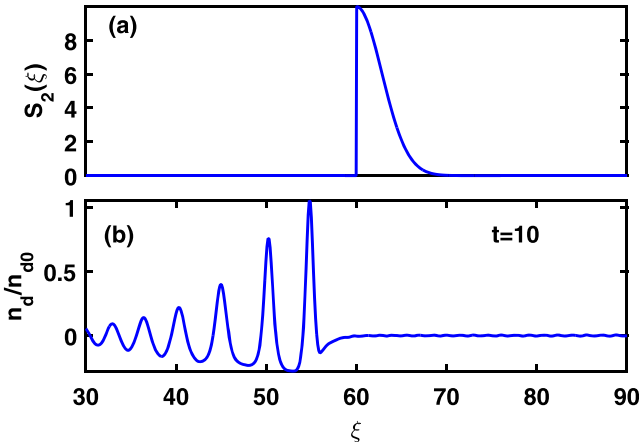


FIG. 11. Time evolution of numerical solution of the f-KdV equation using the half Gaussian function as the source function to replicate the triangular shaped object.

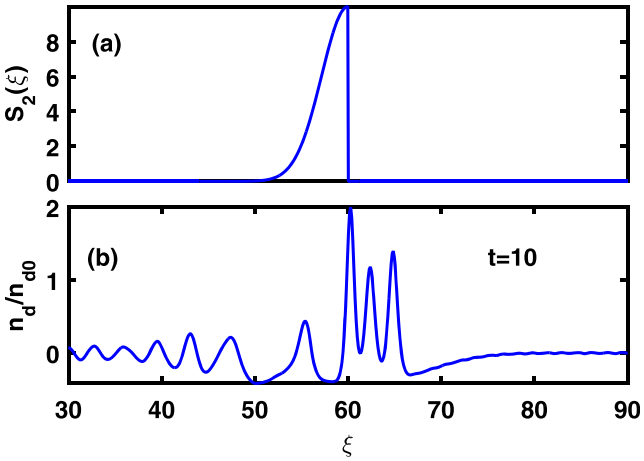


FIG. 13. (a) Source function. (b) Time evolution of numerical solution of the f-KdV equation by reversing the source function as shown in Fig. 11(a).

nonlinear structures. A linear gradient is insufficient to excite the precursor solitons and only gives rise to the customary wakes, whereas a sharp gradient excites both.

IV. SUMMARY AND CONCLUSION

A set of experiments were done to investigate in detail the modifications of the propagation characteristics of precursor solitons which get excited when a supersonic flow of dust fluid is made to flow over a stationary charged object of different sizes and shapes. The experiments were performed in the DPEx device in which dusty plasma was created in a DC glow discharge Ar plasma using kaolin particles. The flow of the dust cloud was initiated by suddenly lowering the height of the potential hill created by a charged object (wire or metallic wedge shaped object). For the case of subsonic dust fluid flow, only wakes were observed in the downstream direction in the frame of the fluid, whereas for a supersonic flow, solitary structures were excited in the upstream direction along with the wakes in the downstream direction.

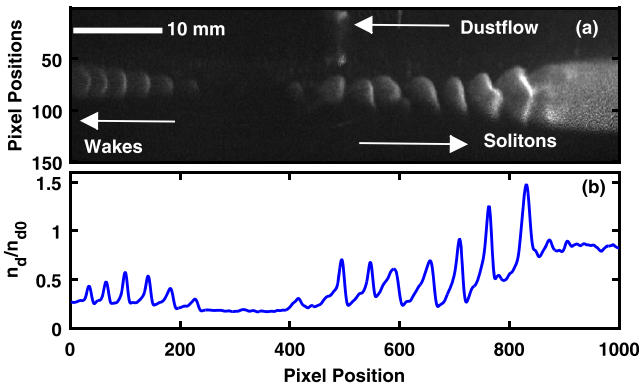


FIG. 12. (a) Generation of wakes and solitons when the flow faces a sharp rise of the potential hill and (b) intensity profiles of these wakes and solitons extracted from Fig. 12(a).

The size and shape of the potential profile were varied by connecting a variable resistance in series with a copper wire and by using the triangular object in different orientations with respect to the flow, respectively. The major outcomes of our present work are listed below:

- To investigate the effect of the size of the potential hill on the propagation of precursor solitons, the height of the potential hill was varied by drawing current through a variable resistance. It was found that the amplitude and velocity of the solitons decreased, whereas their widths increased with a decrease in the height of the potential hill. The number of emitted solitonic structures also decreased with the decrease in the hill height. It was also discovered that there is a threshold height of the potential hill below which the dust fluid simply flows over the object without exciting any structures.
- The f-KdV equation was once again solved numerically by changing the height and width of the Gaussian source function. The numerically obtained amplitudes and widths of solitonic structures followed a similar trend to that observed in the experiments.
- In another set of experiments, the shape of the potential profiles of the charged object was changed by replacing the wire by a solid triangular shaped object. In this specific set of experiments, the flow was only generated by switching the charged object from ground to floating potential. When the dust fluid flowed supersonically over this triangular object facing the linearly increasing slope, only wakes were found to be excited in the downstream direction and no nonlinear structures were seen to propagate in the upstream direction. However, when the experiments were carried out by reversing the object so that the dust fluid faced the sharp jump of the potential created by the charged object, both solitons propagating in the upstream direction and wakes propagating in the downstream direction were seen.
- These results were also modeled and compared qualitatively with the experimental findings by taking the source function to be a half Gaussian in the forward and reverse directions, respectively.

Hence, to summarize, the excitation of precursor solitons and their propagation characteristics are found to depend on the shape and size of the potential profiles of the charged object over which the fluid flows. Our experimental findings not only confirm and consolidate earlier experimental observations of precursor solitons but bring

Published under license by AIP Publishing

DISTRIBUTION A: Distribution approved for public release. Distribution unlimited

to light new fundamental results regarding the excitation process. These insights should prove helpful in interpreting the manifestation of this concept in natural occurrences such as in excitations triggered by solar wind interactions with the earth and moon or space debris or satellite interactions with the ionospheric plasma. The findings may also stimulate further experimental and theoretical studies toward more fundamental investigations of this yet poorly explored topic in plasma physics.

ACKNOWLEDGMENTS

A.S. is thankful to the Indian National Science Academy (INSA) for their support under the INSA Senior Scientist Fellowship scheme and to AOARD for their research grant FA2386-18-1-4022.

REFERENCES

[1]D.-B. Huang, O. Sibul, W. Webster, J. Wehausen, D.-M. Wu, and T. Wu, "Ships moving in the transcritical range," in Proceeding Conference on Behaviour of Ships in Restricted Waters, Varna, Bulgaria (1982), pp. 26–21.
[2]R. Ertekin, "Ship-generated solitons," in Proceedings of the 15th Symposium on Naval Hydrodynamics, Hamburg, Germany, (1985).
[3]R. Ertekin, W. Webster, and J. Wehausen, "Waves caused by a moving disturbance in a shallow channel of finite width," J. Fluid Mech. **169**, 275–292 (1986).
[4]T. Y.-T. Wu, "Generation of upstream advancing solitons by moving disturbances," J. Fluid Mech. **184**, 75–99 (1987).
[5]H.-L. A. Huang, *Dynamics of Surface Waves in Coastal Waters* (Springer, 2010).
[6]M. G. Sun, "The evolution of waves created by a ship in shallow canal," in *the 60th Anniversary Volume*, Zhongshan University, Mechanics Essays Guangzhow, China, 1985, pp. 17–25 (in Chinese).
[7]N. Rao, P. Shukla, and M. Yu, "Dust-acoustic waves in dusty plasmas," Planet. Space Sci. **38**, 543–546 (1990).
[8]A. Barkan, R. L. Merlino, and N. D'Angelo, "Laboratory observation of the dust-acoustic wave mode," Phys. Plasmas **2**, 3563–3565 (1995).
[9]P. K. Shukla and V. P. Silin, "Dust ion-acoustic wave," Phys. Scr. **45**, 508 (1992).
[10]F. Melandso, "Lattice waves in dust plasma crystals," Phys. Plasmas **3**, 3890–3901 (1996).
[11]N. Rao and P. Shukla, "Nonlinear dust-acoustic waves with dust charge fluctuations," Planet. Space Sci. **42**, 221–225 (1994).
[12]P. Bandyopadhyay, G. Prasad, A. Sen, and P. K. Kaw, "Experimental study of nonlinear dust acoustic solitary waves in a dusty plasma," Phys. Rev. Lett. **101**, 065006 (2008).
[13]P. K. Shukla and A. A. Mamun, "Dust-acoustic shocks in a strongly coupled dusty plasma," IEEE Trans. Plasma Sci. **29**, 221–225 (2001).
[14]J. Heinrich, S.-H. Kim, and R. L. Merlino, "Laboratory observations of self-excited dust acoustic shocks," Phys. Rev. Lett. **103**, 115002 (2009).
[15]E. Thomas, K. Avinash, and R. L. Merlino, "Probe induced voids in a dusty plasma," Phys. Plasmas **11**, 1770–1774 (2004).
[16]J. Goree, G. E. Morfill, V. N. Tsytovich, and S. V. Vladimirov, "Theory of dust voids in plasmas," Phys. Rev. E **59**, 7055–7067 (1999).
[17]A. M. Lipaev, S. A. Khrapak, V. I. Molotkov, G. E. Morfill, V. E. Fortov, A. V. Ivlev, H. M. Thomas, A. G. Khrapak, V. N. Naumkin, A. I. Ivanov, S. E. Tretschev, and G. I. Padalka, "Void closure in complex plasmas under microgravity conditions," Phys. Rev. Lett. **98**, 265006 (2007).
[18]M. Kaur, S. Bose, P. K. Chattopadhyay, D. Sharma, J. Ghosh, and Y. C. Saxena, "Observation of dust torus with poloidal rotation in direct current glow discharge plasma," Phys. Plasmas **22**, 033703 (2015).
[19]G. E. Morfill, H. M. Thomas, U. Konopka, H. Rothermel, M. Zuzic, A. Ivlev, and J. Goree, "Condensed plasmas under microgravity," Phys. Rev. Lett. **83**, 1598–1601 (1999).
[20]M. Choudhary, S. Mukherjee, and P. Bandyopadhyay, "Experimental observation of self excited co-rotating multiple vortices in a dusty plasma with inhomogeneous plasma background," Phys. Plasmas **24**, 033703 (2017).
[21]A. Usachev, A. Zobnin, O. Petrov, V. Fortov, M. Thoma, M. Kretschmer, S. Ratynskaia, R. Quinn, H. Hoefner, and G. Morfill, "The project "plasmakristall-4"(pk-4)-a dusty plasma experiment in a combined dc/rf (i) discharge plasma under microgravity conditions," Czech. J. Phys. **54**, C639 (2004).
[22]D. H. E. Dubin, "The phonon wake behind a charge moving relative to a two-dimensional plasma crystal," Phys. Plasmas **7**, 3895–3903 (2000).
[23]L.-J. Hou, Z. L. Mišković, K. Jiang, and Y.-N. Wang, "Energy loss of a charged particle moving over a 2d strongly coupled dusty plasma," Phys. Rev. Lett. **96**, 255005 (2006).
[24]D. Samsonov, J. Goree, Z. W. Ma, A. Bhattacharjee, H. M. Thomas, and G. E. Morfill, "Mach cones in a coulomb lattice and a dusty plasma," Phys. Rev. Lett. **83**, 3649–3652 (1999).
[25]D. Samsonov, J. Goree, H. M. Thomas, and G. E. Morfill, "Mach cone shocks in a two-dimensional yukawa solid using a complex plasma," Phys. Rev. E **61**, 5557–5572 (2000).
[26]O. Havnes, F. Li, F. Melandso, T. Aslaksen, T. W. Hartquist, G. E. Morfill, T. Nitter, and V. Tsytovich, "Diagnostic of dusty plasma conditions by the observation of mach cones caused by dust acoustic waves," J. Vac. Sci. Technol., A **14**, 525–528 (1996).
[27]A. A. Mamun, P. K. Shukla, and G. E. Morfill, "Theory of mach cones in magnetized dusty plasmas with strongly correlated charged dust grains," Phys. Rev. Lett. **92**, 095005 (2004).
[28]L.-J. Hou, Y.-N. Wang, and Z. L. Mišković, "Theoretical study of laser-excited mach cones in dusty plasmas," Phys. Rev. E **70**, 056406 (2004).
[29]S. Jaiswal, P. Bandyopadhyay, and A. Sen, "Experimental observation of precursor solitons in a flowing complex plasma," Phys. Rev. E **93**, 041201 (2016).
[30]S. Kumar Tiwari and A. Sen, "Wakes and precursor soliton excitations by a moving charged object in a plasma," Phys. Plasmas **23**, 022301 (2016).
[31]S. K. Tiwari and A. Sen, "Fore-wake excitations from moving charged objects in a complex plasma," Phys. Plasmas **23**, 100705 (2016).
[32]S. Jaiswal, P. Bandyopadhyay, and A. Sen, "Dusty plasma experimental (dpex) device for complex plasma experiments with flow," Rev. Sci. Instrum. **86**, 113503 (2015).
[33]S. A. Khrapak, S. V. Ratynskaia, A. V. Zobnin, A. D. Usachev, V. V. Yaroshenko, M. H. Thoma, M. Kretschmer, H. Höfner, G. E. Morfill, O. F. Petrov, and V. E. Fortov, "Particle charge in the bulk of gas discharges," Phys. Rev. E **72**, 016406 (2005).
[34]S. A. Khrapak and G. E. Morfill, "Grain surface temperature in noble gas discharges: Refined analytical model," Phys. Plasmas **13**, 104506 (2006).
[35]U. Konopka, "Wechselwirkungen geladener staubteilchen in hochfrequenzplasmen," Ph.D. thesis (Ruhr-Universität-Bochum, 2000).
[36]Y. Feng, J. Goree, and B. Liu, "Accurate particle position measurement from images," Rev. Sci. Instrum. **78**, 053704 (2007).
[37]S. Jaiswal, P. Bandyopadhyay, and A. Sen, "Flowing dusty plasma experiments: generation of flow and measurement techniques," Plasma Sources Sci. Technol. **25**(6), 065021 (2016).
[38]G. Arora, P. Bandyopadhyay, M. G. Hariprasad, and A. Sen, "Micro-dynamics of neutral flow induced dusty plasma flow," Phys. Plasmas **26**, 023701 (2019).
[39]W. Thielicke and E. Stamhuis, "Pivlab-time-resolved digital particle image velocimetry tool for matlab (version: 1.35)," J. Open Res. Software **2**, e30 (2014).
[40]A. Sen, S. Tiwari, S. Mishra, and P. Kaw, "Nonlinear wave excitations by orbiting charged space debris objects," Adv. Space Res. **56**, 429–435 (2015).
[41]G. Arora, P. Bandyopadhyay, M. G. Hariprasad, and A. Sen, "A dust particle based technique to measure potential profiles in a plasma," Phys. Plasmas **25**, 083711 (2018).

Published under license by AIP Publishing

DISTRIBUTION A: Distribution approved for public release. Distribution unlimited

PHYSICAL REVIEW E **103**, 013201 (2021)

Experimental observation of pinned solitons in a flowing dusty plasma

Garima Arora,* P. Bandyopadhyay, M. G. Hariprasad, and A. Sen
Institute For Plasma Research, HBNI, Bhat, Gandhinagar, Gujarat, India 382428

(Received 1 April 2020; revised 4 November 2020; accepted 17 December 2020; published 5 January 2021)

Pinned solitons are a special class of nonlinear solutions created by a supersonically moving object in a fluid. They move with the same velocity as the moving object and thereby remain pinned to the object. A well-known hydrodynamical phenomenon, they have been shown to exist in numerical simulation studies but to date have not been observed experimentally in a plasma. In this paper we report the first experimental excitation of pinned solitons in a dusty (complex) plasma flowing over a charged obstacle. The experiments are performed in a Π shaped dusty plasma experimental (DPEx) device in which a dusty plasma is created in the background of a DC glow discharge Ar plasma using micron sized kaolin dust particles. A biased copper wire creates a potential structure that acts as a stationary charged object over which the dust fluid is made to flow at a highly supersonic speed. Under appropriate conditions nonlinear stationary structures are observed in the laboratory frame that correspond to pinned structures moving with the speed of the obstacle in the frame of the moving fluid. A systematic study is made of the propagation characteristics of these solitons by carefully tuning the flow velocity of the dust fluid by changing the height of the potential structure. It is found that the nature of the pinned solitons changes from a single-humped one to a multihumped one and their amplitudes increase with an increase of the flow velocity of the dust fluid. The experimental findings are then qualitatively compared with the numerical solutions of a model forced Korteweg de Vries (fKdV) equation.

DOI: 10.1103/PhysRevE.103.013201

I. INTRODUCTION

Solitons are a well-known class of stable localized nonlinear structures that have been widely observed and studied in a variety of natural and laboratory settings including ocean waves [1], excitations in optical fibres [2,3] and semiconductors [4], plasmas systems [5–9], laser plasma interactions [10–12], etc. A number of model nonlinear evolution equations that are known to be fully integrable yield soliton solutions. The Korteweg-de Vries (KdV) equation [13–16] is one such nonlinear partial differential equation that has been extensively employed as a model to study low frequency nonlinear wave phenomena in a plasma under conditions of weak dispersion and weak nonlinearity. The emergent nonlinear self-reinforcing wave packets that maintain their shape and identity while propagating at a constant velocity over a large distance are well represented by the exact mathematical soliton solutions of the KdV equation. While the KdV model works well for impulsive excitations of nonlinear pulses where the excitation source provides only an initial perturbation, the model is inadequate to describe experimental situations where the source continues to be operational in a continuous manner. Such is the case for example when a moving object continuously excites waves in a fluid medium. To model such a situation a KdV equation with a driving term—the so-called forced KdV (fKdV) equation—has been adopted and used successfully in the past to interpret nonlinear phenomena in hydrodynamics, e.g., to study nonlinear waves excited by fast moving objects in water [17–20]. The fKdV model yields some interesting and novel nonlinear solutions such as precursor solitons that travel ahead of the moving object at a speed faster than the object. These precursors can be excited when the speed of the moving object crosses the sound speed of the medium. The fKdV model also yields another class of soliton solutions that travel at the same speed as the moving object and remain pinned to the object as an envelope structure. These pinned solitons can be excited at a much higher speed of the object than what is required for the precursor solitons.

Precursor solitons in a plasma were recently observed for the first time under controlled laboratory conditions by flowing a dust fluid supersonically over a stationary charged object [21]. In a frame where the fluid is stationary and the object is moving, the solitons were shown to propagate in the upstream direction as precursors while linear wake structures were seen to propagate in the downstream direction [21]. In a subsequent experiment, the propagation characteristics of these nonlinear structures were shown to depend on the shape and size of the charged object [22] over which the fluid flows. Experimental observations of this fore-wake phenomenon were well explained qualitatively with the help of the forced KdV model equation [21,22].

While propagating precursor solitons in plasmas appear to be well established both experimentally and theoretically the topic of pinned solitons has so far not received much attention. A detailed theoretical study on them over a range of amplitudes, widths, and the velocities of the moving charged object was carried out by Tiwari *et al.* [23] using extensive fluid simulations. To the best of our knowledge, there has yet been no

*garimagarora@gmail.com

 ©2021 American Physical Society

DISTRIBUTION A: Distribution approved for public release. Distribution unlimited

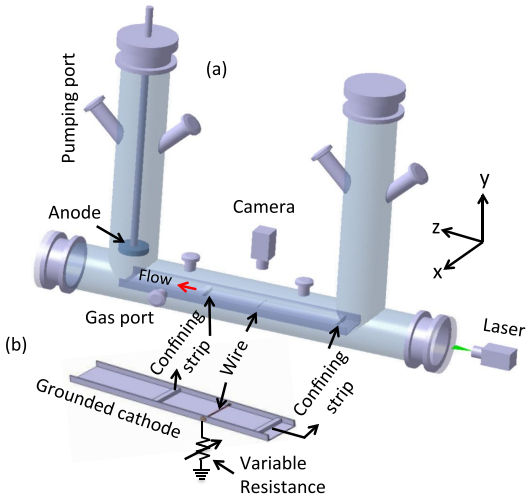


FIG. 1. (a) A schematic diagram of the dusty plasma experimental (DPEx) setup. (b) A zoomed view of the tray shaped grounded cathode showing the copper wire (connected with a variable resistance) and two confinement strips.

experimental study on pinned solitons in plasmas. Our present work addresses that topic and we report on the first successful excitation of such structures in a dusty plasma medium. A dusty plasma provides a convenient medium to study wave phenomena since the massive dust particles suspended in the plasma medium can be easily visualized and their low frequency behavior captured in a nonintrusive manner in a video recording. Our experiments have been carried out in the DPEx device [24] that has been successfully used in the past to study precursor solitons [21,22]. The major difference from past experimental conditions is in the speed of the dust flow which is kept highly supersonic and in the fine tuning of this speed by careful control of the height of the potential barrier created by a biased copper wire placed in the path of the dust flow. Our experiments show not only the existence of single-humped pinned solitons enveloping the moving source but also multihumped solutions as predicted in the theoretical studies of Tiwari *et al.* [23]. Our present findings provide the first experimental evidence of the existence of these interesting nonlinear structures and have the potential of stimulating further experimental and theoretical explorations in this area of nonlinear physics.

II. EXPERIMENTAL SETUP AND PROCEDURE

Figure 1 shows the schematic diagram of the dusty plasma experimental (DPEx) device in which the experiments have been carried out. It is basically an inverted Π shaped vacuum chamber consisting of a primary cylindrical glass tube which is radially attached with two secondary tubes. There are several radial and axial ports connected with the primary as well secondary chambers to serve various experimental needs. A disk-shaped anode suspended axially from the top of the left secondary chamber and a tray-type grounded cathode housed in the primary chamber are used for the production of the plasma. Two confining potential strips are placed on the cathode for confining the dust particles in the axial direction whereas the bent sides of the cathode tray provide radial confinement. A more detailed description of the device along with its associated diagnostics are available in Ref. [24]. A biased copper wire of diameter 1 mm and length 50 mm mounted radially on the cathode creates a potential sheath around it which acts as a stationary charged obstacle in the path of the dust flow and leads to the excitation of the pinned structures. The potential of the wire can be varied between grounded to floating by changing a variable resistor (ranging between 10 kΩ–10 MΩ) that is connected in series with the wire. The variable bias changes the height of the potential barrier and thereby the speed of the dust flow. A DC power supply (with a range of 0–1 kV and 0–500 mA) is used to strike a discharge between the electrodes. Micron-sized polydispersive particles of diameter ranging from 2 to 5 μm are sprinkled on the cathode in between the wire and the right strip for producing a dusty plasma. The average mass of these micron sized dust particles is estimated to be $\sim 8.6 \times 10^{-14}$ kg.

Initially, the chamber is pumped down to a base pressure of 0.1 Pa by fully opening the gate valve attached at the mouth of the pump. The working pressure is set to 9–15 Pa by closing the gate valve to 20% and opening the flow meter attached to the gas port to 5–10% as shown in Fig. 1. An equilibrium pressure inside the chamber is maintained through out the experiments by balancing the pumping rate and the gas flow rate. An Argon plasma is formed between the electrodes by applying a voltage in the range of 290–360 V and the plasma parameters are measured using a single Langmuir probe and an emissive probe over a range of discharge parameters. For the present range of discharge conditions, the plasma density (n_i) is in the range of ~ 0.5–$1.5 \times 10^{15}/\mathrm{m}^3$ and the electron temperature (T_e) is found to be 2–5 eV. The above parameters are consistent with past reported measurements in similar DC glow discharge argon plasmas by several researchers [7,25–28]. The profiles of plasma parameters over a wide range of discharge parameters are the same as presented in Ref. [24].

To create a dusty plasma, an equilibrium pressure $P = 9$ Pa is first set and then the applied voltage is increased to 400 V so that a high electric field is created and the particles sprinkled on the cathode get charged. These particles acquire a negative charge in the plasma environment and form an equilibrium dust cloud by the balance of electrostatic and gravitational forces. In the vertical direction, the gravitational force pulls the particles in the downward direction whereas the electrostatic force (arising from the cathode sheath electric field) pushes the negatively charged particles in the upward direction. When these two forces balance each other the particle levitates in the vertical direction. The outward repulsive interactions among the negatively charged dust particles in the horizontal direction are countered by the inward repulsive force of the sheath electric field of the cathode edges in the radial direction and by that of the grounded copper wire and the right strip in the axial direction. The force balance in axial, radial, and vertical directions provide the overall confinement to create an equilibrium dust cloud. At equilibrium, the dust particles only show their thermal motion. The levitated particles are visualised by shining a green laser light of thickness ~ 1 mm in the x-z plane and their dynamics is captured by a fast CCD camera looking in the same plane. The voltage

DISTRIBUTION A: Distribution approved for public release. Distribution unlimited

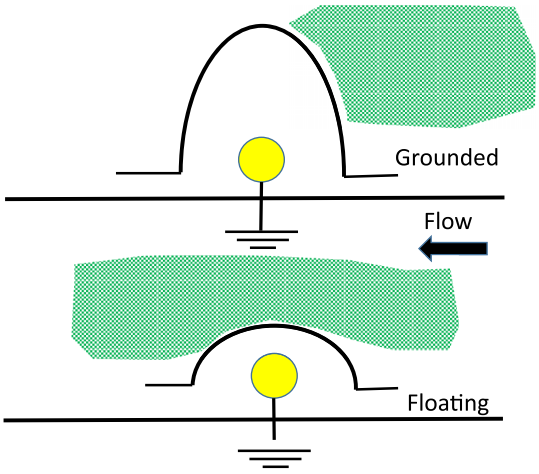


FIG. 2. (a) Illustration of the equilibrium configuration of the dust cloud in the y-z plane prior to generating the flow. (b) Flow in the dust fluid is initiated from right to left by lowering the potential hill suddenly. The yellow circle represents the location of the copper wire shown in Fig. 1(b).

is then reduced to 300 V at which a highly dense dust cloud is seen in between the grounded wire and the right confining strip. Fig. 2(a) shows the y-z plane of the dust fluid, which is confined in between the grounded wire and the right strip. At this specific discharge condition, the potential of the wire remains highly negative with respect to the plasma (∼290 V) and floating (∼270 V) potentials, whereas the surface potential of the dust as predicted by the CEC model [29,30] is ~ -7 V with respect to plasma potential. In other words, the potential around the grounded wire becomes negative with respect to the surface potential of the dust and as a result the particles remain confined in the potential well created by the wire and the strip.

The present set of experiments have been carried out at a discharge voltage of $V_d = 300$ V and a background pressure of 9 Pa, which are lower as compared to the past experiments on precursor solitons [21,22]. For the present discharge conditions, the particles levitate at a height of 2.75 cm from the cathode, which is higher than the (∼2.1 cm) height of the earlier experiments on the excitation of precursor solitons [21,22]. This allows us to generate a higher supersonic flow, $M(v_f/C_{da}) \sim 1.4$–3 in the dust fluid compared to past experimental values of $M(\sim 1.1$–$1.3)$ [21,22]. In addition, as mentioned above, we have performed our experiments at a pressure of 9 pa which is comparatively lower than that of the previous experiments (11–12 Pa) [31]. This leads to a lower dust neutral collision frequency of about 9 s^{-1} [24,32] which is half the value of 18 s^{-1} reported for earlier experiments carried out on this device [31]. We have chosen this lower dust neutral collisional regime so that dissipation becomes less important thereby avoiding the excitation of shock waves. The ion density and electron temperature values, measured using a single Langmuir probe, are found to be $n_i \sim 0.5\times 10^{15}/\mathrm{m}^3$ and $T_e \sim 5$ eV. The dust density (n_d) is approximately estimated as $\sim 10^{11}/\mathrm{m}^3$ from the high resolution camera images, whereas the dust temperature (T_d) is estimated by tracking the individual particles of the tail part of the dust cloud for 100 consecutive frames using a super particle identification tracking (sPIT) [33] code and comes out to be $T_d \sim 0.6$–1.2 eV. The charge $Q_d \sim 10^4$e is estimated from the collision-enhanced plasma collection [29,30] (CEC) model for the present set of discharge conditions. With the help of plasma and dusty plasma parameters, the dust acoustic speed is theoretically estimated to be $C_{da} \sim 22$–25 mm/s. We have also conducted a separate experiment to excite dust acoustic waves (DAW) in the same experimental regime but in the absence of flow to independently determine the dust acoustic velocity. The waves were excited by applying a small electrical pulse to the wire [34]. The average phase velocity (C_{da}) was obtained by tracking different crests of DAWs over time. For the range of discharge conditions of the present set of experiments, the measured phase velocity comes out to be $C_{da} \sim 20$ mm/s. This is in good agreement with the theoretical estimation as discussed above and the earlier measurements of Jaiswal *et al.* [34].

To investigate the propagation characteristics of the nonlinear waves, a highly supersonic flow of the dust fluid ranging from 30 to 60 mm/s (corresponding to $M = 1.4$ to 3) is initiated by altering the confining potential for a particular discharge condition, $p = 9$ Pa and $V = 300$ V. The height of the potential hill is suddenly reduced from grounded potential to an intermediate potential (a potential which is less negative with respect to the particles), which generates a flow of the dust fluid from right to left as shown in Fig. 2(b). Within a few ms, the dust particles attain a constant velocity due to the neutral drag force [34,35] and the magnitude of this constant velocity is varied by changing the value of the intermediate potential and it is found that the maximum velocity is achieved when the wire is switched to floating potential. The flow velocity of the dust fluid is estimated using the particle image velocimetry (PIV) technique [36]. It is worth mentioning that the same technique of flow generation was used by Jaiswal *et al* [21] to excite precursor solitons in the upstream direction and wakes in downstream direction. In their experiments the range of fluid flow velocity was $M = 1.0$–1.2. In the present experiments the fluid velocity is kept higher than these earlier values and the consequent excitations of nonlinear structures studied.

III. RESULTS AND DISCUSSION

The flow technique discussed above is used to generate a flow in the dust fluid with flow velocities ranging from $M \sim 1.4$–3 along the axis of the chamber. The initial experiments are carried out by adjusting the resistance value in such a way that the flow velocity of the dust fluid becomes $M \sim 1.5$. Figure 3(a) shows a snapshot of the wave excitations occurring at this flow velocity, whereas Fig. 3(b) shows the axial profile of density compression, which is extracted from Fig. 3(a). We see a distinct one-humped nonlinear structure close to the yellow dashed line which marks the location of the charged object and lower amplitude wake structures to the left of the yellow line. It is to be noted that the size of the obstacle is not the physical dimension of the wire but the width of the electrostatic sheath created by the potential of the wire. The dashed line in Fig. 3 indicates the physical location of the wire, whereas the actual charged object

DISTRIBUTION A: Distribution approved for public release. Distribution unlimited

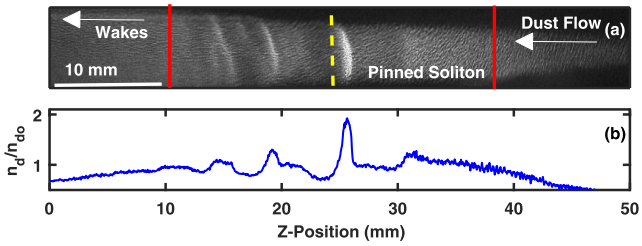


FIG. 3. (a) A typical experimental image of excitation of single pinned soliton. The dashed vertical line marks the position of the wire, whereas the distance between the two red (solid) vertical lines, placed at distances of 1.5 cm on either side of the wire, is the approximate spatial extent of the potential sheath. (b) Axial profile of compression factor of density perturbation extracted from Fig. 3(a).

(the sheath) extends approximately 1.5 cm on both sides of the wire [22] as indicated by the red (solid) vertical lines. The distance from the wire to the single soliton in Fig. 3 is ∼0.8 mm; hence, the soliton is located within the sheath and remains stationary. However, within the experimental errors, it is hard to ascertain whether it is exactly at the center of the sheath.

For a quantitative analysis, the amplitude and the width of these nonlinear structures are calculated by following a standard technique used in the past [7,9,37,38]. The amplitude, A (defined as $\frac{n_d}{n_{dq}} - 1$, where n_d and n_{do} are the instantaneous and equilibrium dust densities, respectively) is calculated from the average pixel intensities of the images of perturbed (I) and equilibrium (I_0) dust densities using the formula $A = \frac{I}{I_o} - 1$. It is to be noted while calculating the amplitude, we have assumed that the light intensity captured by the camera is directly proportional to the dust density due to the linear response of the camera [39,40]. The width (L) of the pinned soliton is measured from the full width at half maximum (FWHM) of the intensity profile of perturbed dust density. The experimental data associated with the high amplitude essentially corresponds to an intense wave crest (indicative of stronger nonlinearity) as shown in Fig. 3, whereas the higher width signifies broadened structures. The amplitude (A), width (L) and the parameter (AL^2) for a typical single-humped nonlinear structure, measured over a number of frames for which it remained stationary, was found to be $A \sim 1.3310 \pm 0.0649$, $L \sim 0.8575 \pm 0.0765$, and $AL^2 \sim$

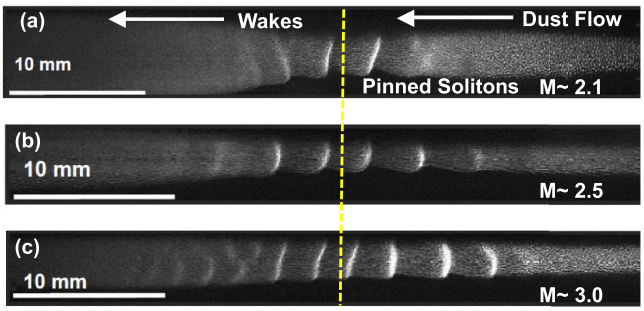


FIG. 4. Typical image of excitation of (a) double, (b) four, and (c) many pinned solitons along with the wakes. The yellow dashed line represents the location of the charged object.

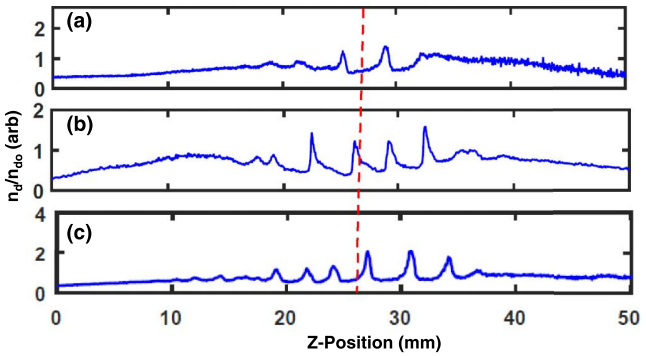


FIG. 5. Density compression factor of (a) two, (b) four, and (c) many sharp peaks extracted from Figs. 4(a), 4(b) and 4(c). The dashed line represents the location of the wire.

0.9859 ± 0.0179. As is well known, the electrostatic single-humped soliton is formed when there is an exact balance of the nonlinear steepening of a wave with the broadening associated with dispersion. As shown theoretically [41,42] and experimentally [7,21,38] in the past, solitons with larger amplitude always propagate with higher velocity and smaller width in such a manner that the product of the amplitude and the square of the width remains constant. To test this conservation property, a slightly different set of experiments was carried out by lowering the fluid flow velocity to $M \sim 1.4$ but keeping the plasma parameters to be the same. The amplitude and width of the consequent excited single-peaked solitary structure were found to be $A = 1.2721 \pm 0.0265$ and $L = 0.8645 \pm 0.0728$, respectively, giving a value of $AL^2 \sim 1.0997 \pm 0.01581$, which is very close to the value

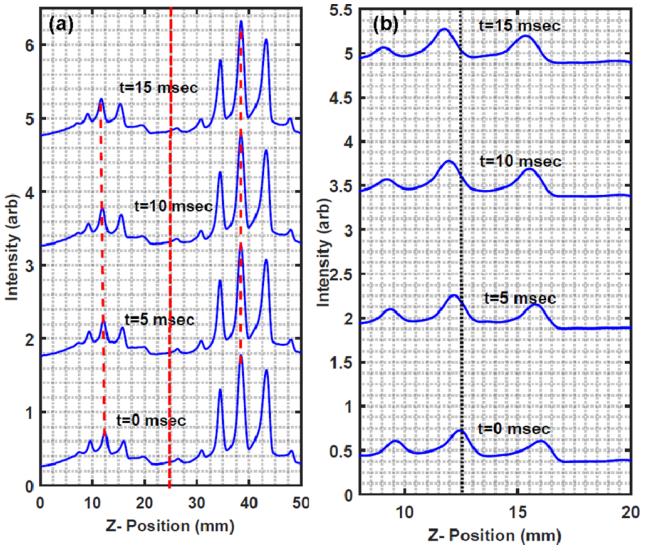


FIG. 6. (a) Intensity profile of a three-humped pinned soliton and wakes over time. The dashed lines show that the higher amplitude soliton remains stationary in the laboratory frame, whereas the wakes move along the flow. The dotted line represents the location of the wire. (b) The zoomed view of a portion of Fig. 6(a) clearly shows that the wakes move from right to left.

DISTRIBUTION A: Distribution approved for public release. Distribution unlimited

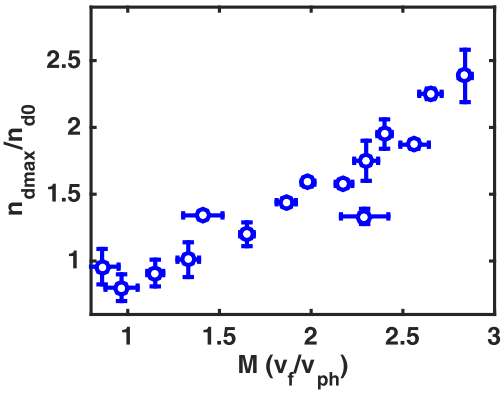


FIG. 7. Variation of maximum density compression $n_{d\max}/n_{d0}$ with the normalized flow velocity M.

obtained in the earlier set of experiments. The constancy of AL^2 provides further evidence that such a structure is indeed a soliton [7,9]—in this case a pinned soliton.

When the flow velocity of the fluid is increased further to $M = 2.1$ and above, by changing the wire potential under the same discharge conditions, we find a significant change in the shape of the pinned soliton. As shown in Fig. 4 a variety of multihumped pinned structures appear for flow velocities $M = 2.1$, 2.5, and 3.0, respectively. Figures 4(a)–4(c) clearly show that the number of humps increases with an increase in the flow velocity. The corresponding intensity profiles of the structures of Figs. 4(a)–4(c) are plotted in Figs. 5(a)–5(c). Figure 5(a) shows the profile of a fully developed two-humped pinned soliton that remains stationary in the laboratory frame, and Fig. 5(b) shows the profile for a similar four-peaked pinned soliton. It is to be noted that the two- and four-peaked structures have a symmetric profile around the wire. Interestingly, in the case of $M \sim 3.0$ [see Fig. 5(c)], the multihumped pinned soliton has an asymmetric structure with respect to the wire with the peaks to the right having a higher amplitude compared to the ones at the left. The characteristics of the wakes however remain the same with the increase of flow velocity and are always found to propagate in the direction of flow or in the downstream direction in the frame of the fluid.

The time evolution of a three-peaked soliton (as captured from subsequent frames) for the case of $M = 2.3$ is plotted in Fig. 6(a) where the high amplitude structures in the figure represent the three-peaked soliton, whereas the lower amplitude structures on the left are wakes. Figure 6(a) also shows that the soliton remains nearly stationary in its position in the laboratory frame of reference like the stationary charged object. In the frame of the fluid, the charged object moves from left to right along with the pinned soliton with the same velocity. The wake structures however are not stationary and propagate in the downstream direction as has been observed earlier in the experiments of Jaiswal *et al.* [21] and also shown in Fig. 6(b), which is a zoomed view of Fig. 6(a) with only the wakes. To summarize, the highly supersonic fluid flow over a stationary charged object excites nonlinear pinned solitons in the upstream direction which maintain their shape and size in the course of time, whereas the wakes propagate in the downstream direction.

To quantify the dependence of the amplitude on the flow velocity the maximum values of the amplitudes of the solitons excited in the range of $M = 1.5$ to 3 are plotted against the Mach number in Fig. 7. It can be seen that with an increase in M, the maximum amplitude of the excited stationary structures increases. This is in qualitative agreement with the scaling observed in earlier fluid simulation studies of pinned solitons [23].

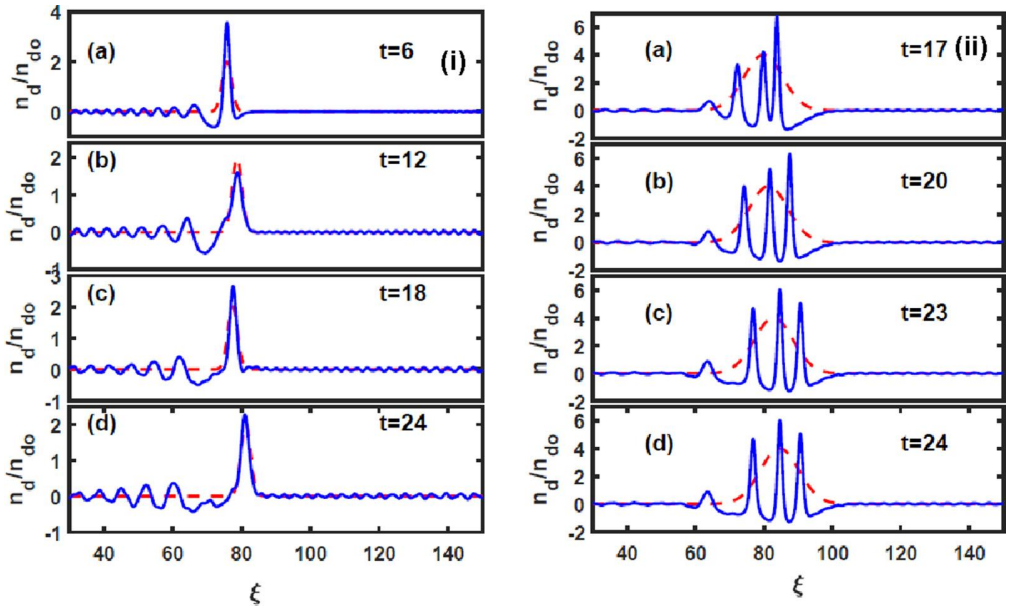


FIG. 8. Time evolution of (i) single ($B = 2.0$, $G = 2.0$, and $v_d = 1.5$.) and (ii) three ($B = 4$, $G = 8$, and $v_d = 2$) pinned solitons obtained numerically by solving the f-KdV equation with $\alpha = 2.0$. Solid lines represents the solitonic structure whereas the dashed line represents the source functions. The time is normalized by the inverse of dust plasma frequency.

DISTRIBUTION A: Distribution approved for public release. Distribution unlimited

TABLE I. Solitonic parameters for different v_d values.

v_d	Amplitude (A)	Width (L)	AL^2
1.1	1.354 ± 0.028	3.18 ± 0.05	13.67 ± 0.71
1.2	1.512 ± 0.045	3.09 ± 0.06	14.48 ± 0.99
1.3	1.816 ± 0.027	2.71 ± 0.05	13.35 ± 0.69
1.4	2.220 ± 0.020	2.38 ± 0.04	12.55 ± 0.54
1.5	2.684 ± 0.020	2.16 ± 0.03	12.44 ± 0.44

IV. COMPARISON WITH MODEL F-KDV EQUATION

For a further qualitative understanding of the experimental results we have solved a model f-KdV equation numerically with a Gaussian source term [43] and compared the numerical results with our experimental observations. The f-KdV equation for a dusty plasma is given by [21]

$$\frac{\partial n_{d1}}{\partial t} + \alpha n_{d1}\frac{\partial n_{d1}}{\partial \xi} + \frac{1}{2}\frac{\partial^3 n_{d1}}{\partial \xi^3} = \frac{1}{2}\frac{\partial S_2}{\partial \xi}, \tag{1}$$

where S_2 represents the source term. n_{d1} is the perturbed dust density normalized to the equilibrium density n_{do} and $\xi = (z - u_{ph}t)$ is the coordinate in the wave frame moving at phase velocity u_{ph} normalized to the dust acoustic speed. The spatial coordinate z is normalized by the dust Debye length (λ_D), whereas time (t) is normalized by the inverse of dust plasma frequency (ω_{pd}).The coefficient $\alpha = [\delta^2 + (3\delta + \sigma_i)\sigma_i + \frac{1}{2}\delta(1+\sigma_i^2)]/(\delta-1)^2$, where δ and σ are the ratio of ion to electron density and temperature, respectively. For our numerical investigations we have used the value of α to be 2 as per the plasma parameters. A Gaussian source function is used in the form $S_2(\xi + Ft) = B\exp[-(\xi + Ft)/G]^2$, where B and G are the amplitude and width of the source function, respectively, and $F = 1 - v_d$, with v_d the velocity of the source function with respect to the frame of fluid. The coefficient α in the unforced part of the model equation is associated with the nonlinear contribution arising from the plasma properties. It is the balance of this contribution with the dispersive term that produces the standard KdV soliton. As a result, the nature of the KdV soliton does depend on the value of α. However, in our case since we are not altering the plasma conditions this dependence remains unchanged. For our driven experiment we are interested in the influence of the driving amplitude (B) and width (G) of the source term as well as its velocity on the nature of the pinned solitons. In general, all these three quantities influence the propagation properties of the emitted soliton. An exact analytic form of such a dependence is not known except for very special forms of the driving term (e.g., a sech^2 driving term gives rise to a sech^2 soliton as discussed in Ref. [43]). For the Gaussian shaped source we have numerically explored various values of the amplitude, width and velocity to investigate the excitation of single-peaked and multipeaked pinned solitons. One guiding factor is that the area of the Gaussian should be sufficient to produce a soliton. The additional amount is radiated away.

In our experiments the sheath around the wire plays the role of the charged object S_2. This wire was also used for the successful excitation of precursor solitons in our earlier experiments [21,22]. The knowledge of the shape and size of the sheath potential from our earlier experimental measurements [44] indicates that it is close to a Gaussian shape. This has prompted our choice for the form of the source function S_2 for the numerical solution of the f-KdV equation. The pinned solitons are numerically obtained by solving Eq. (1) for a Gaussian source with $B = 2.0$, $G = 2.0$ that is made to move with $v_d = 1.5$ in accordance with the experimental condition of $M = 1.5$.

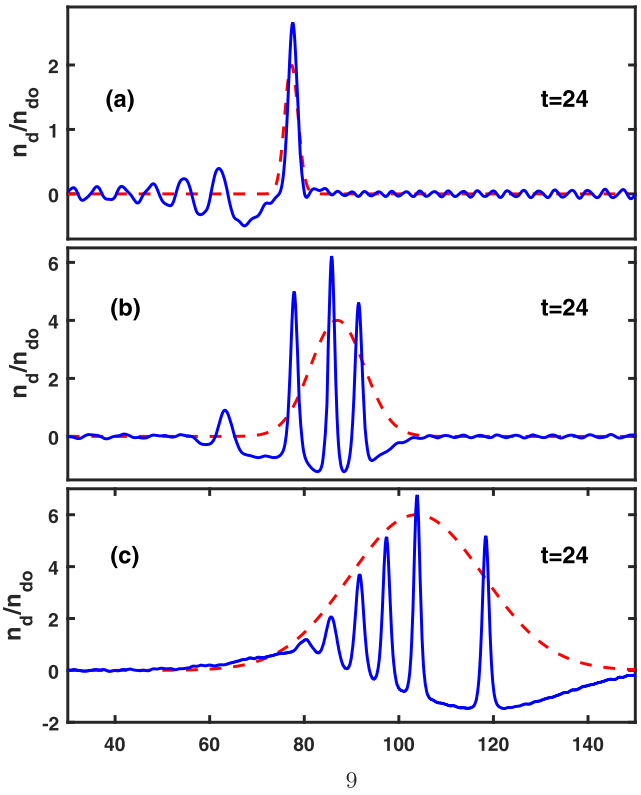


FIG. 9. Time evolution of (a) single ($B = 2.0$, $G = 2.0$, and $v_d = 1.5$), (b) three ($B = 4$, $G = 8$, and $v_d = 2.0$), and (c) multiple ($B = 6$, $G = 20$, and $v_d = 2.2$) pinned solitons obtained by numerically solving the f-KdV equation. Solid lines represent the solitonic structures whereas the dashed lines represents the source function. Time is normalized by the inverse of dust plasma frequency.

The snap shots of S_2 and the normalized perturbed dust density n_d/n_{do} are shown in the left panel of Figs. 8(a)–8(d) for $t = 6, 12, 18, 24$, respectively. The red dashed lines in Fig. 8 represents the position of the charged object that moves with supersonic velocity in the fluid frame. The blue solid lines represent the numerical solution of the fKdV. As can be seen, similar to the experimental results [see Fig. 3(b)], a single-peaked structure representing a single-humped pinned soliton is created near the source and remains stationary with respect to it. The structures to the left of the object consisting of wakes are seen to travel to the left. The slightly oscillating-decaying behavior of the excitation observed in the left panel of Fig. 8 is a consequence of the structure trying to settle down to a soliton state by radiating waves. The right panels of Figs. 8(a)–8(d) show snapshots of a three-peaked structure for $t = 17, 20, 23, 24$, respectively, as it settles down to a quasi-stationary state for a Gaussian source with $B = 4$,

DISTRIBUTION A: Distribution approved for public release. Distribution unlimited

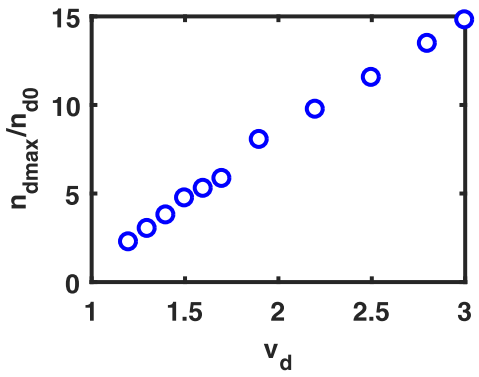


FIG. 10. Variation of maximum density compression $n_{d\max}/n_{d0}$ obtained from numerical solution with the velocity of source function v_d.

$G = 8$ and $v_d = 2.0$. We have also numerically investigated the conservation property (AL^2) by looking at the single peak structure solutions of different amplitudes in the forced KdV model. For this investigation, the values of v_d were changed between 1.1 to 1.5 (see Table I) for a given values of $B = 2$ and $G = 2$. Table I shows that over a range of the flow velocity (v_d), the solitons get excited with different values of amplitudes (A) and widths (L) but the value of the solitonic parameter AL^2 remains nearly constant as also seen in the case of experiments.

For further comparisons with the experiment, Eq. (1) is solved for different values of the amplitude, width and speed v_d of the source term to investigate the dependence of the nature of the pinned solitons on the source parameters.

In the experiments the change in the velocity of the source is brought about by a change in the amplitude and width of the source, e.g., the velocity of the source function was increased by increasing its amplitude which in turn increased the width. Keeping that in mind we have changed the amplitude, width, and the velocity v_d in the source and then solved the f-KdV equation. The results are shown in Figs. 9(a)–9(c) for source parameters with $B = 2, 4, 6$, $G = 2, 8, 20$, and $v_d = 1.5, 2.0, 2.2$, respectively, at $t = 24$. The solid lines correspond to the stationary structures excited by the moving source and the dashed line indicates the position of the source. Similar to the experiments, it can be seen that with an increase in the velocity (v_d) of the source function, the number of peaks of the excited pinned solitons increases as does the value of the maximum amplitude. This is once again in qualitative agreement with the fluid simulation results of Ref. [23], where it was found that the amplitude as well as the number of modulation peaks of the excited pinned solitons increased with an increase in the source velocity and amplitude. The scaling of the density compression with velocity from our numerical solutions is plotted in Fig. 10. Similar to the experimental findings (see Fig. 7), the density compression increases almost linearly with the increase of flow velocity.

V. CONCLUSIONS

To conclude, experimental observations of a new class of stationary solitons, known as pinned solitons, is reported in a flowing complex plasma. These experiments have been performed in the dusty plasma experimental device in which a large dust cloud was created in a DC glow discharge Argon plasma. For the purpose of generating a highly supersonic flow in the dust fluid, the discharge voltage and the background pressure were set such that the dust particles levitated at a height far above the cathode. The flow in the dust fluid was generated over the stationary charged object by changing the height of the potential hill used for the axial confinement. The highly supersonic flow of dust fluid was seen to generate multiple nonlinear stationary structures in the vicinity of the wire. In the frame of the moving fluid, these structures remain attached to the moving object (wire) and constitute propagating pinned solitons. The maximum amplitude of the solitonic structures was found to display an increase with the increase of the fluid flow velocity. In addition, the number of amplitude modulations (peaks) in the density perturbation was also found to increase with the increase in the dust flow velocity. The results are in qualitative agreement with numerical solutions of the forced-KdV equation with a Gaussian source function moving with a supersonic velocity. It must be remarked here that the f-KdV model as well as the previous fluid simulations [23] are based on a one dimensional approximation of the dynamics and hence have inherent limitations. They ignore, for example, effects associated with finite length effects in the direction transverse to the direction of propagation of the soliton that can lead to bending or curving of the soliton profiles that would show up in an experiment carried out in a finite device. Hence, the model results can only serve as a qualitative guide for the interpretation of the results. However, as we see in the present experiment and as has also been observed in past experimental studies of solitons in laboratory plasma devices [7,21,22], a KdV-based model does capture the essential features of soliton excitation and its propagation characteristics. In the present case we are able to qualitatively establish the predominant features of the pinned solitons by their stationary nature, the constancy of the quantity AL^2 for the one-humped structure and the existence of multihumped forms predicted by the model. So it appears that higher dimensional effects may not be important for our experiment. Our present results apart from being of fundamental importance may have some potential applications in real life situations. The experimental conditions in the Earth's bow shock region with a supersonic solar wind impinging on a charged Earth is similar in configuration to our experimental set up. Likewise, in the Earth's ionosphere objects like spacecraft and space debris get naturally charged from the ionospheric plasma and can have similar associated nonlinear excitations. The possibility of such excitations have already been discussed in the literature [43] and recognized for their utility [45]. It is hoped that such potential applications as well as the intrinsic importance of this nonlinear phenomenon can stimulate further explorations on this topic.

ACKNOWLEDGMENTS

A.S. is thankful to the Indian National Science Academy (INSA) for their support under the INSA Senior Scientist Fellowship scheme and to AOARD for their research Grant No. FA2386-18-1-4022.

DISTRIBUTION A: Distribution approved for public release. Distribution unlimited

[1] A. New and R. Pingree, Deep Sea Res. Part A. Oceanogr. Res. Papers **37**, 513 (1990).

[2] M. Gedalin, T. C. Scott, and Y. B. Band, Physi. Rev. Lett. **78**, 448 (1997).

[3] H. A. Haus and W. S. Wong, Rev. Mod. Phys. **68**, 423 (1996).

[4] S. Barland, J. R. Tredicce, M. Brambilla, L. A. Lugiato, S. Balle, M. Giudici, T. Maggipinto, L. Spinelli, G. Tissoni, T. Knoedl *et al.*, Nature **419**, 699 (2002).

[5] N. J. Zabusky and M. D. Kruskal, Physi. Rev. Lett. **15**, 240 (1965).

[6] R. Heidemann, S. Zhdanov, R. Sütterlin, H. M. Thomas, and G. E. Morfill, Phys. Rev. Lett. **102**, 135002 (2009)

[7] P. Bandyopadhyay, G. Prasad, A. Sen, and P. K. Kaw, Phys. Rev. Lett. **101**, 065006 (2008)

[8] Y. Nakamura, H. Bailung, and P. K. Shukla, Phys. Rev. Lett. **83**, 1602 (1999)

[9] D. Samsonov, A. V. Ivlev, R. A. Quinn, G. Morfill, and S. Zhdanov, Phys. Rev. Lett. **88**, 095004 (2002)

[10] P. K. Kaw, A. Sen, and T. Katsouleas, Physi. Rev. Lett. **68**, 3172 (1992).

[11] S. Sundar, A. Das, V. Saxena, P. Kaw, and A. Sen, Phys. Plasmas **18**, 112112 (2011).

[12] A. Kumar, C. Shukla, D. Verma, A. Das, and P. Kaw, Plasma Phys. Control. Fusion **61**, 065009 (2019).

[13] D. J. Korteweg and G. De Vries, London, Edinburgh, Dublin Philos. Mag. J. Sci. **39**, 422 (1895).

[14] R. M. Miura, SIAM Rev. **18**, 412 (1976).

[15] H. Ikezi, Phys. Fluids **16**, 1668 (1973).

[16] J. N. Dinkel, C. Setzer, S. Rawal, and K. E. Lonngren, Chaos, Solitons, Fractals **12**, 91 (2001)

[17] T. Y.-T. Wu, J. Fluid Mech. **184**, 75 (1987).

[18] S.-J. Lee, G. T. Yates, and T. Y. Wu, J. Fluid Mech. **199**, 569 (1989).

[19] M. G. Sun, The 60th Anniversary Volume, Zhongshan University, Mechanics Essays Guangzhow, China, 1985, pp. 17–25 (in Chinese).

[20] B. J. Binder, M. G. Blyth, and S. Balasuriya, Europhys. Lett. **105**, 44003 (2014)

[21] S. Jaiswal, P. Bandyopadhyay, and A. Sen, Phys. Rev. E **93**, 041201(R) (2016)

[22] G. Arora, P. Bandyopadhyay, M. G. Hariprasad, and A. Sen, Phys. Plasmas **26**, 093701 (2019).

[23] S. Kumar Tiwari and A. Sen, Phys. Plasmas **23**, 022301 (2016).

[24] S. Jaiswal, P. Bandyopadhyay, and A. Sen, Rev. Sci. Instrum. **86**, 113503 (2015).

[25] V. E. Fortov, A. G. Khrapak, S. A. Khrapak, V. I. Molotkov, A. P. Nefedov, O. F. Petrov, and V. M. Torchinsky, Phys. Plasmas **7**, 1374 (2000).

[26] C. Thompson, A. Barkan, N. D'Angelo, and R. L. Merlino, Phys. Plasmas **4**, 2331 (1997).

[27] J. D. Williams, E. Thomas, and L. Marcus, Phys. Plasmas **15**, 043704 (2008).

[28] J. Pramanik, B. Veeresha, G. Prasad, A. Sen, and P. Kaw, Phys. Lett. A **312**, 84 (2003).

[29] S. A. Khrapak, S. V. Ratynskaia, A. V. Zobnin, A. D. Usachev, V. V. Yaroshenko, M. H. Thoma, M. Kretschmer, H. Höfner, G. E. Morfill, O. F. Petrov *et al.*, Phys. Rev. E **72**, 016406 (2005)

[30] S. A. Khrapak and G. E. Morfill, Phys. Plasmas **13**, 104506 (2006).

[31] S. Jaiswal, P. Bandyopadhyay, and A. Sen, Phys. Plasmas **23**, 083701 (2016).

[32] P. S. Epstein, Phys. Rev. **23**, 710 (1924).

[33] Y. Feng, J. Goree, and B. Liu, Rev. Sci. Instrum. **78**, 053704 (2007).

[34] S. Jaiswal, P. Bandyopadhyay, and A. Sen, Plasma Sources Sci. Technol. **25**, 065021 (2016).

[35] G. Arora, P. Bandyopadhyay, M. G. Hariprasad, and A. Sen, Phys. Plasmas **26**, 023701 (2019).

[36] W. Thielicke and E. Stamhuis, J. Open Res. Software **2**, e30 (2014).

[37] S. Annibaldi, A. Ivlev, U. Konopka, S. Ratynskaia, H. Thomas, G. Morfill, A. Lipaev, V. Molotkov, O. Petrov, and V. Fortov, New J. Phys. **9**, 327 (2007).

[38] S. K. Sharma, A. Boruah, and H. Bailung, Phys. Rev. E **89**, 013110 (2014).

[39] T. M. Flanagan and J. Goree, Phys. Plasmas **17**, 123702 (2010).

[40] R. Merlino, J. Heinrich, S. Kim, and J. Meyer, Plasma Phys. Control. Fusion **54**, 124014 (2012).

[41] P. K. Shukla and B. Eliasson, Phys. Rev. E **86**, 046402 (2012).

[42] P. Bandyopadhyay, U. Konopka, S. Khrapak, G. Morfill, and A. Sen, New J. Phys. **12**, 073002 (2010).

[43] A. Sen, S. Tiwari, S. Mishra, and P. Kaw, Adv. Space Res. **56**, 429 (2015).

[44] G. Arora, P. Bandyopadhyay, M. G. Hariprasad, and A. Sen, Phys. Plasmas **25**, 083711 (2018).

[45] A. S. Truitt and C. M. Hartzell, J. Spacecr. Rockets **0**, 1 (2020).

DISTRIBUTION A: Distribution approved for public release. Distribution unlimited

New Journal of Physics
The open access journal at the forefront of physics

Deutsche Physikalische Gesellschaft DPG IOP Institute of Physics

PAPER • OPEN ACCESS

Precursor magneto-sonic solitons in a plasma from a moving charge bunch

To cite this article: Atul Kumar and Abhijit Sen 2020 *New J. Phys.* **22** 073057

View the article online for updates and enhancements.

This content was downloaded from IP address 157.32.100.250 on 30/07/2020 at 17:56

DISTRIBUTION A: Distribution approved for public release. Distribution unlimited

New Journal of Physics
The open access journal at the forefront of physics

Deutsche Physikalische Gesellschaft DPG
IOP Institute of Physics

Published in partnership with: Deutsche Physikalische Gesellschaft and the Institute of Physics



OPEN ACCESS

RECEIVED
13 December 2019

REVISED
1 June 2020

ACCEPTED FOR PUBLICATION
10 June 2020

PUBLISHED
29 July 2020

Original content from this work may be used under the terms of the Creative Commons Attribution 4.0 licence.

Any further distribution of this work must maintain attribution to the author(s) and the title of the work, journal citation and DOI.



PAPER

Precursor magneto-sonic solitons in a plasma from a moving charge bunch

Atul Kumar and Abhijit Sen

Institute for Plasma Research, Bhat, Gandhinagar-382428, India

E-mail: atul.j1211@gmail.com

Keywords: electromagnetic precursors, magnetosonic solitons, ion wakes, ion beam, precursor solitons

Abstract

The nature of fore-wake excitations created by a charge bunch moving in a magnetized plasma is investigated using particle-in-cell simulations. Our studies establish for the first time the existence of precursor magneto-sonic solitons traveling ahead of a moving charge bunch. The nature of these excitations and the conditions governing their existence are delineated. We also confirm earlier molecular dynamic and fluid simulation results related to electrostatic precursor solitons obtained in the absence of a magnetic field. The electromagnetic precursors could have interesting practical applications such as in the interpretation of observed nonlinear structures during the interaction of the solar wind with the Earth and the Moon and may also serve as useful tracking signatures of charged space debris traveling in the ionosphere.

1. Introduction

Precursors that travel faster than a source pulse exciting them are of much fundamental and practical interest in many areas of physics. For example, optical precursors that were theoretically predicted many years ago by Sommerfeld and Brillouin [1, 2], provide insights into questions related to group velocity in a dispersive medium [3] and can be potentially useful in applications like underwater communications [4] or deep imaging of biological tissue [5]. Optical precursors have been experimentally observed when light pulses have been launched in a deionized water column [4] and also in a linear dispersive medium consisting of a gas of cold potassium atoms [6]. Their occurrence is associated with the existence of anomalous dispersion in the medium, namely, a negative value of the derivative of the refractive index with respect to frequency at the source pulse carrier frequency. In principle, such a linear phenomenon can also take place in a gaseous plasma medium as has been pointed out in past studies [7–9]. However in a plasma there can be other competing mechanisms of precursor generation that do not depend on anomalous dispersion but exploit the nonlinear properties of the medium. One such process is the excitation of nonlinear structures like solitons or shocks that can propagate faster than the moving excitation source. The generation of such nonlinear precursor pulses has been conjectured a long time ago in hydrodynamics and studied in the context of fore-wake structures generated by moving ships [10–12] but has received scant attention in plasmas until recently. Theoretical studies in the framework of a fluid model have now shown the existence of electrostatic precursor pulses ahead of a super-sonically moving charged object in a plasma [13–15] and experimental support has come from observations in a laboratory dusty plasma device [16, 17]. One of the advantages of these solitonic precursors over the Brillouin or Sommerfeld type precursors is that they can propagate over long distances without any attenuation and can thus prove more useful in communication applications or in transferring packets of energy to a target. To date, the theoretical/simulation studies of such precursors in plasmas have been limited to the excitation of low frequency electrostatic pulses in a fluid plasma model [13, 14] or in a strongly coupled Yukawa fluid system [15]. In the present work we take a more fundamental approach of investigating this phenomenon at a particulate level and also consider the excitation of electromagnetic pulses. Using two dimensional

© 2020 The Author(s). Published by IOP Publishing Ltd on behalf of the Institute of Physics and Deutsche Physikalische Gesellschaft

DISTRIBUTION A: Distribution approved for public release. Distribution unlimited

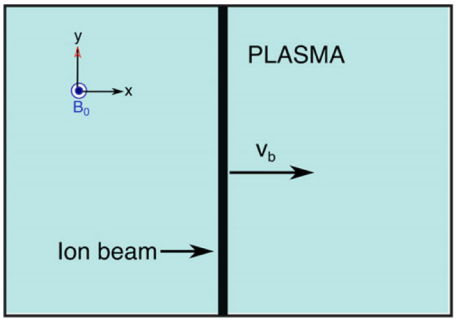


Figure 1. Schematic diagram (not to scale) of the simulation geometry where an ion beam (thick black line) representing an idealized finite charge source is moving with a speed V_b in the positive $\hat{x}$-direction. A magnetic field is applied in the positive $\hat{z}$ direction.

particle-in-cell simulations we establish from first principles the existence of precursor magnetosonic solitons propagating ahead of a moving charge bunch in a magnetized plasma and explore the excitation conditions and the nature of these solitons. We also point out the potential uses of our results in a few practical applications ranging from space debris detection to interpretation of precursor waves in Earth solar wind interactions.

The paper is organized as follows. In section 2 we briefly describe the physical model used for our simulations and also give the essential computational details. Our main results are presented in section 3 with separate subsections devoted to confirmation of earlier electrostatic precursor results section 3.1, magnetosonic solitons section 3.2, pinned solitons section 3.3 and precursors from a two dimensional source section 4. Section 5 gives a summary of our results and discusses their possible occurrences in nature and also their potential applications.

2. Simulation model

Our 2d-3V particle-in-cell simulations have been carried out using the OSIRIS-4.0 code [18–20] for a quasi-neutral plasma system consisting of positive ions and electrons. For simplicity and shorter simulation times the ion to electron mass ratio has been taken to be 25. In this system a short pulsed beam of positive (or negative) ions is made to travel at various velocities and the resultant wave excitations are studied. A constant magnetic field B_0 is imposed in the $\hat{z}$ direction while the beam travels in the perpendicular $\hat{x}$ direction. A schematic of the simulation geometry and the start-up scenario is shown in figure 1. The magnetic field strength is chosen to be such that the following condition holds, namely, $\omega_{ci} < \omega_{pi} \ll \omega_{pe} < \omega_{ce}$, where ω_{ci}, ω_{ce}, ω_{pe} and ω_{pi} are the ion cyclotron, the electron cyclotron, the electron plasma and the ion plasma frequencies respectively. In this situation the electrons are strongly magnetized while the ions are not. The beam width in the direction of propagation is chosen to be of the order of a few electron skin depths, c/ω_{pe}, where c is the velocity of light in vacuum. The beam pulse, which acts as a moving current source for the electromagnetic excitations and a moving charge density source for the electrostatic excitations, is considered to be rigid and free streaming with no loss in its energy as it propagates through the plasma. Its typical charge density is $\sim 1.15 n_0 e$ where n_0 is the equilibrium plasma density and e is the electronic charge. A rectangular area of $1500c/\omega_{pe} \times 100c/\omega_{pe}$) in the $x-y$ plane has been chosen for the simulations with $n_0 = 3.19 \times 10^{20}\text{cm}^{-3}$. The spatial resolution chosen in the simulation is 10 cells per electron skin depth (c/ω_{pe}) with 64 particles per cell for each species corresponding to a grid size of $\Delta x = 0.1c/\omega_{pe}$ and the temporal resolution is given by the time step $\Delta t = 0.0707\omega_{pe}^{-1}$. The cubic order interpolation schemes and sufficient number of particles per cell used in the simulations carried out in this work reduces the intrinsic noise to very very low level [19]. For our own simulations, the accuracy of our results has been verified by decreasing the time steps and grid sizes by factors of 10 and found no significant changes. Therefore, a tiny initial noise in the form of thermal velocities $v_{th_1} = 0.000\,442c$ and $v_{th_2} = 0.000\,0884c$ (corresponding to 0.1 eV for each species), is added to electrons and ions respectively to trigger excitations in our system. This is then supplemented by providing an actual temperature to the electrons, for the $B = 0$ case where one is looking for electrostatic ion acoustic excitations which require warm electrons and cold ions. The electron temperature is such that the ion acoustic sound speed in the medium is $0.1c$. For the electromagnetic case the electrons are once again assumed to be cold (i.e. at $v_{the} = v_{th1} = 0.000\,442c$) so that they remain magnetised in the presence of the background magnetic field. The boundary conditions for the electromagnetic fields and particles are

DISTRIBUTION A: Distribution approved for public release. Distribution unlimited

periodic in the $\hat{y}$ direction and absorbing in the $\hat{x}$ direction. The value of the magnetic field is taken to be $B_0 = 2.5 m_e e c \omega_{pe}/e$ where m_e is the electronic mass.

3. Results

3.1. Electrostatic precursors

Prior to investigating electromagnetic precursors we carried out a series of simulations in the absence of the background magnetic field ($B = 0$) in order to benchmark our code and to also examine the earlier fluid and molecular dynamic results of electrostatic precursors in the framework of a PIC simulation. As is well known [21, 22], a charged source traveling in a dielectric medium can excite various collective modes of the medium depending on its speed relative to the phase velocities of the modes. In the present case we therefore make the pulsed beam travel close to the ion acoustic speed in order to study the excitation of low frequency electrostatic waves. For undamped ion acoustic waves to exist in the plasma we need to have $T_e \gg T_i$. Accordingly, as discussed in the previous section we assign an appropriate temperature to the electrons and define the ion acoustic speed (in the absence of the beam) as $V_{cs} = \sqrt{\frac{k_B T_e}{m_i}} = v_{the}/\sqrt{m_i/m_e}$ where v_{the} is the electron thermal velocity and k_B is the Boltzmann constant. To test the earlier fluid results we examine two cases, namely when (i) $V_b < V_{cs}$ and (ii) $V_b > V_{cs}$ where V_b is the beam velocity. For our simulations we have chosen $V_{cs} = 0.1c$ and (i) $V_b = 0.06c$ and (ii)$V_b = 0.11c$ so that the two cases correspond to $M = 0.6$ and $M = 1.1$ respectively, where $M = V_b/V_{cs}$ is the Mach number. It may be noted that our definition of the Mach number is based on the definition of the ion acoustic speed in the unperturbed plasma and ignores any change in the sound speed due to the presence of the beam. In practice, as we show later, the measured phase velocities of the linear ion acoustic waves excited as wakes by the beam are in fact very close (upto a few percent) of the V_{cs} value used in our definition of the Mach number.

Figure 2 illustrates the simulation results for these two cases in the form of 2d snapshots of the electron density at $t = 353.5$ and $t = 700.0$. Superposed on the snapshots we have plotted the y averaged density values (line plots) as a function of x. From the figures it is evident that for $V_b < V_{cs}$ one only gets wake fields excited behind the source whereas for $V_b > V_{cs}$ a series of precursor pulses are generated ahead of the traveling source. These precursor pulses are formed in front of the source due to the rapid piling up of the density at the expense of a density depression behind the source. If the beam is moving at a subsonic speed then the accumulated mass at its front can disperse away at the linear phase velocity of the sound waves in that region. However if the beam moves supersonically then the accumulated mass cannot disperse away fast enough and it keeps growing leading to nonlinear steepening. When this steepening balances the dispersion it can lead to the formation of a soliton which can move at a speed faster than the speed of the beam and thereby move away from it. The pile up develops again leading to the formation of another soliton and thereby resulting in a series of solitons ahead. We have independently ascertained the solitonic nature of these pulses by checking the constancy of the product of their amplitudes with the square of their widths—a procedure that will be described in more details when we discuss the electromagnetic solitons. We have also examined the nature of the trailing wakes behind the charge bunch which according to the linear theory of wakes should consist of ion acoustic waves [21–23]. To verify this in our simulations we have obtained the frequency spectrum of these waves in the far-wake region and shown it in figure 3(a).

The wavelength of these structures is estimated from the distance between the oscillation peaks and then the phase speed is estimated as ω/k. For an additional confirmation we have also directly obtained the phase velocity of the waves from the simulation data by measuring the distance traveled by a wave peak over a prescribed time period. This is shown in figure 3(b) and the measured phase speed comes out to be $0.0925c$ which differs from the theoretical ion sound speed value (in the absence of the beam) of $0.1c$ by about 7.5%.

Figure 4 shows the plots of the electric fields in the x and y directions. The extremely weak values of the electromagnetic component E_y compared to E_x further establishes the electrostatic nature of these excitations. Our electrostatic PIC simulation results are thus in accord with the earlier fluid and MD simulation results and not only serve as a good benchmark of our code but also provide a first principles confirmation of this phenomenon at a particulate level.

3.2. Electromagnetic precursors

We now discuss our simulation results carried out in the presence of an ambient magnetic field with the short pulse beam source traveling perpendicular to the field (as shown schematically in figure 1). For this case we take the both electrons and ions to be cold i.e. at a noise level with thermal velocities

DISTRIBUTION A: Distribution approved for public release. Distribution unlimited

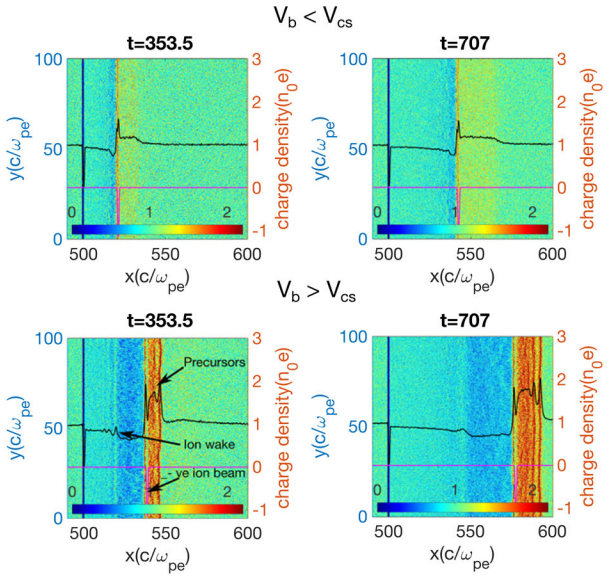


Figure 2. Two dimensional snap shots of the electron density at $t = 353.5$ and $t = 707$ for subsonic ($V_b < V_{cs}$) and super-sonic ($V_b > V_{cs}$) propagation velocities of the beam. The line plots superposed on the snapshots are the y averaged density values providing a one dimensional profile of the perturbations as a function of x.

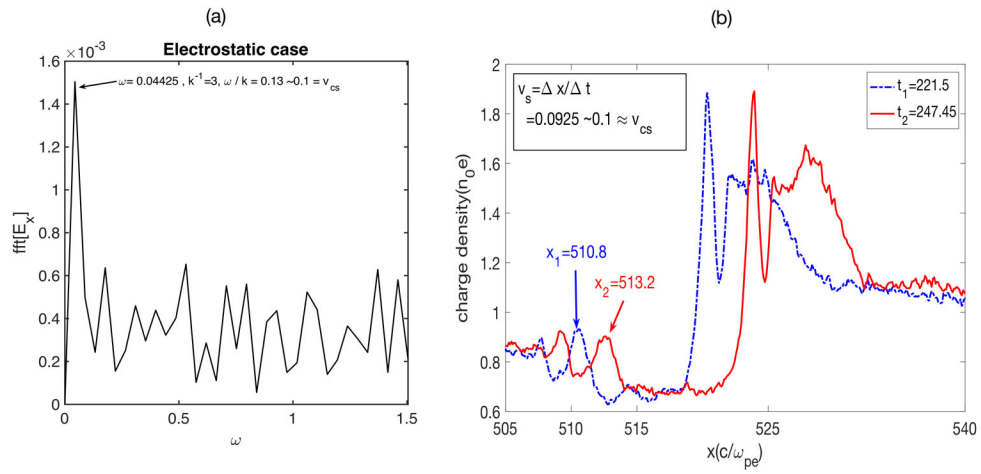


Figure 3. Spectrum analysis of far wake region for electrostatic case.

$v_{th_1} = 0.000\,442c$ and $v_{th_2} = 0.000\,0884c$ for electrons and ions respectively, corresponding to a temperature of $0.1ev$. We discuss two cases, namely, (i) $V_b < V_{ms}$ and (ii) $V_b > V_{ms}$, where V_{ms} is the phase velocity of linear magneto-sonic waves and which for our cold plasma case is close to the Alfven velocity $V_A = (m_e/m_i)^{1/2}\omega_{ce}/\omega_{pe} = 0.5c$ for our choice of parameters. For our simulations we have chosen (i) $V_b = 0.3c$ and (ii) $V_b = 0.505$ so that the two cases correspond to $M = 0.6$ and $M = 1.01$ respectively. Here $M = V_b/V_{ms}$ is the Mach number. Figure 5 illustrates the simulation results for these two cases where we have again superposed the y averaged density values as line plots on the 2d density snapshots.

Figure 6 displays the electric field components of the wake-fields and precursors. Unlike the electrostatic case we now find that the excitations have both an E_x as well as an E_y component thereby establishing their electromagnetic nature. These are in fact nonlinear magneto-sonic waves of the fast kind with the precursors taking the form of magneto-sonic solitons. In the present case the solitons are found to propagate with a Mach speed of around $M = 1.13$ with the taller solitons moving faster than the smaller amplitude ones. In fact their peaks lie on an ascending straight line as shown in figure 6 which is a characteristic of soliton solutions of the Korteweg de Vries (KdV) equation [24]. Another signature of a KdV type soliton is the constancy of the product of its amplitude (a) with the square of their width (L). To

DISTRIBUTION A: Distribution approved for public release. Distribution unlimited

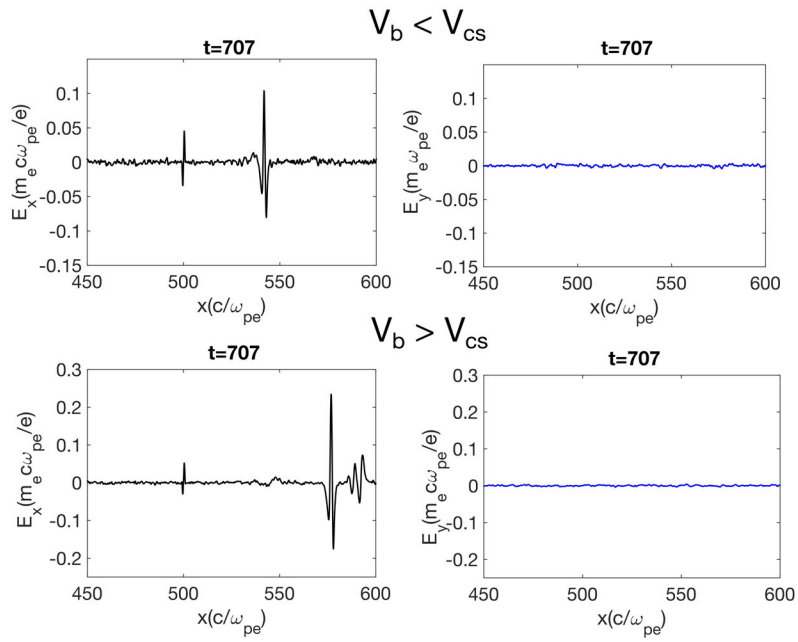


Figure 4. Plots of the electric fields in the x and y directions for the $V_b < V_{cs}$ and $V_b > V_{cs}$ cases.

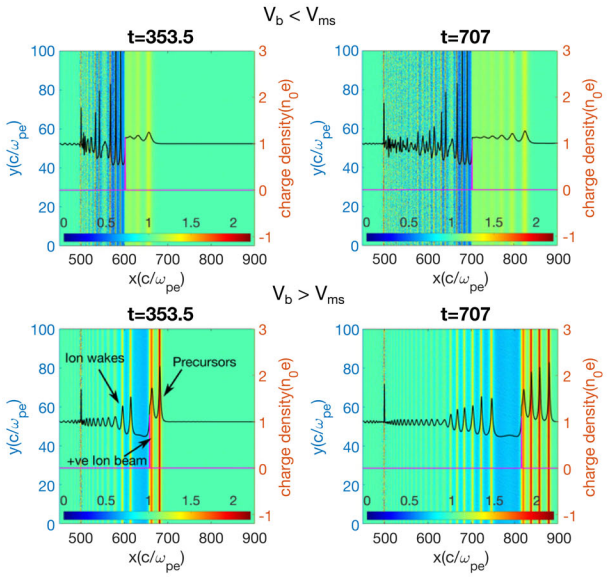


Figure 5. Two dimensional snap shots of the electron density at $t = 353.5$ and $t = 707$ for ($V_b < V_{ms}$) and ($V_b > V_{ms}$) propagation velocities of the beam. The line plots superposed on the snapshots are the y averaged density values providing a one dimensional profile of the perturbations as a function of x.

further establish the solitonic nature of the precursors we have measured the amplitudes and widths of a number of them and checked the constancy of aL^2. Our findings are given in table 1.

As can be seen from the table, the parameter aL^2 changes very little in simulations and essentially remains constant for the observed precursor magnetosonic KdV solitons A, B and C of figure 6. The percentage variation in a is 24% and 22% for L^2 but aL^2 varies only by 4.3% in the data shown above.

We also notice from figure 5 that precursors are generated even when $V_b < V_{ms}$ but they are considerably weaker than the $V_b > V_{ms}$ case. This is distinctly different from the electrostatic case where for $V_b < V_{cs}$ no precursors were generated at all and therefore is suggestive of a fundamental difference in the excitation mechanism of the two kinds of solitons. Electrostatic solitons are born in front of the source pulse due to a rapid pile up of the density when its velocity exceeds the phase velocity of the ion acoustic

DISTRIBUTION A: Distribution approved for public release. Distribution unlimited

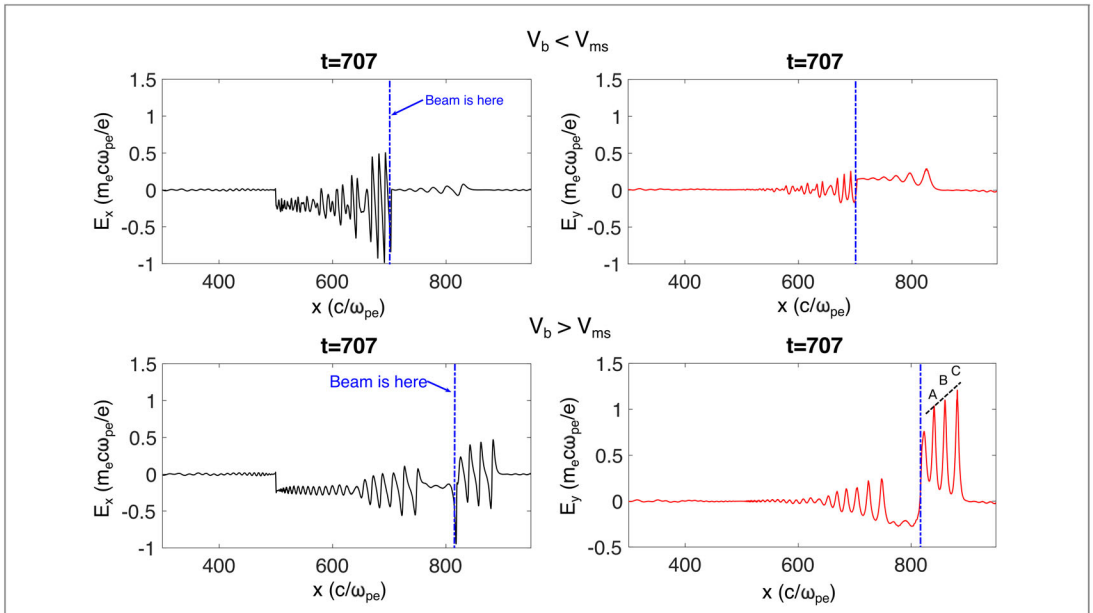


Figure 6. Plots of E_x and E_y for the $V_b < V_{ms}$ and $V_b > V_{ms}$ cases.

Table 1. Constancy of aL^2 for the precursor solitons A, B, and C of figure 6.

Soliton	$t(\omega_{pe}^{-1})$	$a(\delta n_i/n_0)$	$L(c/\omega_{pe})$	aL^2
A	700	0.5325	4.1	8.95
B	700	0.5865	3.9	8.92
C	700	0.6605	3.6	8.56

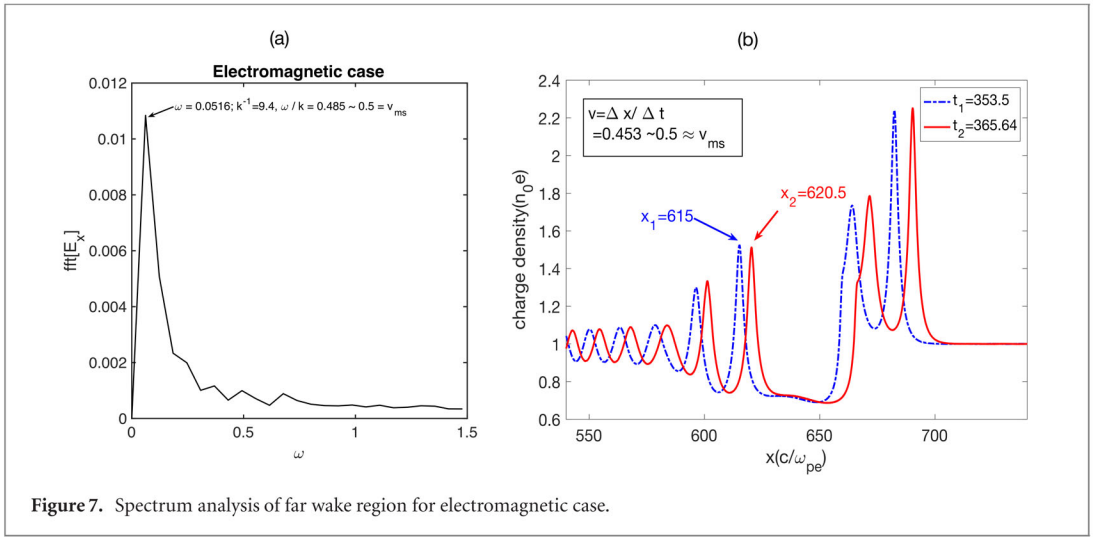


Figure 7. Spectrum analysis of far wake region for electromagnetic case.

wave. The electromagnetic solitons on the other hand are primarily created in the wake region when the wake fields become nonlinear and can then overtake the source pulse due to their faster velocity when $V_b < V_{ms}$. As in the electrostatic case, we have also analyzed the nature of the wakes for the magnetized plasma case, particularly in the far wake region where the waves are expected to be linear. As before we have looked at the frequency spectrum as well as the phase velocity of the waves as measured from the simulation data. The results are shown in figure 7(a) and figure 7(b) which show them to be magneto-sonic waves.

Magneto-sonic solitons have been studied in the past both analytically (using the KdV and its variants) [25–27] as well as in various numerical simulation studies [28, 29]. Most recently they have been observed in PIC simulations in the wake region of an intense laser pulse passing through a plasma [30]. However, we

DISTRIBUTION A: Distribution approved for public release. Distribution unlimited

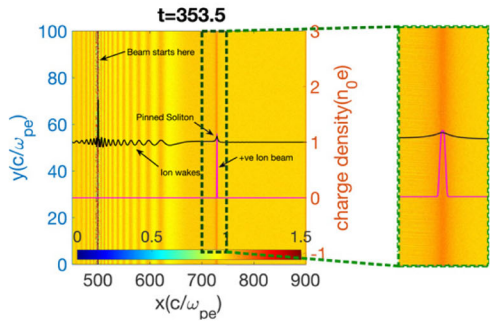


Figure 8. The excitation of a pinned soliton when the beam travels at $V_b = 0.85$ corresponding to $M = 1.7$. The inset shows a magnified view of the structure of the soliton that envelops the source and travels at the same speed as the source.

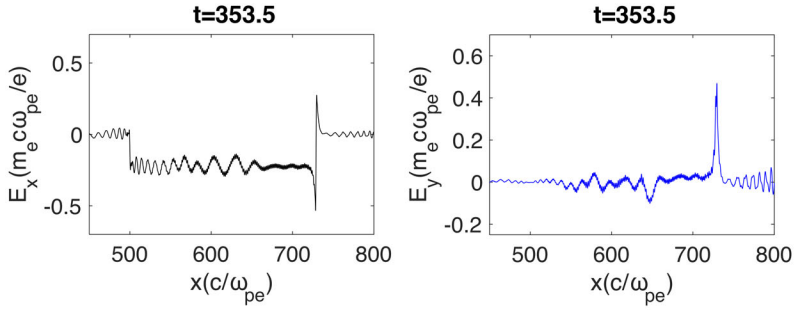


Figure 9. Plots for E_x and E_y for Pinned soliton case where beam is moving with $0.85c$ ($M = 1.7$). It is evident from the figure that the pinned solitons are also electromagnetic, magnetosonic solitons.

believe they have never been studied or seen in the context of precursor pulses and our present results are the first to establish their existence ahead of a charged source traveling in a magnetized plasma.

3.3. Pinned solitons

As discussed in the previous section, the precursor magneto-sonic solitons are of the KdV type and propagate with velocities that have $M > 1$. In our case when the beam velocity was $M = 1.01$ the precursor soliton speed was found to be $M = 1.13$. What happens if we increase the beam speed to higher Mach numbers? To explore this question we have carried out simulations at $M = 1.7$ and the results are shown in figure 8. One notices that there are no precursor solitons ahead of the moving source but an envelope structure develops around the source which travels at the same speed as the source. Such a structure known as a 'pinned' soliton has been predicted theoretically for a driven KdV equation [31, 32] but has not been captured in any PIC simulation studies. The structure is a few electron skin depths wide and has the characteristic bell shape form of a soliton. The longitudinal and transverse electric fields associated with the pinned soliton are shown in figure 9 establishing once more that these are electromagnetic structures.

4. Two dimensional sources

Our simulation results, presented in the preceding sections, were based on a simplification of the source term by assuming it to be of a one dimensional nature. This helped us to establish in principle the existence of the precursor and pinned solitons and to appropriately compare them to past fluid simulation results. However in an actual physical situation the moving charged object will be of a three dimensional nature and the size and shape of the object will likely influence the nature of the excitations. While a detailed study based on 3d-3V simulations is presently in progress and will be reported by us later, we present here a preliminary result obtained with a two dimensional circular source term that illustrates such an effect. Figure 10 shows a typical snapshot of the electron density for a circular source (of radius $r = 2c/\omega_{pe}$) moving at $M = 1.01$ across the magnetic field in the plasma. The basic results remain the same, namely, the excitation of wake structures in the downstream region and precursor pulses in the upstream region. The only noticeable difference from the 1d simulation is in the shape of the wakes and precursors which are now

DISTRIBUTION A: Distribution approved for public release. Distribution unlimited

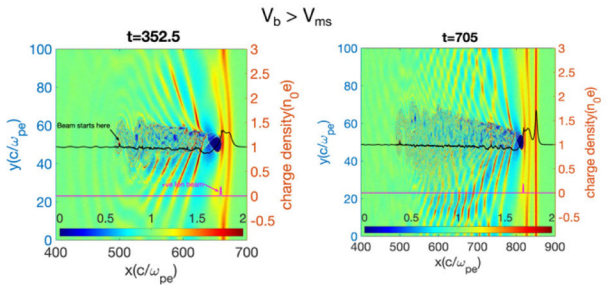


Figure 10. Typical snapshots of the electron density for a circular charged source moving at a Mach speed of 1.01 in the magnetized plasma.

curved in nature. This means that the presence of the wakes and precursors will not be uniformly felt in the y direction due to the curvature effect.

5. Discussion

To summarize, we have carried out detailed PIC simulations to study the phenomenon of precursor excitations of nonlinear pulses ahead of a charged source moving in a plasma. Our particular focus has been on the emission of electromagnetic pulses which have hitherto not been studied in this context. Our simulations establish for the first time the existence of such precursors in the form of magneto-sonic solitons that can either travel faster than the source or appear as stationary structures pinned to the source. Pinned solitons appear when the source speed is at a Mach number that is higher than about 1.6. As a benchmark exercise we have also confirmed the existence of electrostatic precursors in the form of ion acoustic solitons when the simulations were done in the absence of a magnetic field. These electrostatic results agree well with previously obtained fluid and molecular dynamic simulations. A comparison between the electrostatic and electromagnetic precursors reveals some interesting differences. The electrostatic wake fields are quite weak for low Mach numbers in comparison to those for the electromagnetic runs. Also while electrostatic precursors in the form of ion acoustic solitons occur only when the beam speed is supersonic ($V_b > V_{cs}$) the (electromagnetic) magnetosonic solitons appear even when $V_b < V_{ms}$. The difference can be traced to the basic mechanism for the creation of the solitons. The ion acoustic solitons arise from the pile up of the density in front of the charged source due to a balance between the nonlinear steepening and thermal broadening effects. Once formed they detach from the source and move away as their speed is faster than the source. The electromagnetic solitons on the other hand are not dependent on the density pile up and are created from the large amplitude wake fields that arise in the downstream region. If the source is moving at a sub-magnetosonic speed then the solitons can easily overtake the source and move ahead of it. The wake field excitations get larger as the source speed approaches or slightly exceeds the magnetosonic speed and the resultant solitons then acquire a higher speed and again move ahead of the source. If the source speed exceeds a certain limit (in this case $M = 1.6$) then one does not get any precursors but the soliton generated from the wake sticks to the source as a pinned soliton. Our simulations also reveal that the strength of the electromagnetic wake fields not only depends on the Mach number but also on the sign of the electrical charge of the source. Thus a positive ion beam source creates larger and sharper wakes than a corresponding negative ion beam of the same strength. Correspondingly the precursors created by the positive ion beam are sharper and larger in magnitude. These and other features of the wakes associated with the characteristics of the beam are currently under further investigation. Furthermore, the above studies have been carried out assuming an unrealistic mass ratio of ions to electrons $m_i/m_e = 25$. This has been done primarily to reduce the computation time. However we believe that increasing the mass ratio to a realistic value will not change the fundamental nature of our findings but might require a stronger impulse (by increasing the amount of charge and/or size of the charge bunch) in order to sufficiently disturb the ions for excitation of wakes and precursors.

We now briefly discuss the possible natural occurrences of such solitons and also their potential practical applications. Flowing plasmas interacting with obstacles or charged objects moving through a plasma are common occurrences in nature. The most common example is the streaming solar wind plasma impinging on the Earth and giving rise to the magnetosphere and a host of wave activity. From the perspective of our present simulations one could view the Earth as moving through the solar wind in the latter's frame of reference. The solar wind has components that can be supersonic or even super-Alfvenic. One can thus

DISTRIBUTION A: Distribution approved for public release. Distribution unlimited

expect precursor pulses to be generated in the vicinity of the Earth's bow shock and travel in the upstream (sun ward) direction. There have indeed been several satellite observations of upstream waves that range in frequency from mHz to tens of kHz [33] and comprise of both electrostatic and electromagnetic disturbances. Some of these structures have also been identified with electrostatic solitons and occasionally with electromagnetic solitons that correspond to magnetic holes or magnetosonic solitons. Our simulation results provide a new paradigm for the interpretation of these wave structures by appropriately correlating them with the solar wind flow dynamics in these regions. It should be mentioned here that although our simulations have been done for an idealized 'charged object' which does not change its mass or charge as it travels through the plasma—factors that would influence a real object—our fundamental findings could still be realistically applied in many practical situations. For example, objects like artificial satellites and space debris that become naturally charged through interactions with the ionospheric plasma and other processes, possess so much kinetic energy and the collision mean free path in the ionosphere is so long that they do not suffer much energy change. The charge fluctuations due to interaction with the plasma are also of the order of a few percent of the ambient charge and can be neglected. Such objects can therefore give rise to precursors as they travel. Such precursors traveling ahead of the objects can be detected from the ground using radar scattering for example, and could prove useful in tracking dangerous objects like small scale space debris that can damage live satellites [13]. Electromagnetic solitons would be particularly useful in this regard as their spatial extent of a few electron skin depths would have a large footprint in the ionosphere and therefore be easy to remotely detect.

Acknowledgments

AS is thankful to the Indian National Science Academy (INSA) for their support under the INSA Senior Scientist Fellowship scheme and to AOARD for their research grant FA2386-18-1-4022. The authors would like to acknowledge the OSIRIS Consortium, consisting of UCLA and IST (Lisbon, Portugal) for providing access to the OSIRIS4.0 framework which is the work supported by NSF ACI-1339893. The simulations for the work described in this paper were performed on Uday, an IPR Linux cluster.

ORCID iDs

Atul Kumar https://orcid.org/0000-0002-7747-5210
Abhijit Sen https://orcid.org/0000-0001-9878-4330

References

[1] Sommerfeld A 1914 Über die Fortpflanzung des Lichtes in disperdierenden Medien *Ann. Phys.* **44** 177–202
[2] Brillouin L 1914 Über die Fortpflanzung des Licht in disperdierenden Medien *Ann. Phys.* **44** 204–40
[3] Brillouin L 1960 *Wave Propagation and Group Velocity* (New York: Academic)
[4] Choi S-H and Österberg U 2004 Observation of optical precursors in water *Phys. Rev. Lett.* **92** 193903
[5] Albanese R, Penn J and Medina R 1989 Short-rise-time microwave pulse propagation through dispersive biological media *J. Opt. Soc. Am.* A **6** 1441–6
[6] Jeong H, Andrew M, Dawes C and Gauthier D J 2006 Direct observation of optical precursors in a region of anomalous dispersion *Phys. Rev. Lett.* **96** 143901
[7] Peter P and Palócz I 1969 Experimental observation of sommerfeld and brillouin precursors in the microwave domain *Phys. Rev. Lett.* **22** 1201–4
[8] Buckley R and Sammut C A P 1979 Wave packets in dispersive media: an approximation encompassing both main signal and precursors *J. Plasma Phys.* **22** 563–70
[9] Cartwright N and Oughstun K E 2009 Ultrawideband pulse propagation through a homogeneous, isotropic, lossy plasma *Radio Sci.* **44**
[10] Ertekin R C, Webster W C and Wehausen J V 1984 Ship-generated solitons *Proc. 15th Symp. Naval Hydrodyn. Hamburg* pp 347–61
[11] Akylas T R 1984 On the excitation of long nonlinear water waves by a moving pressure distribution *J. Fluid Mech.* **141** 455–66
[12] Lee S-J, Yates G T and Yaotsu Wu T 1989 Experiments and analyses of upstream-advancing solitary waves generated by moving disturbances *J. Fluid Mech.* **199** 569–93
[13] Sen A, Tiwari S, Mishra S and Kaw P 2015 Nonlinear wave excitations by orbiting charged space debris objects *Adv. Space Res.* **56** 429–35
[14] Tiwari S K and Sen A 2016 Wakes and precursor soliton excitations by a moving charged object in a plasma *Phys. Plasmas* **23** 022301
[15] Tiwari S K and Sen A 2016 Fore-wake excitations from moving charged objects in a complex plasma *Phys. Plasmas* **23** 100705
[16] Jaiswal S, Bandyopadhyay P and Sen A 2016 Experimental observation of precursor solitons in a flowing complex plasma *Phys. Rev.* E **93** 041201(R)

DISTRIBUTION A: Distribution approved for public release. Distribution unlimited

[17] Arora G, Bandyopadhyay P, Hariprasad M G and Sen A 2019 Effect of size and shape of a moving charged object on the propagation characteristics of precursor solitons *Phys. Plasmas* **26** 093701
[18] Hemker R G 2000 Particle-in-cell modeling of plasma-based accelerators in two and three dimensions *Ph.D. Thesis* University of California, Los Angeles
[19] Fonseca R A *et al* 2002 *OSIRIS: A Three-Dimensional, Fully Relativistic Particle in Cell Code for Modeling Plasma Based Accelerators* (Berlin: Springer) pp 342–51
[20] Fonseca R A, Martins S F, Silva L O, Tonge J W, Tsung F S and Mori W B 2008 One-to-one direct modeling of experiments and astrophysical scenarios: pushing the envelope on kinetic plasma simulations *Plasma Phys. Control. Fusion* **50** 124034
[21] Sanmartin J R and Lam S H 1971 Far-wake structure in rarefield plasma flows past charged bodies *Phys. Fluid.* **14** 62–71
[22] Chen L, Landon A B and Lieberman M A 1973 Shielding of moving test particles in warm, isotropic plasma *J. Plasma Phys.* **9** 311–24
[23] Lampe M, Joyce G, Ganguli G and Gavrishchaka V 2000 Interactions between dust grains in a dusty plasma *Phys. Plasmas* **7** 3851–61
[24] Zabusky N J and Kruskal M D 1965 Interaction of 'solitons' in a collisionless plasma and the recurrence of initial states *Phys. Rev. Lett.* **15** 240–3
[25] Gardner C S and Morikawa G K 1965 The effect of temperature on the width of a small-amplitude, solitary wave in a collision-free plasma *Commun. Pure Appl. Math.* **18** 35–49
[26] Kever H and Morikawa G K 1969 Korteweg-de Vries equation for nonlinear hydromagnetic waves in a warm collision-free plasma *Phys. Fluid.* **12** 2090–3
[27] Tidman D A and Krall N A 1971 *Shock Waves in Collisionless Plasmas* (New York: Wiley) pp 29–54
[28] Ogino T and Takeda S 1975 Computer simulation for the fast magnetosonic solitons *J. Phys. Soc. Jpn.* **38** 568–75
[29] Gueroult R, Fruchtman A and Fisch N J 2018 Cumulative displacement induced by a magnetosonic soliton bouncing in a bounded plasma slab *Phys. Plasmas* **25** 062118
[30] Kumar A, Shukla C, Verma D, Das A and Kaw P 2019 Excitation of KdV magnetosonic solitons in plasma in the presence of an external magnetic field *Plasma Phys. Control. Fusion* **61** 065009
[31] Wu T Y 1987 Generation of upstream advancing solitons by moving disturbances *J. Fluid Mech.* **184** 75–99
[32] Zhao J-X and Guo B-L 2009 Analytic solutions to forced KdV equation *Commun. Theor. Phys.* **52** 279–83
[33] Burgess D 1997 What do we really know about upstream waves? *Adv. Space Res.* **20** 673–82

DISTRIBUTION A: Distribution approved for public release. Distribution unlimited

Signatures of an energetic charged body moving in a plasma ‡

Vikram Dharodi[1], Atul Kumar[2] and Abhijit Sen[1]

[1]Institute for Plasma Research, HBNI, Bhat, Gandhinagar - 382428, India
[2]Oak Ridge National Laboratory, Oak Ridge, TN 37831, United States of America

E-mail: vikram.ipr@gmail.com

Abstract. A charged body moving in a plasma can excite a variety of linear and nonlinear waves in the form of trailing wakes, fore-wake shocks and precursor solitons. These structures can further interact with the background plasma to create secondary effects that can serve as signatures of the passage of the charged body. Using particle-in-cell simulations we investigate in detail the dynamics of a plasma system that is being traversed by an energetic positively charged body. Using two different shapes of this charged source, namely, an idealized one dimensional line source and a two dimensional thin rectangular source we examine the differences in the nature of the excited wave structures and their consequent impact on the background plasma. Our simulations reveal interesting features such as the dependence of the precursor speeds on the total charge on the driving source, local particle trapping, and energization of the trapped ions in various regions along the traversal path leading to the formation of energetic ion beam-lets. The collective excitations and the signatures in the ambient plasma could prove useful in practical applications such as in analysing the trajectories of charged objects like space debris orbiting in the ionosphere.

1. Introduction

One of the well known phenomenon associated with the passage of an object in a neutral fluid is the excitation of trailing waves, more popularly known as wakes or wake fields, behind the object. In a plasma, such wake fields in the form of plasma waves can arise when a charged source or an intense laser pulse travels through it. Plasma wake fields have been intensely studied in recent times because of their potential application as a means of accelerating charged particles. An electron or an ion injected in such a structure and moving with the same speed as the wake experiences a nearly DC electric

‡ This manuscript has been authored by UT-Battelle, LLC, under contract DE-AC05-00OR22725 with the US Department of Energy (DOE). The US government retains and the publisher, by accepting the article for publication, acknowledges that the US government retains a nonexclusive, paid-up, irrevocable, worldwide license to publish or reproduce the published form of this manuscript, or allow others to do so, for US government purposes. DOE will provide public access to these results of federally sponsored research in accordance with the DOE Public Access Plan (http://energy.gov/downloads/doe-public-access-plan).

DISTRIBUTION A: Distribution approved for public release. Distribution unlimited

field and thereby gains energy from it.[1,2] Since a plasma can sustain large electric fields, these wake fields can accelerate particles to very high energies and the wake field based accelerator scheme has made spectacular progress over the past several years.[3–6]

Apart from these wake fields which trail a moving charged source, it is also possible to excite nonlinear wave structures in the fore-wake region i.e. ahead of the source. Such a phenomenon, well known in hydrodynamics, has not received much attention in plasma physics, except in very recent years.[7–10] It has been shown that when a charged source moves in an unmagnetized plasma at a speed greater than the ion acoustic speed, a train of nonlinear structures in the form of precursor solitons can arise ahead of the traveling source and move away from it at a faster speed.[7] This nonlinear phenomenon is best understood in terms of a fluid picture. As the object moves through the fluid it causes an accumulation of matter in front of it causing a rise in the density. Since the object is moving at a supersonic speed the density perturbations ahead of it cannot linearly disperse because the linear sound velocity is less than the speed of the object. As the density continues to build up in the front, nonlinear effects set in. When the nonlinear steepening is balanced by the dispersive broadening a soliton can be formed whose velocity is supersonic and can be much faster than the moving object. Hence it moves away from the object. The process is repeated after some time leading to a chain of solitons. The existence of such precursor solitons in a plasma has been experimentally confirmed in controlled experiments carried out in a dusty plasma device with the dust fluid made to flow over a charged obstacle at a speed faster than the dust acoustic speed.[9] In principle, such excitations can arise in a magnetized plasma as well in the form of magnetosonic or Alfvenic solitons. A proof of principle evidence of the existence of such electromagnetic precursor solitons was provided in an earlier publication[11] using particle-in-cell [PIC] simulations. It was shown that a rigid charged particle source, in the form of a nearly one dimensional line source could excite these solitons when its velocity exceeded the magneto-sonic speed. The simulations also confirmed the existence of electrostatic solitons, by turning off the ambient magnetic field and moving the source at a speed faster than the ion acoustic speed. The focus of the earlier study was on delineating the conditions for the excitation of the ion acoustic and magnetosonic precursors in an unmagnetized and magnetized plasma set-up, respectively. The precursors were also identified as solitons from their propagation characteristics. The topic of the subsequent interaction of these wave structures with the ambient plasma was not addressed nor was the dependence of the wave properties on the nature of the charged source explored. Our present study is devoted to an investigation of these questions. We investigate in greater detail the nature of the excited structures using a 2d simulation and investigate the influence of the source size and strength on the precursors. This is done by comparing the results of propagating a thin rectangular shaped source with different transverse extents with those obtained for an idealized one dimensional source. An important difference is found in the propagation characteristics of the two dimensional precursors compared to the one dimensional ones. While the one dimensional precursors (solitons)

DISTRIBUTION A: Distribution approved for public release. Distribution unlimited

maintain a constant amplitude and width during the course of their propagation, the amplitudes of the two dimensional ones decrease with distance while their widths keep increasing. In both cases the product of their amplitude with the square of the width remains constant. We also look at the subsequent interactions of the excited waves with the background plasma in various regions along the path of the charged source. These include the wake region, the density depleted region just behind the moving source and the region ahead of the source where precursor solitary structures propagate. For this we carry out a detailed study of the temporal evolution of the particle density and energy density in various regions as well as some individual particle kinetics in special regions. For simplicity we restrict ourselves to excitations created by a positively charged source propagating in an unmagnetized plasma.

Our simulations also show some other interesting differences for the two cases both in the characteristics of the wave structures and their subsequent interaction with the plasma particles. The finite size of the source is seen to introduce a magnetic field component in the excited structures. The propagation speed of the precursors is found to have a direct dependence on the strength of the charge in the source. We also observe significant self-injection of ions in the ion-depleted region immediately behind the charged source. These ions experience energization and focusing effects leading to the formation of beam like structures. Ions are also seen to be trapped between precursor structures and to get energized due to multiple bounces off these structures. The trajectories of these particles are analysed using particle tagging techniques. The implications and potential applications of these secondary signatures created by the passage of an energetic charged body in the plasma are discussed.

The paper is organized as follows. In section 2 we briefly describe the physical model used for our simulations and also give the essential computational details. Our main results are presented in section 3 with separate subsections devoted to energization due to collective excitations arising from an idealized thin line source (3.1) and a two dimensional thin rectangular source (3.2). Section 4 gives a summary of our results and discusses their possible occurrences in nature as well as their potential applications.

2. Simulation model and details

We have carried out 2d-3V particle-in-cell simulations using the OSIRIS-4.0 code[12–14] for a quasi-neutral plasma system where the ions are taken to be cold such that the ion thermal velocity $v_{thi} = 8.85\times10^{-5}c$, while the electrons are warm with a thermal velocity $v_{the} = 0.5c$. At this electron temperature the ion acoustic sound speed in the medium is[11] $V_{cs} = 0.1c$ ($V_{cs} = \sqrt{k_B T_e/m_i} = v_{the}/\sqrt{m_i/m_e}$). For simplicity and shorter simulation times the ion to electron mass ratio m_i/m_e has been taken to be 25. This is not an uncommon practice in PIC simulations[15–17] and is acceptable provided it can be justified for a realistic scenario as will be done later in the paper. We consider a rectangular box of $L_x(= 1000\delta s) \times L_y(= 100\delta s)$ in the $x-y$ plane, where $\delta s(= c/\omega_{pe})$ is the skin-depth of the plasma. L_x and L_y are the system lengths in the x and y directions. The equilibrium

DISTRIBUTION A: Distribution approved for public release. Distribution unlimited

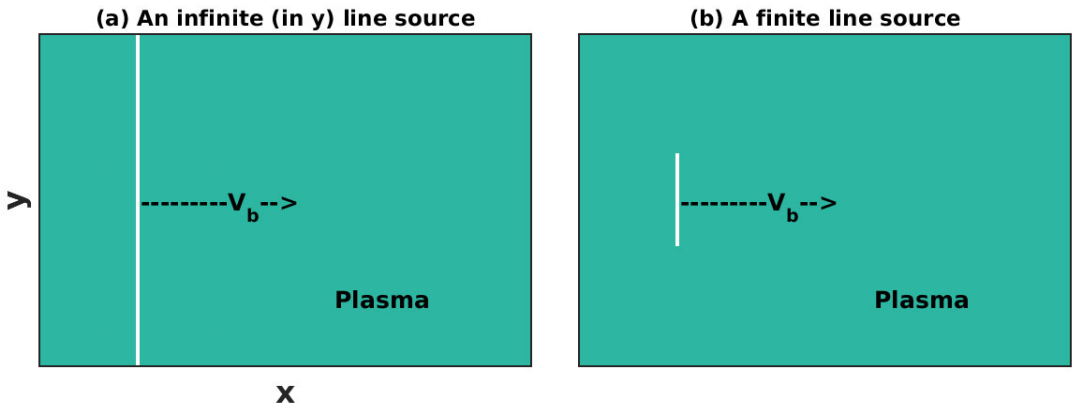


Figure 1. Schematic diagram (not to scale) of the simulation geometry showing two different shaped charge sources (a) an infinite (in y) thick line source and (b) a finite thin rectangular source. They move with speed V_b in the positive $\hat{x}$-direction.

plasma density is taken as $n_0 = 3.10 \times 10^{20} cm^{-3}$. The perturbed density is normalized by the equilibrium plasma density and the electric and magnetic fields are normalised by $m_e c\omega_{pe}/e$. The spatial resolution chosen in the simulation is 20 cells per electron skin depth with 10×10 particles per cell for each species corresponding to a grid size of $\Delta x = 0.05c/\omega_{pe}$ and the temporal resolution is given by the time step $\Delta t = 0.0283\omega_{pe}^{-1}$. In such a plasma system a positively charged thin (in the x direction) rigid body is made to travel in order to create linear and nonlinear wave excitations in the plasma. We consider two specific shapes of the charged body: (i) an infinite (in y) and finite thickness (in x) line source and (ii) a finite thin rectangular source. Schematic diagrams corresponding to these two cases are shown in Fig. 1(a) and Fig. 1(b), respectively. For all the simulation runs, the line source is initially positioned at $x = 500\delta s$. In most cases it is made to travel at $V_b = 0.11c$ that is a bit faster than the ion acoustic speed $V_{cs} = 0.1c$. The corresponding Mach number is $M = 1.1$ (where $M = V_b/V_{cs}$). As has been established in molecular dynamics[18] as well as PIC studies,[11] precursors happen when the Mach number is greater than one. The speed of the precursor is always faster than the source implying that as the Mach number increases the precursor speed also increases. Beyond a certain Mach number one obtains dispersive shock structures[18] or pinned solitons.[11] In our present study we do not consider the variation of the precursor propagation as a function of the Mach number but focus on the influence of the shape and size of the source. For simplicity we have considered a rigid charged source that retains its shape and amount of charge and also does not change its velocity while propagating through the plasma. Real life examples of such a model source can be found, for example, in the form of a charge body representing a space debris object orbiting in the ionosphere.

DISTRIBUTION A: Distribution approved for public release. Distribution unlimited

3. Simulation results and Observations

The prime objectives of this section are to numerically explore the evolution of wave structures generated using two types of positively charged sources shown in Fig. 1 and their consequent impact on the background plasma. Both types of sources have constant charge density $\rho^c_{bm} = 1.1$ and the same width $\delta x = 1.02$ (along $\hat{x}$ direction). The source length δy (along $\hat{y}$ direction) is the only parameter that is varied. All the simulations are performed with absorbing boundary conditions in the $\hat{x}$ direction and periodic in the $\hat{y}$ direction for both the particles and the fields.

3.1. Idealized one dimensional thin line source

We first discuss an infinite length source case, which develops only longitudinal perturbations in the background plasma. In our 2D simulation (where z is the ignored coordinate) our 1D line charge represents an ideally thin sheet (infinite in the $x - z$ plane) propagating in the x direction. Its projection in the $x - y$ plane is an infinite line. The choice of this source is to provide a benchmark for studying the effect of a finite size (in the y direction) and to also relate to early fluid and PIC simulations done for such a shaped source. We have then varied the aspect ratio (length in the y direction / width in the x direction) of the source to study its impact on the precursor excitations. By changing the orientation of the object by 90 degrees we could also make it a cylinder like object. Debris objects come in all shapes and sizes including large planar ones which are called HAMR[19,20] (high area to mass ratio) objects. Our present work is a representative study of the aspect ratio dependence of a typical source which can be extended in the future to explore other geometrical effects. Understanding this case allows us to determine the impacts of a finite length source. For example, it is of interest to know whether the speed of the perturbations is affected by the transverse dimension of the source and whether it can provide a means of controlling the speed. Figure 2 shows the late-time evolution of the ion charge density $\rho^c_i(x, y)$ due to the passage of an infinite line source (vertical white-solid line) through the plasma. The solid line plots (in black) superposed on these 2d density snapshots represent its one dimensional profile $\rho^c_i(x)$ as a function of x for the fixed value of $y = 50.03$. This traveling source generates a strong density inhomogeneity in the longitudinal direction. It is clearly seen that this inhomogeneity is the result of the creation of precursor waves ahead of the source (yellow-colored disturbances), the formation of a region with a depleted number of ions just behind the source (a dark-blue-coloured region) and wake structures following this depressed region (cyan-colored disturbances). Such structures were previously observed in the simulations reported by Kumar and Sen[11] for the case when the ambient magnetic field was taken to be zero. They were obtained to benchmark the code and to also establish connections with previous one dimensional electrostatic results obtained in fluid simulations. In the present paper we examine these structures in greater detail in order to characterize them and to also study their impact on the background plasma.

DISTRIBUTION A: Distribution approved for public release. Distribution unlimited

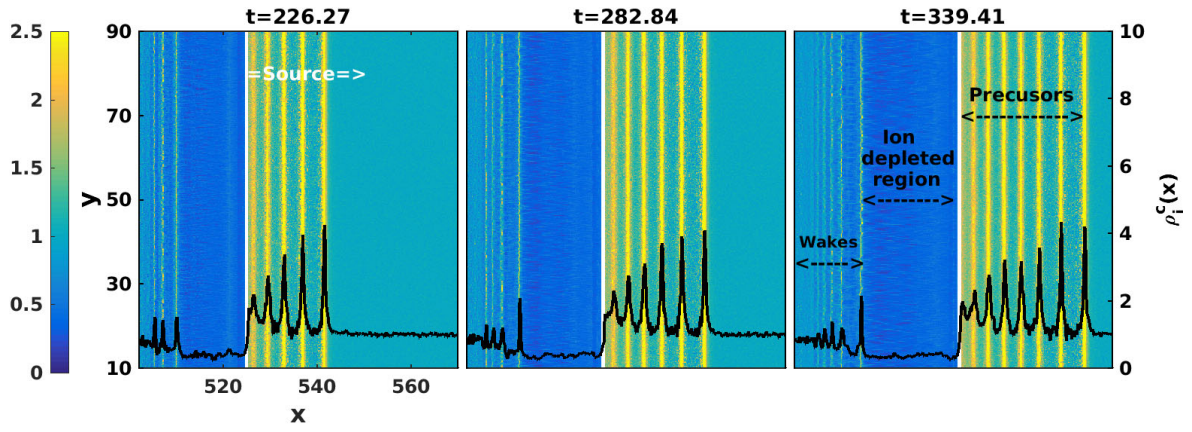


Figure 2. Time evolution of the ion charge density $\rho_i^c(x, y)$ due to passage of an infinite line source ($\delta x = 1.02, \delta y = L_y$). The source creates well developed trailing wake fields and precursor structures moving ahead of it. The line plots superposed on the snapshots are the profiles of the density $\rho_i^c(x)$ as a function of x for $y = 50.03$ (its scale is given on right y axis).

To establish the basic character of these structures we first look at the electric field components of these waves. In Fig. 3 we have superposed on the ion charge density colour plot, the longitudinal field component, $E_x(x)$, as a black-solid curve, and the transverse component, $E_y(x)$, as a red-dotted curve, at a time $t = 395.98$. For these components of the electric field, the right y-axis defines the scale. As can be seen from this figure, the transverse component is extremely weak compared to the longitudinal component indicating that the waves are primarily electrostatic in nature. Furthermore the density depleted region is nearly free of any electric field and the ion density is uniform in this region. $E_x(x)$ has sharp spikes at either edge of this region that is consistent with the creation of a region of density depression behind the moving source. A careful analysis of Fig. 3 tells us that the electrostatic force for ions in the density depleted region is acting in the forward direction and which can lead to acceleration of any self injected ions in the direction of the source propagation. We next look at the time evolution of the various structures described above and the changes in the background plasma as a result of their creation. This is best captured in Fig. (4) which shows the temporal evolution of the density and the kinetic energy as a function of x for a fixed value of $y = 50.03$. Since in this 1d simulation case there is uniformity in the y direction, this plot provides a comprehensive picture of the spatio-temporal evolution of wave excitations as well as the background density (Fig. 4(a)) and kinetic energy (Fig. 4(b)) of the system. From Fig. 4(a) we can clearly see that with time the source excites more and more precursor structures ahead of it which move faster than the source. These precursor structures with enhanced ion densities (yellow color) travel along x at a steady pace with a super sonic velocity of $0.2004c$. The velocity can be deduced from the straight line fit (magenta dotted slant line) of $x = 0.2004t + 496.07$

DISTRIBUTION A: Distribution approved for public release. Distribution unlimited

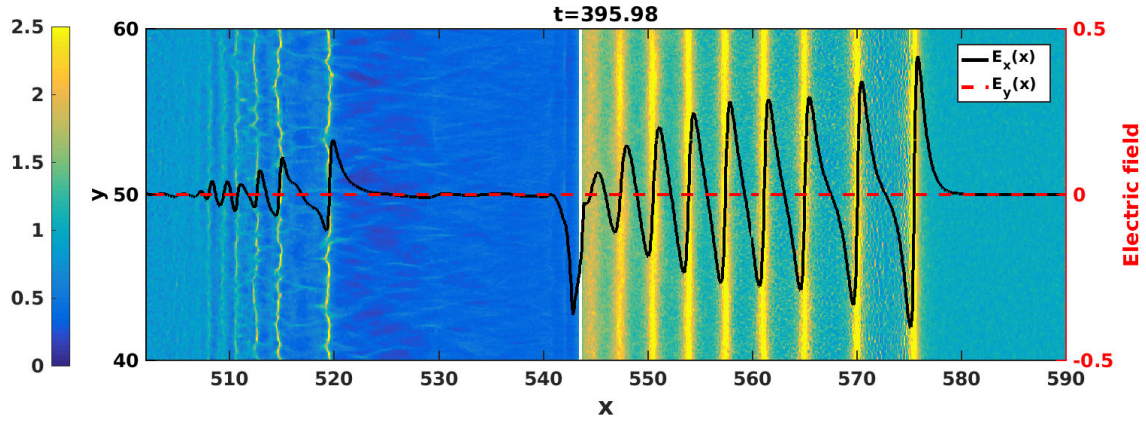


Figure 3. Spatial variation of electric field components (longitudinal electric field E_x and E_y, normalised to $m_e c\omega_{pe}/e$) with respect to x at a particular instant of time $t = 395.84$.

to the trajectory of the precursor. This is consistent with earlier fluid[7,8] and PIC simulations[11] which have identified these structures as precursor ion acoustic solitons. Fig. 4(a) also shows that with the passage of time the region of depressed density keeps on expanding. This can be understood from mass conservation arguments. Basically as the source generates more and more density enhanced structures (precursor solitons) ahead of it, mass is transferred from the region behind the source to enable this process and hence the depressed region grows in size. Trailing behind the depressed region are the wake structures. Unlike the precursor solitons these are dispersive structures whose amplitudes die down as a function of the distance behind the depressed region. Far away from the depressed region the amplitudes are quite small and the waves travel with the group velocity of the linear ion acoustic wave, namely,

$$C_g = \frac{\partial \omega}{\partial k} = \frac{C_s}{(1 + k^2\lambda_d^2)^{3/2}} \tag{1}$$

where k is the wave number and λ_d is the electron Debye length. For our simulation parameters, $\lambda_d \sim 0.5c/\omega_{pi}$. The wave number $k \sim 1.8\omega_{pi}/c$ so that $k\lambda_d \sim 0.9$. Using (1) this yields a group velocity of $\sim 0.4C_s$. The velocity of these linear wakes can be deduced from a straight line fit (white dotted slant line) to the green lines shown in the far left portion of Fig. 4(a) and the velocity is found to be $\sim 0.04c \sim 0.4C_s$. The lead portion of the wake, seen as a wave structure with a substantial amplitude, that remains attached to the rear end of the depressed region, travels somewhat faster than the linear wakes. A linear fit (red dotted slant line) to its trajectory yields a velocity of $0.0564c \sim 0.564C_s$. The enhanced velocity can be attributed to finite amplitude effects giving the lead wake structure a nonlinear character. Finally, in Fig 4(b), we look at the spatio-temporal evolution of the kinetic energy of the system as the source passes through it. The energy of the source and the precursors are predominantly due to their directed velocities. There is no significant heating of the background plasma in

DISTRIBUTION A: Distribution approved for public release. Distribution unlimited

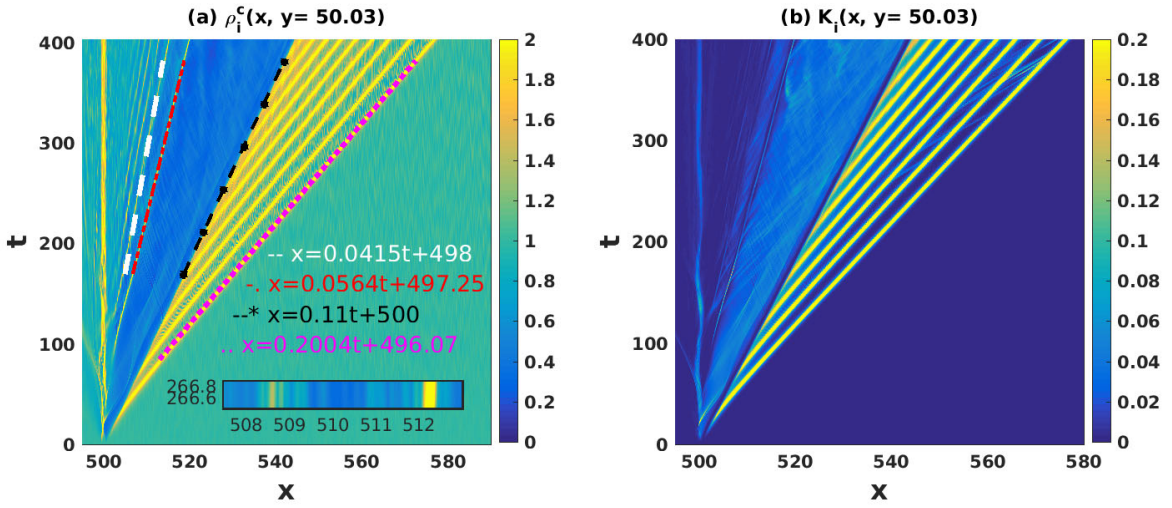


Figure 4. The temporal evolution of (a) the ion charge density and (b) the kinetic energy at $y = 50.03$

the fore-wake region. Some traces of weakly energetic ion beam-lets are seen in regions between some of the precursors which could be due to trapping and repeated bouncing of some ions between them. Such an effect becomes more pronounced in 2d simulations which will be discussed in the next section. We also note that the density depressed region shows evidence of background heating of the ions in that region. The weak wake structures do not impact the background energy in any noticeable manner.

3.2. A two dimensional thin rectangular source

We now turn to the case of a two dimensional thin rectangular source moving through the plasma as shown schematically in Fig. 1(b). In contrast to the one-dimensional case described in the previous section, the source now has a finite transverse dimension δy along the $\hat{y}$ direction. The finite transverse dimension has a profound influence on the nature of the induced excitations as well as on the interactions of these structures with the background plasma. A quick comparative overview of the influence of the transverse length on the nature of the wave excitations is shown in Fig. 5 where snapshots of the background ion charge density $\rho_i^c(x, y)$ are presented at $t = 282.84$ for simulations with $\delta y = 100, 50, 28, 20, 14$ and 8 respectively. All other parameters are kept the same for these runs. The vertical white line shows the location of the source. One of the first difference one notices is in the shapes of the precursors which now bend back at the tips to give rise to a crescent like structure. The bending becomes more pronounced as the transverse length of the source diminishes - a distinctly hydrodynamic phenomenon as the movement of the plasma flow around the source tries to attain a streamlined form. Note that this is different from a hydrodynamic bow wave that is normally formed around a ship's prow[21] or the plasma structure observed in PIC simulations, around an intense short laser pulse propagating in an underdense plasma.[22] These bow waves remain attached to the moving source quite unlike our precursor structures which separate from the source and move away from it at a faster speed. We also notice a slight decrease in the speed of the precursor with a reduction in the transverse size of the source. This can be discerned (as marked in Fig. 5) from the distances travelled

DISTRIBUTION A: Distribution approved for public release. Distribution unlimited

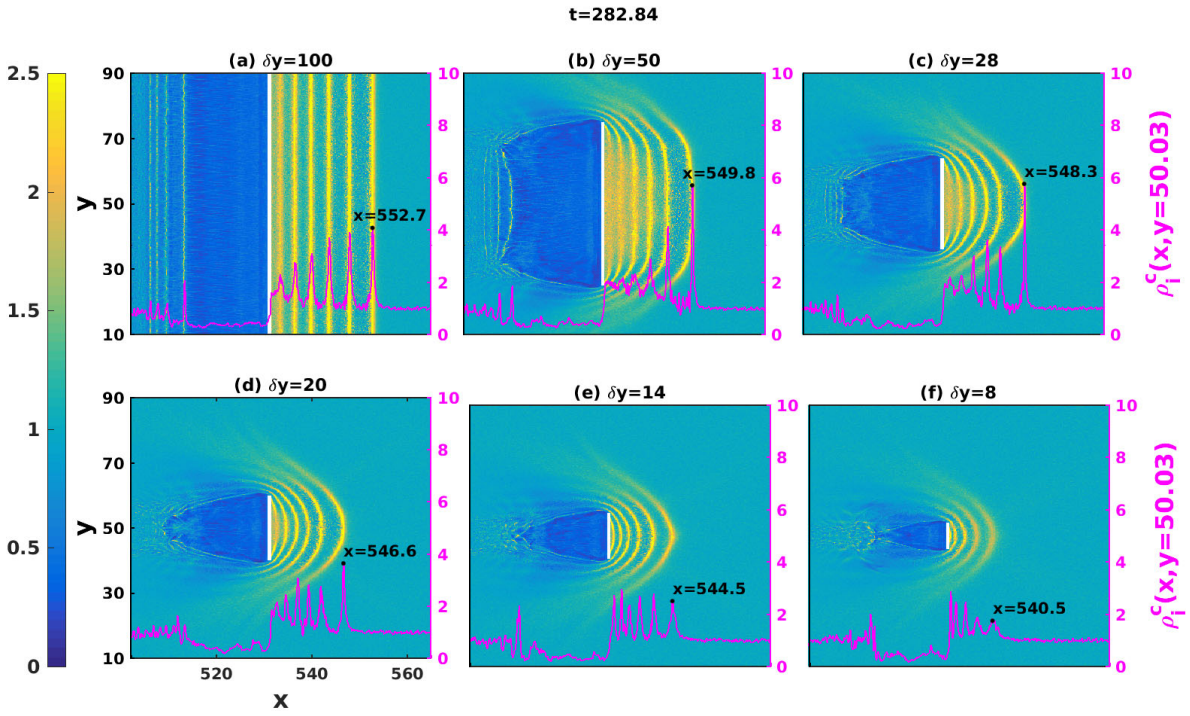


Figure 5. The snapshots of the background ion charge density $\rho_i^c(x, y)$ for charged sources of various transverse lengths $\delta y = 100, 50, 28, 20, 14$ and 8 at $t = 282.84$. The vertical white line shows the location of the source.

by the peaks of the leading precursors for the different cases within the same fixed period of time. The physical reason for this reduction in speed can be attributed to the decrease in the charge strength of the source as the transverse length decreases. The decrease in the strength of the source is also responsible for the fewer number of precursors generated for the $\delta y = 8$ case compared to the others and the decrease in the number of wakes. One also notices a reduction in the size of the ion depleted region - a geometric consequence of the decrease in the transverse source length. This "bubble" region (a terminology borrowed from the plasma wakefield acceleration literature) now displays both longitudinal and transverse inhomogeneity in density. We will now take a closer look at the $\delta y = 8$ case in order to discuss the propagation characteristics of the precursor and also the dynamics of the background particles in the various regions. In order to characterize the nature of their propagation an enlarged image of the $\delta y = 8$ case has been shown in Fig. 6 at t=339.41. In this figure the superposed line plots again give the density profiles of the precursors. As can be seen the amplitudes of the precursors diminish with distance while their widths keep increasing. The values of these quantities are given in Table I which shows that the product of their amplitudes a with the square of their widths L^2 remains constant. This is a characteristic property of a two dimensional soliton.[23–25] This is in contrast to 1d solitons which are known to keep their amplitudes and widths constant during the course of their propagation.

DISTRIBUTION A: Distribution approved for public release. Distribution unlimited

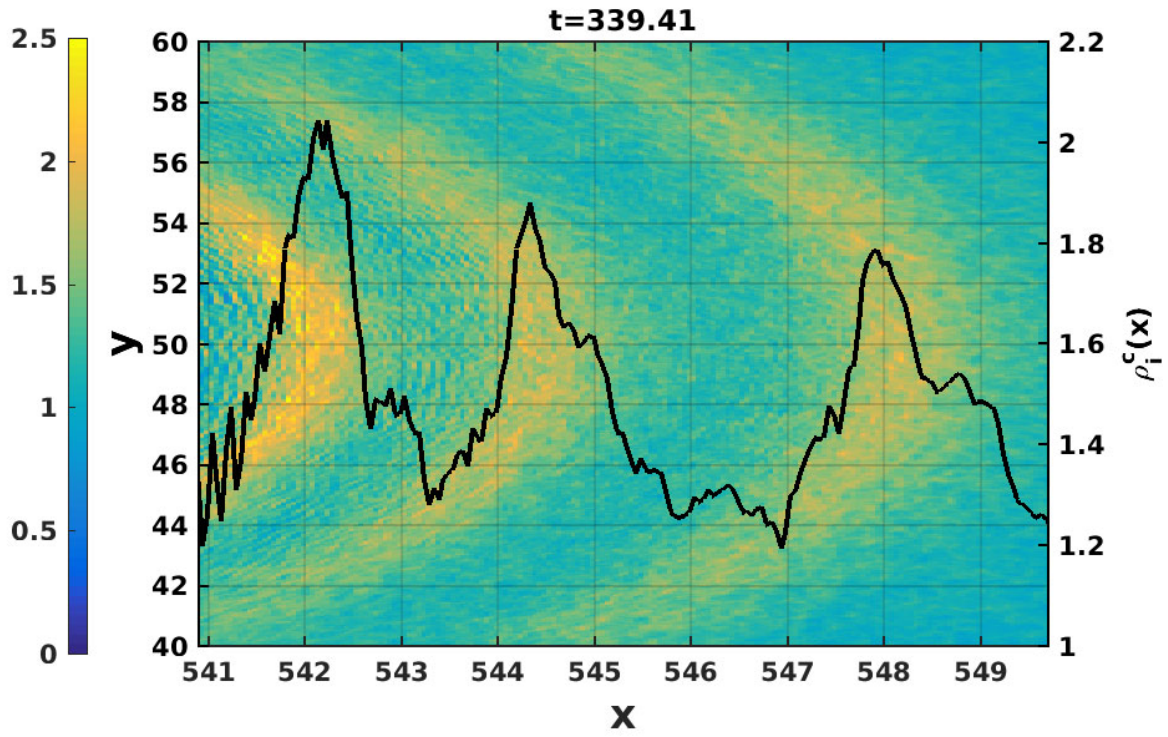


Figure 6. Zoomed view of the ion charge density $\rho_i^c(x, y = 50.03)$ at t=339.41 for the case of $\delta y = 8$.

Table 1. Constancy of aL^2 for the precursor solitons of Fig. 6.

Soliton	t (ω_{pe}^{-1})	a $(\delta n_i/n_0)$	L (c/ω_{pe})	aL^2
Left	339.41	0.7311	0.8	0.4679
Middle	339.41	0.5665	0.93	0.4795
Right	339.41	0.4771	1.0	0.4771

Next we look at their impact on the background plasma. Figure 7(a) shows a series of snapshots of the ion charge density $\rho_i^c(x, y)$ for this case, taken at various times while Fig. 7(b) displays the corresponding snapshots of the ion kinetic energy $K_i(x, y)$. One observes a number of interesting features in Fig. 6 both in the bubble region and in the precursor region. As the source propagates, the bubble region starts filling up with particles that are self-injected from the background plasma. This is evident at $t = 113.14$ and beyond, through the appearance of an increase in the ion population (shown in light blue in the plots of $\rho_i^c(x, y)$) in the evacuated bubble region that was originally in dark blue. In Fig. 6(b) one also sees evidence of the energization of these self-injected ions inside the bubble region and a focusing effect leading to the formation of a beam like structure. The injected ions enter through the tail region of the bubble where they are swept in from the region ahead of the source by the action of the curving precursor waves. Such a self-injection is not seen in the 1d case since the ions ahead of the source

DISTRIBUTION A: Distribution approved for public release. Distribution unlimited

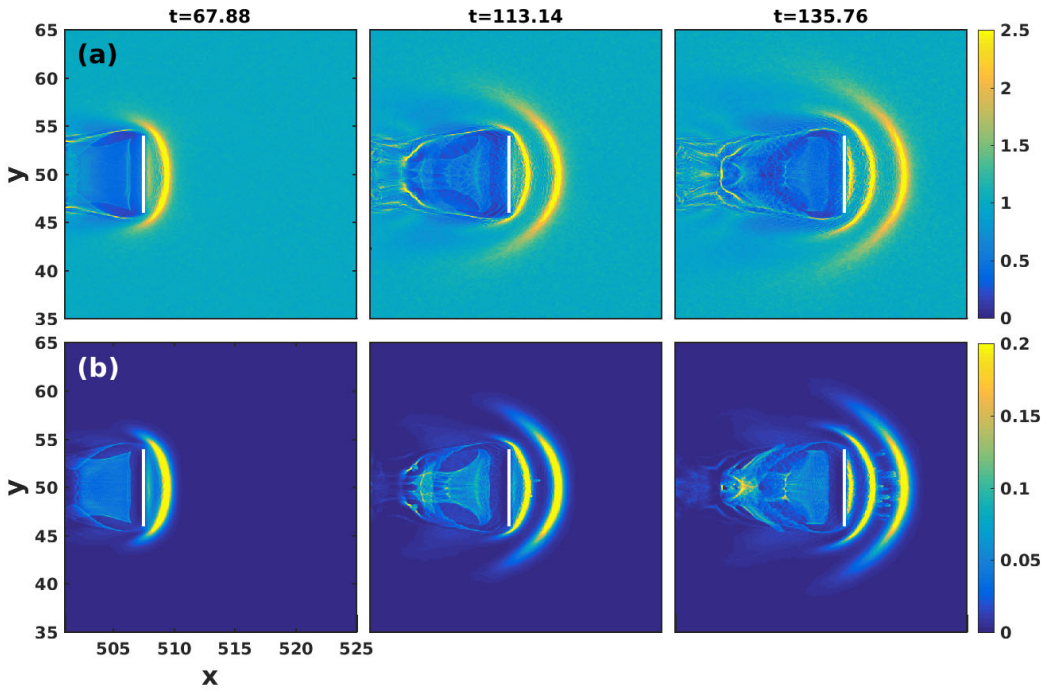


Figure 7. The evolution of (a) the ion charge density $\rho_i^c(x, y)$ at various times while (b) displays the corresponding ion kinetic energy $K_i(x, y)$. Some self-injection of ions is evident in the bubble region as light blue regions showing ion accumulation in the otherwise dark blue ion evacuated region of the bubble.

cannot go around it due to the infinite length of the source. The physical phenomenon of self-injection and energization of the ions within the bubble is analogous to what happens to electrons in a wake-field acceleration scheme. Another interesting feature, distinctly visible in the rightmost plot of Fig. 6(b) is the trapping of particles between two precursors. These particles get energized by bouncing back and forth between the two wave fronts. This is brought out more clearly in Fig. 8 where the progress of four tagged particles p_1, p_2, p_3 and p_4 are monitored. At $t = 362.04$, these four particles are tagged at different location of the simulation domain: p_2 and p_4 are the particles tagged between the two precursors whereas p_1 and p_3 are tagged at the back end of the bubble. The time evolution of these particles shown in Fig.8 explains their overall dynamics. The particles p_2 and p_4 originally tagged between the two precursor structures get entrapped. As time progresses, they bounce back and forth between those two wave fronts, get energized and eventually in this process, they get untrapped. The trapping of these two particles between two precursor wave fronts are shown more clearly in Fig. 9 where the positions of the particles in the x direction are plotted as a function of time. As can be seen the particle orbit exhibits a back and forth motion in x indicating a trapping phenomenon. Eventually as these particles gain more energy they are pushed ahead of the precursors in the forward direction. These particles then travel faster than the precursors. In certain cases groups of ions undergo such an acceleration and emerge

DISTRIBUTION A: Distribution approved for public release. Distribution unlimited

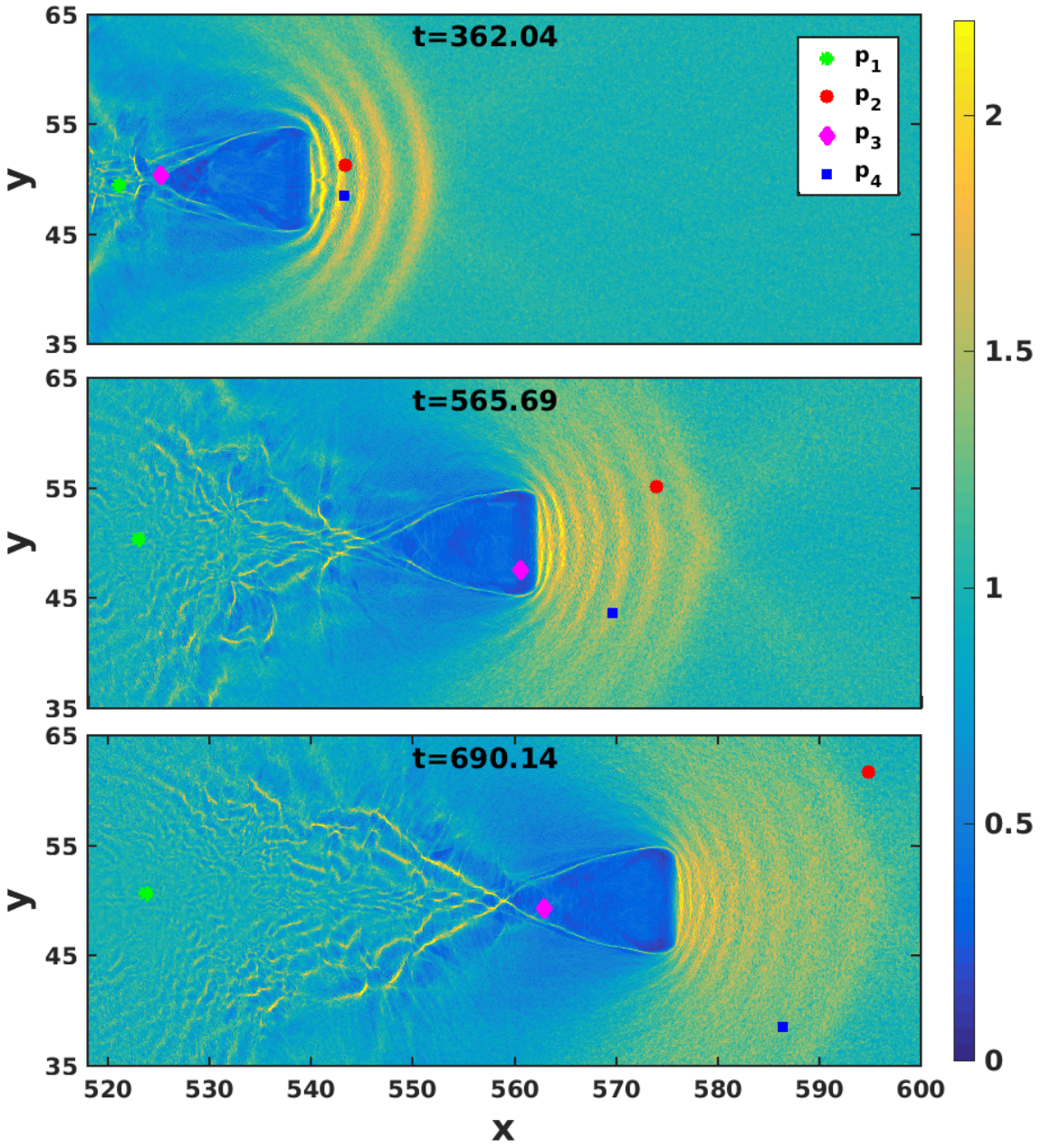


Figure 8. Tagging and tracking. p_1, p_2, p_3 and p_4 are the four tagged particles. Initially p_2 and p_4 are the particles tagged between the two precursors and p_1 and p_3 are tagged at the back end of the bubble. Out of these four particles, one particle p_3 gets accelerated in the ion bubble/wake-field region and particle p_4 gets energized and eventually gets untrapped.

in the form of thin beam-lets. Traces of the formation of such beam-lets were observed in the 1d case, as remarked earlier, but the acceleration is rather weak in that case. Furthermore, the particle $p3$ which is placed exactly at the back end of the bubble sees a huge electrostatic force acting in the forward direction. This force pulls this particle inside the bubble and accelerates it in the forward direction. The particle $p1$ which

DISTRIBUTION A: Distribution approved for public release. Distribution unlimited

was placed slightly away from the back end of the bubble does not suffer any kind of acceleration.

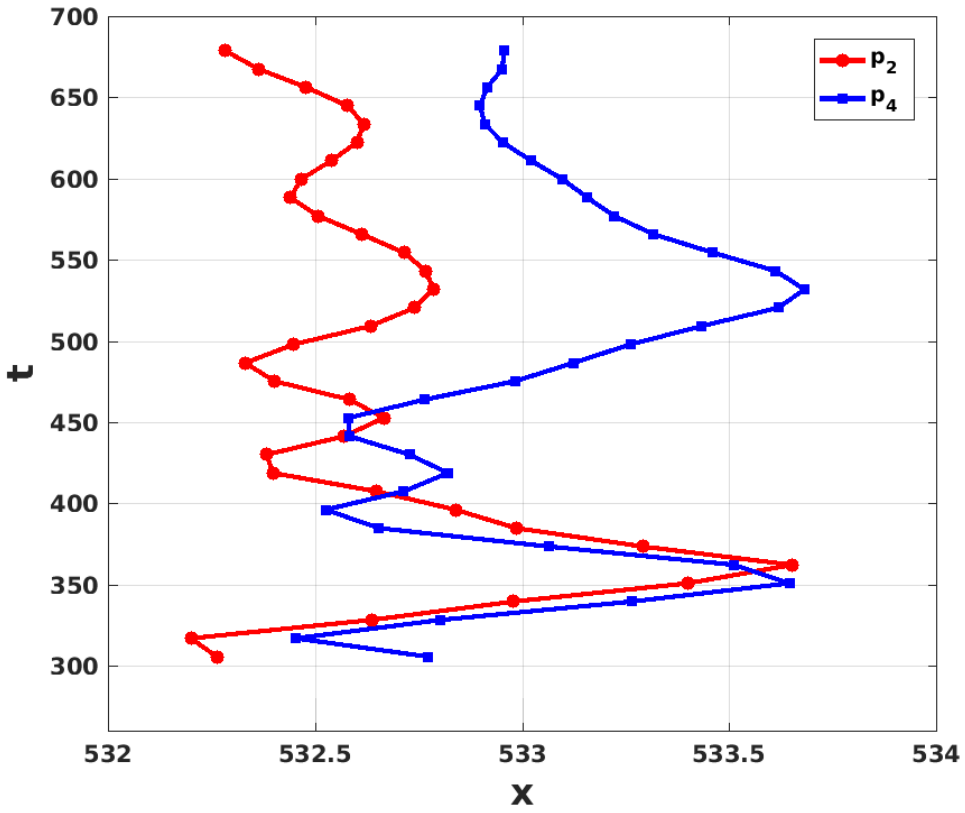


Figure 9. The bouncing motion of the particles p_2 and p_4 as evident from their trajectories in the x direction.

Finally we discuss one more marked difference between the 1d case and the present 2d simulation. This is in the nature of the wave excitations. Figure 10 shows the field components of the excited waves. Unlike the 1d case we now have both E_x and E_y and also a finite magnetic field component B_z. In other words, these near-field wave components are no longer purely (or predominantly) electrostatic, as was seen for the infinite line charge source case, but have a non-negligible magnetic component. This is seen in all regions of the wave propagation - precursors, bubble region and the wake region. It is important to point out that the wave excitations (wakes as well as precursors) in our simulations are due to a charged source that is *moving uniformly* in the plasma. This has to be distinguished from radiation emerging from an accelerating charge or an oscillating charge (as in an antenna). Thus in our case the near field measurements are the relevant ones unlike those carried out for standard antenna outputs. We identify the presence of such a magnetic component as one more signature of a finite sized charged object moving in the plasma. Similar signatures have been noted earlier in other contexts in the literature and our observations are in line

DISTRIBUTION A: Distribution approved for public release. Distribution unlimited

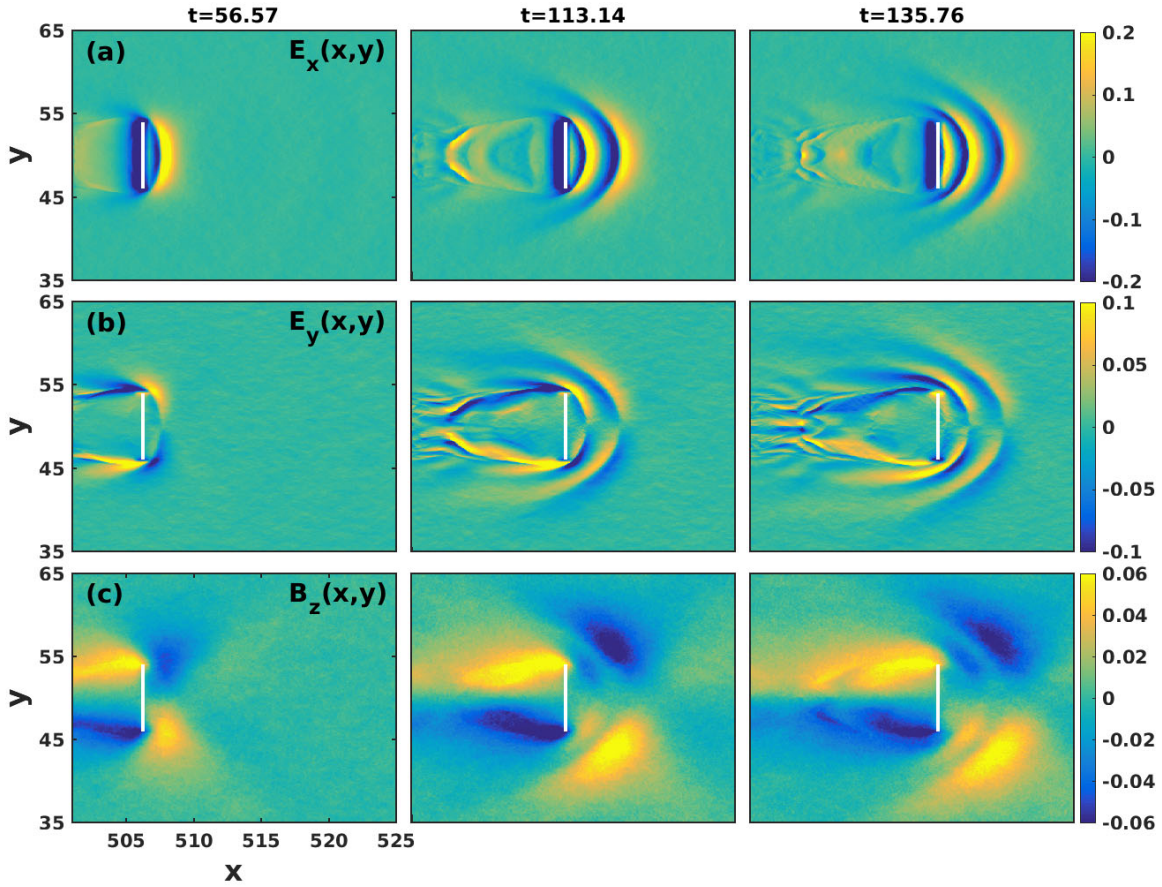


Figure 10. The field components (normalised to $m_e c\omega_{pe}/e$) of the excited waves: (a) $E_x(x,y)$, (b) $E_y(x,y)$ and (c) $B_z(x,y)$.

with those[26–28]

4. Discussion

In this work we have investigated the nature of linear and nonlinear collective excitations arising from the passage of an energetic positively charged body in a plasma. Furthermore, we have examined the interaction of these waves with the ambient plasma. These excitations include both trailing wakes and fore-wake structures. While trailing wakes excited behind a moving source have received a lot of attention in the past for particle acceleration applications, the fore-wake structures in plasmas have remained relatively unexplored. Our investigations are concerned with such scenarios where both trailing wake and fore-wake excitations can occur, as distinct from the earlier works. Such structures are likely to arise whenever the source speed exceeds the phase speeds of some of the basic collective modes of the system. In the present study we have restricted ourselves to cases where the source speed exceeds the ion acoustic speed of the plasma and where the plasma is unmagnetized. We have then varied the transverse dimension of the source to create different configurations of the source ranging from a

DISTRIBUTION A: Distribution approved for public release. Distribution unlimited

nearly one dimensional line source to various two dimensional thin rectangular sources. We find that the shape and size of the beam have a profound influence on the nature of the precursor waves. One significant difference between the 1d and 2d precursor solitons is in the nature of their evolution in space. While a 1d precursor maintains a constant amplitude and width during its propagation, the amplitude of the 2d precursor decreases with distance and its width increases. In both cases the product of the amplitude and square of the width remains a constant. This is in accord with theoretical predictions of 1d and 2d solitons.[23,24] Furthermore, it is seen that reducing the transverse dimension of the source causes a slowing down of the precursor and also bends it at the edges to create a crescent like structure. Since the charge density of the source is kept constant, reducing the transverse length reduces the area of the source and hence the amount of charge on it. The reduction of the charge and hence the strength of the source leads to a reduction of the speed of the precursor and also to the number of precursors created in a given amount of time. The bending of the precursors is a geometric effect directly related to the shape of the source influencing the flow of the plasma around it. The finite transverse size of the source also introduces a modification in the field characteristics of the precursor and other source induced excitations in that they are no longer purely electrostatic but have a magnetic component to it. Such a modification arising from finite size effects had been predicted theoretically[26–28] and observed experimentally[29] in other contexts. This is the first time that they have been observed for precursor waves.

As regards the interaction of these waves with the ambient plasma we observe interesting features some of which have a commonality with phenomena well known from wake-field particle acceleration studies. These include the formation of a bubble region and the trapping of ions and their subsequent acceleration inside the bubble. Our particle tagging studies demonstrate this very clearly. The formation of beam-lets provides a distinct signature of such an acceleration and focusing within the bubble region. The existence of the precursors, a novel feature of the present scenario, provides an additional mechanism for particle trapping and energization of ions. The basic mechanism is akin to Fermi acceleration due to repeated bouncing off these intense field structures. We also see evidence of beam-let formation in the fore-wake region arising due to particle trapping and acceleration in regions between precursors.

We now discuss some of the assumptions and simplifications made in our simulations and their impact on our results. A major simplification is in the evolution of the source which is assumed to maintain its rigidity and also not lose any energy or charge during its propagation. Our source model is motivated by and based on real life examples like an orbiting space debris object. Such an object gets quickly charged by the ionospheric plasma and the amount of charge does not change apart from small fluctuations due to the dynamic nature of the plasma charging process. The object also possesses a large kinetic energy due to its large mass (compared to that of the plasma electrons and ions) and its high orbital velocity. By comparison the energy of the precursors and wake structures would be negligibly small and hence the source would not suffer any

DISTRIBUTION A: Distribution approved for public release. Distribution unlimited

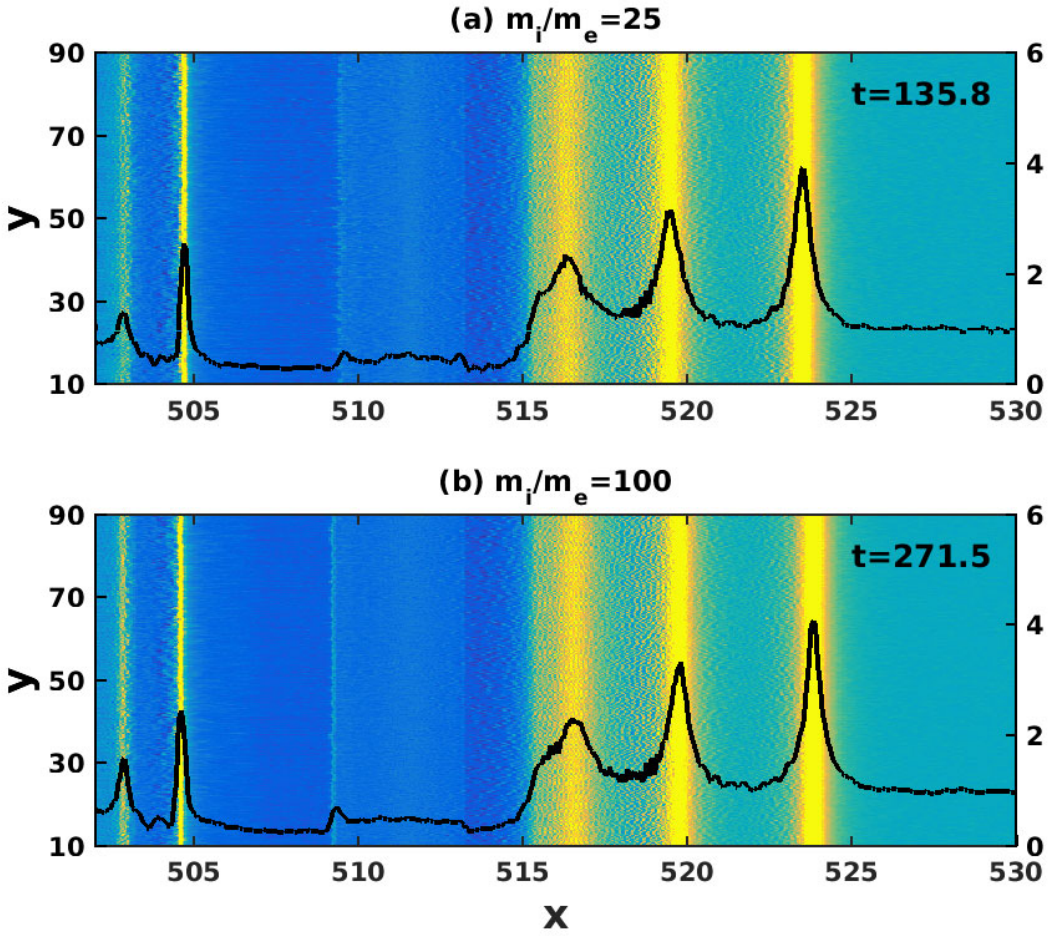


Figure 11. A comparison of the precursor excitations by a line source for two different values of the mass ratio, namely 25 and 100 while maintaining the same Mach number of 1.1. As can be seen the basic phenomenon of precursor excitation and the nature of the precursor remains the same in both cases with a time delay that is linearly proportional to the ion acoustic speeds for the two cases. For the higher mass ratio of 100 the phenomenon occurs at twice the time period compared to that of 25.

significant energy loss. This can be seen from the following estimates for the ionospheric case. The electric field energy density of a wake or precursor structure can be estimated as $\frac{E^2}{8\pi} \sim \alpha n k_B T_e/2$ where n is the plasma density in the ionosphere, E is the electric field of the precursor, T_e is the electron temperature, k_B is the Boltzmann constant and α is a factor that determines the amplification of the field over the thermal fluctuation due to nonlinear effects. The typical size of an ion acoustic soliton is about a few Debye lengths (λ_d), hence the energy lost, $\mathcal{E}_{loss}$, by the source in creating a single soliton would be $\mathcal{E}_{loss} \sim \frac{E^2\lambda_d^3}{8\pi} \sim \alpha k_B T_e n \lambda_d^3$. The kinetic energy of the source is given by $m_s v_s^2/2 \sim m_s k_B T_e/m_i$ where m_s is the mass of the source and v_s its velocity is assumed to be of the order of the ion acoustic velocity $k_B T_e/m_i$ where m_i is the ion mass. Thus the ratio R of the soliton energy to the source energy is $\sim R \sim \alpha(m_i/m_s)(n\lambda_d^3)$. In the ionosphere taking an oxygen ion and a centimetre sized solid debris object the ratio

DISTRIBUTION A: Distribution approved for public release. Distribution unlimited

m_i/m_s would be of the order of 10^{-27} and hence the debris object would suffer negligible drag due to the excitation of solitons and wake fields in the ionosphere. Based on such a consideration we have taken a source model that maintains a constant velocity and a constant charge.

Our next major assumption has been that of taking an unrealistic ion to electron mass ratio of 25 as well as a very high value of the electron temperature. As mentioned above this has been done to reduce the simulation time and is justified provided one can show the scaling of the results to realistic scenarios. In our case, the above mentioned quantities determine the ion acoustic speed and concomitantly the speed of the source for a fixed Mach number. The ion acoustic speed determines how rapidly the precursors separate from the source and from each other since their speeds are supersonic. A low ion acoustic speed (and hence also a low source speed) would imply a longer period for a reasonable separation of the precursors and one would have to carry out a longer simulation run. The time scale is linear with the ion acoustic speed. We have confirmed this by carrying out a run in which the ion acoustic speed was lowered by a factor of two by increasing the mass ratio by a factor of 4. The source speed was accordingly lowered by a factor of two to maintain the same Mach number. A comparison of the two runs is shown in Fig. 11. As can be seen, the bottom panel recreates exactly the phenomenon observed in the top panel but at a time that is two times later. Thus our basic physics conclusions regarding the occurrence and nature of precursors remains the same for the two different choices of the mass ratio.

Finally, we would like to mention that although our present simulations are restricted to unmagnetized plasmas they can be easily extended to magnetized plasmas where in the past we have demonstrated the existence of magneto-sonic precursors.[11] Such an investigation is presently in progress and is also being extended to three dimensional simulations to provide a more realistic assessment for practical applications. These results will be reported separately.

5. Acknowledgements

A.S. acknowledges AOARD for their research grant FA2386-18-1-4022 and is grateful to the Indian National Science Academy for the Honorary Scientist position. This work is partially supported by the U.S. Department of Energy, Office of Science, Office of Fusion Energy Sciences, under Contract No. DEAC05-00OR22725. The authors would like to acknowledge the OSIRIS Consortium, consisting of UCLA and IST (Lisbon, Portugal) for providing access to the OSIRIS4.0 framework which is the work supported by NSF ACI-1339893. The simulations for the work described in this paper were performed on Antya, an IPR Linux cluster.

DISTRIBUTION A: Distribution approved for public release. Distribution unlimited

6. References

[1] Toshiki Tajima and John M Dawson. Laser electron accelerator. *Physical Review Letters*, 43(4):267, 1979.

[2] Pisin Chen, J. M. Dawson, Robert W. Huff, and T. Katsouleas. Acceleration of electrons by the interaction of a bunched electron beam with a plasma. *Phys. Rev. Lett.*, 54:693–696, Feb 1985.

[3] C Joshi, WB Mori, T Katsouleas, JM Dawson, JM Kindel, and DW Forslund. Ultrahigh gradient particle acceleration by intense laser-driven plasma density waves. *Nature*, 311(5986):525–529, 1984.

[4] C Joshi, Erik Adli, W An, CE Clayton, Sebastian Corde, S Gessner, MJ Hogan, M Litos, W Lu, KA Marsh, et al. Plasma wakefield acceleration experiments at facet ii. *Plasma Physics and Controlled Fusion*, 60(3):034001, 2018.

[5] Toshiki Tajima, XQ Yan, and T Ebisuzaki. Wakefield acceleration. *Reviews of Modern Plasma Physics*, 4(1):1–72, 2020.

[6] T Kurz, T Heinemann, MF Gilljohann, YY Chang, JP Couperus Cabadağ, A Debus, O Kononenko, R Pausch, S Schöbel, RW Assmann, et al. Demonstration of a compact plasma accelerator powered by laser-accelerated electron beams. *Nature communications*, 12(1):1–9, 2021.

[7] Abhijit Sen, Sanat Tiwari, Sanjay Mishra, and Predhiman Kaw. Nonlinear wave excitations by orbiting charged space debris objects. *Advances in Space Research*, 56(3):429–435, 2015.

[8] Sanat Kumar Tiwari and Abhijit Sen. Wakes and precursor soliton excitations by a moving charged object in a plasma. *Physics of Plasmas*, 23(2):022301, 2016.

[9] Surabhi Jaiswal, P Bandyopadhyay, and A Sen. Experimental observation of precursor solitons in a flowing complex plasma. *Physical Review E*, 93(4):041201, 2016.

[10] Garima Arora, P Bandyopadhyay, MG Hariprasad, and A Sen. Effect of size and shape of a moving charged object on the propagation characteristics of precursor solitons. *Physics of Plasmas*, 26(9):093701, 2019.

[11] Atul Kumar and Abhijit Sen. Precursor magneto-sonic solitons in a plasma from a moving charge bunch. *New Journal of Physics*, 22(7):073057, 2020.

[12] RG Hemker. *Particle-in-cell modeling of plasma-based accelerators in two and three dimensions*. University of California, Los Angeles, 2000.

[13] Ricardo A Fonseca, Luis O Silva, Frank S Tsung, Viktor K Decyk, Wei Lu, Chuang Ren, Warren B Mori, S Deng, S Lee, T Katsouleas, et al. Osiris: A three-dimensional, fully relativistic particle in cell code for modeling plasma based accelerators. In *International Conference on Computational Science*, pages 342–351. Springer, 2002.

[14] RA Fonseca, SF Martins, LO Silva, JW Tonge, FS Tsung, and WB Mori. One-to-one direct modeling of experiments and astrophysical scenarios: pushing the envelope on kinetic plasma simulations. *Plasma Physics and Controlled Fusion*, 50(12):124034, 2008.

[15] Rudolf Treumann and Wolfgang Baumjohann. Collisionless magnetic reconnection in space plasmas. *Frontiers in Physics*, 1, 2013.

[16] A Mishchenko, A Biancalani, A Bottino, T Hayward-Schneider, Ph Lauber, E Lanti, L Villard, R Kleiber, A Könies, and M Borchardt. Numerics and computation in gyrokinetic simulations of electromagnetic turbulence with global particle-in-cell codes. *Plasma Physics and Controlled Fusion*, 63(8):084007, jun 2021.

[17] Gregory R. Werner, Scott Robertson, Thomas G. Jenkins, Andrew M. Chap, and John R. Cary. Accelerated steady-state electrostatic particle-in-cell simulation of langmuir probes. *Physics of Plasmas*, 29(1):013502, 2022.

[18] Sanat Kumar Tiwari and Abhijit Sen. Fore-wake excitations from moving charged objects in a complex plasma. *Physics of Plasmas*, 23(10):100705, 2016.

[19] T. Schildknecht, R. Musci, and T. Flohrer. Properties of the high area-to-mass ratio space debris population at high altitudes. *Advances in Space Research*, 41(7):1039–1045, 2008.

[20] Carolin Früh, Tom Kelecy, and Moriba K. Jah. Coupled orbit-attitude dynamics of high area-to-

DISTRIBUTION A: Distribution approved for public release. Distribution unlimited

mass ratio (hamr) objects: influence of solar radiation pressure, earth's shadow and the visibility in light curves. *Celestial Mechanics and Dynamical Astronomy*, 117:385–404, 2013.

[21] H. Lamb. *Hydrodynamics*. Cambridge University Press, Cambridge, UK, 1993.

[22] T Zh Esirkepov, Y Kato, and S V Bulanov. Bow wave from ultraintense electromagnetic pulses in plasmas. *Physical Review Letters*, 101(26):265001, 2008.

[23] Stephen Maxon and James Viecelli. Cylindrical solitons. *The Physics of Fluids*, 17(8):1614–1616, 1974.

[24] Stephen Maxon and James Viecelli. Spherical solitons. *Phys. Rev. Lett.*, 32:4–6, Jan 1974.

[25] T. Romesser and N. Hershkowitz. Experimental observations of the dimensionless scaling of planar and cylindrical ion acoustic solitons. *Physics Letters A*, 53(2):180–182, 1975.

[26] SV Yadavalli. Electromagnetic wake of a charged-particle pulse in a plasma. *The Physics of Fluids*, 8(5):956–967, 1965.

[27] Ratan Kumar Bera, Devshree Mandal, Amita Das, and Sudip Sengupta. Effect of transverse beam size on the wakefields and driver beam dynamics in plasma wakefield acceleration schemes. *AIP Advances*, 10(2):025203, 2020.

[28] Amita Das, Atul Kumar, Chandrasekhar Shukla, Ratan Kumar Bera, Deepa Verma, Devshree Mandal, Ayushi Vashishta, Bhavesh Patel, Y Hayashi, KA Tanaka, et al. Boundary driven unconventional mechanism of macroscopic magnetic field generation in beam-plasma interaction. *Physical Review Research*, 2(3):033405, 2020.

[29] Gourab Chatterjee, Kevin M Schoeffler, Prashant Kumar Singh, Amitava Adak, Amit D Lad, Sudip Sengupta, Predhiman Kaw, Luis O Silva, Amita Das, and G Ravindra Kumar. Magnetic turbulence in a table-top laser-plasma relevant to astrophysical scenarios. *Nature communications*, 8(1):1–5, 2017.

DISTRIBUTION A: Distribution approved for public release. Distribution unlimited

Annexure V

Electromagnetic Pinned Solitons for Space Debris Detection

Abhijit Sen,[1] Rupak Mukherjee,[2] Sharad K. Yadav,[3] Chris Crabtree,[4] and Gurudas Ganguli[4]

[1)] *Institute for Plasma Research, Bhat, Gandhinagar 382428, India*

[2)] *Princeton Plasma Physics Laboratory, Princeton, N.J., U.S.A.*

[3)] *Department of Physics, S.V.N.I.T. Surat, Surat 395007, India.*

[4)] *Naval Research Laboratory, Washington, DC 20375, U.S.A.*

(Dated: 16 May 2022)

Electromagnetic "pinned" solitons in the form of stationary nonlinear waves are studied within the framework of an inertial magneto-hydrodynamic model. These structures that can arise when a charged source moves in a magnetized plasma have a velocity that is equal to the source velocity and hence appear as "pinned" structures that envelope the source. We investigate the excitation of such solitons in the Low Earth Orbit (LEO) region due to the passage of charged space debris objects. The spatial size of these electromagnetic solitons, typically of the order of a few ion skin depths, can be very large in this region and may be easily detected using ground-based radar back scattering. Such solitons can therefore provide a convenient means of tracking small sized debris objects that cannot be easily spotted using optical methods.

DISTRIBUTION A: Distribution approved for public release. Distribution unlimited

I. INTRODUCTION

The population of 'space debris' also known as 'space junk', consisting of dead or destroyed satellites, their fragmented parts, rocket bodies and mission related debris continues to grow at an alarming rate thereby posing a serious threat to active space assets[1]. Space debris concerns have delayed mission launches and space walks by astronauts. It is estimated that at the present time there are over half a million pieces of debris with sizes ranging from 1 to 10 cms and nearly 100 million particles that are less than a centimetre orbiting the earth[2–4]. The majority of the debris population resides in the region between 600 kms to 1200 kms altitude in sun-synchronous Low Earth Orbit (LEO) region where they pose the greatest threat to the high population of active orbiting space craft[1]. Since the debris objects have a high orbital velocity (of the order of 8 kms/s in the LEO region) even a small centimetre sized particle has tremendous kinetic energy and can cause enormous damage if it collides with a satellite[5]. According to NASA, a collision with even a millimeter-size debris at orbital speed can be mission ending[6]. Individual small sized objects are difficult to detect using optical techniques or even directly by radar scatterings. Therefore, modelling the dynamics of these objects and devising better methods of detecting them remain a high priority research area of Space Situational Awareness[7,8].

An important physical characteristic of the space debris is that they are highly charged objects. This is because they are moving in the space plasma environment of the ionosphere and the flow of electron and ion currents on them can lead to the accumulation of a large amount of surface charge (usually negative) and the development of a surface potential on these objects. Thus debris are subject to electromagnetic forces from the surrounding plasma and the ambient magnetic field[9] and in turn can also excite electromagnetic perturbations in the plasma[10]. While the electromagnetic forces acting on the debris have been investigated in detail and found to be negligible to affect orbital motion compared to other primary forces like gravity[9], the consequences of the charge interactions with the ambient plasma leading to electromagnetic emissions by the debris have not received much attention. In a series of investigations, we examined this topic and suggested an alternate way of tracking small sized debris by exploiting these collective perturbations induced by them in the plasma[10–13]. The basic idea is that these nonlinear excitations, which take the form of long-lived soliton

DISTRIBUTION A: Distribution approved for public release. Distribution unlimited

structures and travel ahead of the debris object, can give rise to a cloud of plasma irregularity with a dimension much larger than the debris size. Such irregularities can be detected from ground or space based radars and thereby provide an indirect means of detecting the debris object. This theoretical idea of the possibility of exciting a precursor soliton in a plasma was confirmed experimentally in a laboratory device using a flowing dusty plasma interacting with a static charged obstacle[11]. It was shown that when the magnitude of the flow exceeded a critical value (in this case the dust acoustic speed) precursor pulses were created in addition to the customary trailing wake fields. The pulses were analysed for their propagation characteristics and found to be fast propagating dust acoustic solitons. Subsequent experiments also explored the nature of these solitons as a function of the size and shape of the charged obstacle[14]. In a detailed feasibility study, Truitt and Hartzell[15] have worked out the amplitude, width, and production frequency of ion acoustic solitons that may be produced by millimeter and centimeter-scale orbital debris as a function of the debris' size, velocity, and location (altitude, latitude, and longitude) about the Earth. Finally, a new class of solitons, also theoretically predicted earlier[10], was identified in a dusty plasma experiment[16]. These solitons do not move away from the source but cling to it as an envelope forming an electric sheath around it and are known as "pinned" solitons. Typically, the envelope can be quite large compared to the normal Debye shield around the source and could again provide a means of detecting the debris using radar scattering.

All these past works[10–16] were confined to electrostatic excitations *e.g.* ion acoustic waves or dust acoustic waves which are easy to model theoretically and also test experimentally. Ion acoustic waves excited by the debris in the ionosphere are likely to have short lifetimes due to Landau damping effects particularly in the LEO region where the electron and ion temperatures are nearly equal. Although ion Landau damping can be eliminated by an inhomogeneous ion flow[17], that can arise from a speeding debris, a better alternative would be to excite electromagnetic waves which would not suffer such damping and can be longer lived. Electromagnetic solitons would also have a larger spatial extent, of the order of a few ion skin depths, and would be easier to detect with radar back scattering. Since a moving charge constitutes a current, the orbiting debris can be seen as current sources and hence, in principle, should be able to emit electromagnetic waves. In the presence of an ambient magnetic field these could be in the form of Alfven waves or magnetosonic waves. However there still remains the question of whether they can emit electromagnetic precursor

DISTRIBUTION A: Distribution approved for public release. Distribution unlimited

waves and what would be their characteristics. The question was addressed in Ref.[18] where particle-in-cell simulations provided a first principles proof of existence of driven electromagnetic solitons. It was shown that a charge bunch moving in a magnetized plasma could excite precursor waves in the form of fast magneto-sonic solitons. Under other conditions, the simulations also observed the existence of fast magneto-sonic pinned solitons. While the PIC simulations have helped establish the existence of electromagnetic precursor solitons, for information about their spectrum and physical characteristics a fluid simulation is more convenient and provides good physical insights[19,20]. The present paper is devoted to such an investigation where we look for a wide class of driven nonlinear stationary solutions of the magneto-hydrodynamic set of equations. We pay special attention to pinned solitons which move at the same speed as the charge source (the debris object) and discuss their propagation characteristics. Our results are primarily numerical but we also discuss analytic solutions and reduced nonlinear models in certain simplifying limits. Finally we discuss the relevance and applicability of our results to the debris detection problem in the LEO region.

The paper is organized as follows. The next section, section II, is devoted to a description of the model equations as well as the equilibrium configuration and parameters. Section III provides a reduced nonlinear model in the form of a forced Korteweg de Vries (fKdV) equation that is derived from the full model equations by employing a reductive perturbation method. Some analytic and numerical results of the fKdV are presented. Section IV presents nonlinear stationary solutions for arbitrary amplitudes in various limits through numerical solutions of the full set of model equations in the frame of the moving source. In section V we discuss the physical significance of our solutions and their relevance and applicability to the debris detection problem.

II. MODEL EQUATIONS

Our model equations are derived from the standard two fluid model equations[21], by making the MHD approximation of quasi-neutrality ($n_e = n_i = n$) and defining the mass $M = m_e + m_i \approx m_i$ and the MHD fluid velocity as, $\vec{v} = \frac{m_1}{M}\vec{v}_i + \frac{m_e}{M}\vec{v}_e \approx \vec{v}_i$. Here $m_j, n_j, \vec{v}_j$ refer to the two fluid electron ($j = e$) and ion ($j = i$) quantities.

DISTRIBUTION A: Distribution approved for public release. Distribution unlimited

Then the continuity equation is given by,

$$\frac{\partial n}{\partial t} + \nabla \cdot (n\vec{v}) = 0 \tag{1}$$

By adding the electron and ion momentum equations, one gets the following MHD momentum equation,

$$\frac{d\vec{v}}{dt} = \frac{1}{Mnc}\vec{J} \times \vec{B} - \frac{1}{nM}\nabla p \tag{2}$$

where $\vec{J} = en(\vec{v}_i - \vec{v}_e)$ and $p = n(T_e + T_i)$. To account for the effect of the moving charged debris source we introduce an additional current source $\vec{S}$ in the Ampere's law which is now given by,

$$\nabla \times \vec{B} = \frac{4\pi}{c}\vec{J} + \vec{S} \tag{3}$$

Finally, we have Faraday's law,

$$\frac{\partial \vec{B}}{\partial t} = -\nabla \times \vec{E} \tag{4}$$

Using (3) to substitute for $\vec{J}$ in (2) we get

$$\frac{d\vec{v}}{dt} = \frac{1}{4\pi nM}(\nabla \times \vec{B}) \times \vec{B} - \frac{1}{\pi nM}\vec{S} \times \vec{B} + \frac{1}{nM}\nabla(p) \tag{5}$$

The electric field is calculated from the ion momentum equation to get,

$$\begin{aligned} \vec{E} &= -\frac{1}{c}\vec{v}_i \times \vec{B} + \frac{m_i}{e}\frac{dv_i}{dt} \\ &\approx -\frac{1}{c}\vec{v} \times \vec{B} + \frac{M}{e}\frac{dv}{dt} \end{aligned} \tag{6}$$

Substituting for $\vec{E}$ in Faraday's law one gets,

$$\frac{\partial \vec{B}}{\partial t} = \nabla \times \left(\vec{v} \times \vec{B}\right) - \frac{Mc}{e}\nabla \times \frac{d\vec{v}}{dt} \tag{7}$$

The last term in eq.(2) comes from retaining the ion inertial contribution and provides a dispersive contribution. Equations (1),(2) and (7) constitute our full set of model equations.

We next assume that the debris is moving in the x direction ($\vec{S} = S\hat{e}_x$) and thus only consider perturbations with x variation. We take the equilibrium magnetic field to be $\mathbf{B_0} = B_{0x}\hat{e}_x + B_{0z}\hat{e}_z$ with $B_{0x} = B_0 sin\theta$ and $B_{0z} = B_0 cos\theta$ where θ is the angle between the magnetic field and z, the direction perpendicular to the direction of the wave propagation (see Fig.1). We now write eqns.(1), (2) and (7) in component form and further use the following normalizations,

DISTRIBUTION A: Distribution approved for public release. Distribution unlimited

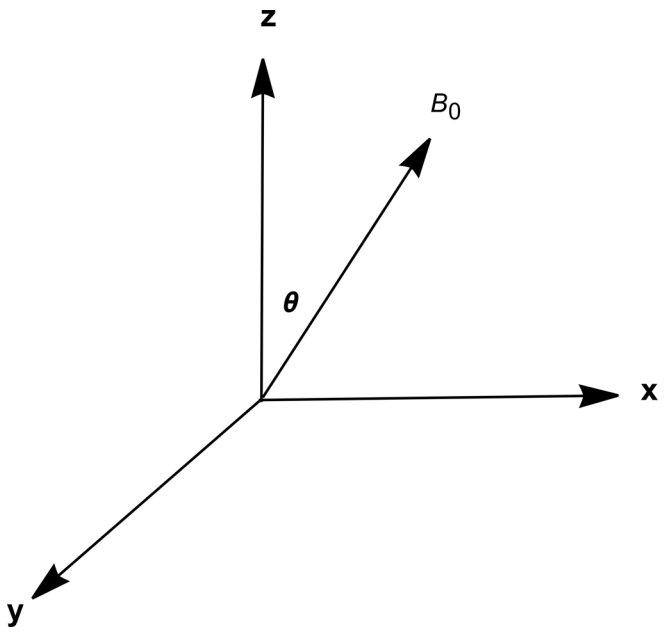


FIG. 1: Configuration of the equilibrium magnetic field with respect to the wave propagation direction, $\hat{e}_x$.

$$x = \frac{x}{\delta} \; ; \; t = \frac{tV_A}{\delta}$$

$$n = n/n_0 \; ; \; \vec{v} = \vec{v}/V_A \; ; \; \vec{B} = \vec{B}/B_0$$

where $\delta = \frac{c}{\omega_{pi}}$ is the ion skin depth, $V_A = \frac{B_0}{\sqrt{4\pi n_0 m_i}}$ is the Alfven velocity and $\omega_{pi} = \sqrt{4\pi n_0 e^2/m_i}$ is the ion plasma frequency. The normalized set of evolution equations are then given by,

$$\frac{\partial n}{\partial t} + \frac{\partial}{\partial x}\left(n v_x\right) = 0 \tag{8}$$

$$\frac{\partial v_x}{\partial t} + v_x \frac{\partial v_x}{\partial x} = -\frac{1}{2n}\frac{\partial}{\partial x}\left((b_z + \cos(\theta))^2 + b_y^2\right) - \frac{\beta}{n}\frac{\partial n}{\partial x} \tag{9}$$

$$\frac{\partial v_y}{\partial t} + v_x \frac{\partial v_y}{\partial x} = \frac{1}{n}\sin\theta \frac{\partial b_y}{\partial x} + \frac{S}{n}(\cos(\theta) + b_z) \tag{10}$$

DISTRIBUTION A: Distribution approved for public release. Distribution unlimited

$$\frac{\partial v_z}{\partial t} + v_x \frac{\partial v_z}{\partial x} = \frac{1}{n}\sin\theta \frac{\partial b_z}{\partial x} - \frac{S}{n} b_y \tag{11}$$

$$\frac{\partial b_y}{\partial t} = -\frac{\partial}{\partial x}(v_x b_y - v_y \sin\theta) + \frac{\partial}{\partial x}(\frac{1}{n}\sin\theta \frac{\partial b_z}{\partial x} - \frac{S b_y}{n}) \tag{12}$$

$$\frac{\partial b_z}{\partial t} = \frac{\partial}{\partial x}\left(v_z \sin\theta - v_x(\cos\theta + B_z)\right) - \frac{\partial}{\partial x}\left(\frac{1}{n}\sin\theta \frac{\partial b_y}{\partial x} + \frac{S}{n}(\cos(\theta) + b_z)\right) \tag{13}$$

where $\beta = C_s^2/V_A^2$ with $C_s = \sqrt{T/m_i}$ being the sound velocity. Furthermore, b_y, b_z denote perturbed magnetic field components and $b_x = 0$ follows from the x component of Faraday's law.

For $S = 0$, linearising the above equations and taking the linear quantities to be of the form $\tilde{f} \sim \exp(-i\omega t + ikx)$, one gets the following dispersion relation:

$$M_1^6 - M_1^4(1 + \sin^2\theta + k^2\delta^2 \sin^2\theta + \beta) + M_1^2 \sin^2\theta \left(1 + \beta(2 - k^2\delta^2)\right) - \beta \sin^4\theta = 0 \tag{14}$$

where $M_1 = \omega/kV_A$. The above dispersion relation can be solved to obtain the full spectrum of MHD waves including the Alfven waves and the fast and slow magneto-sonic waves. The $k^2\delta^2$ term in (14) is the ion inertia contribution and provides the essential dispersion contribution for the formation of a soliton for very low frequency waves in the cold plasma limit. We will discuss these waves in the context of applications to the LEO region.

III. SMALL AMPLITUDE NONLINEAR SOLUTIONS - THE FKDV LIMIT

Before attempting to solve the full set of model equations for arbitrary amplitudes of the variables, we first discuss a reduced model equation that can be obtained from (8-13) in the limit of weak nonlinearity (small but finite amplitude perturbations) and weak dispersion. This leads to a nonlinear evolution equation in the form of a forced Korteweg de Vries (fKdV) equation which is easier to analyze than the full set of model equations. A systematic derivation of such an equation using the reductive perturbation method is given in the Appendix. The equation is,

$$a_1 \frac{\partial b_{z1}}{\partial \tau} + a_2 b_{z1} \frac{\partial b_{z1}}{\partial \xi} + a_3 \frac{\partial^3 b_{z1}}{\partial \xi^3} = a_4 \frac{\partial S_2}{\partial \xi} \tag{15}$$

where, $\xi = \epsilon^{1/2}(x - ut)$ is the stretched variable in the wave frame moving with velocity u, $\tau = \epsilon^{3/2}t$ is a stretched time describing the temporal evolution of the perturbed quantities in

DISTRIBUTION A: Distribution approved for public release. Distribution unlimited

the wave frame and ϵ is the expansion parameter. b_{z1} is the first order perturbed variation in the z component of the wave magnetic field and S_2 is the source term which is assumed to be an order higher than the field perturbations. M the Mach number is defined as $M = u/V_A$ and the coefficients a_n are defined as,

$$a_1 = (\beta + M^2)\cos(\theta) - \frac{(\beta - M^2)((M-\beta)}{M}\sin(\theta)\tan(\theta) + \frac{M(M^2-\beta)(M-\beta)}{\cos(\theta)}$$

$$a_2 = 2\frac{\beta}{M-\beta}\cos^2(\theta) + \left(1 - M + \frac{(M-\beta)^2}{\cos^2(\theta)}\right)\frac{M^2}{M-\beta}\cos^2(\theta) + \frac{(M^2-\beta)(1-M)}{M}\sin^2(\theta)$$
$$+2M(M^2-\beta)$$

$$a_3 = -\frac{(M^2-\beta)(M-\beta)M^2\tan(\theta)\sin(\theta)}{(M^2-\sin^2(\theta))}$$

$$a_4 = M - \beta$$

A similar fKdV equation had earlier been derived for the electrostatic case by Sen *et. al*[10] to model the excitation of ion acoustic precursor solitons by a charged debris object. The above eq.(15) models electromagnetic emissions from a moving charged debris and like the electrostatic case can produce both precursor solitons as well as pinned solitons. For the case of pinned solitons eq.(15) has some exact analytic solutions[10] for particular forms of S_2. For example if,

$$S_2 = AB\mathrm{sech}^2\left[\sqrt{\frac{Aa_2}{12a_3}}\left(\xi - \frac{Aa_2 - 3Ba_4}{3a_1}\tau\right)\right]$$

then a solution of (15) is

$$b_{z1} = A\mathrm{sech}^2\left[\sqrt{\frac{Aa_2}{12a_3}}\left(\xi - \frac{Aa_2 - 3Ba_4}{3a_1}\tau\right)\right]$$

where A and B are constants. Typically $B \ll 1$, since in this approximation the source perturbation is taken to be small. The amplitude of the soliton is larger than the source by a factor of $1/B$. In other words, the source is enveloped by an electromagnetic structure that is much larger than the source size. For arbitrary forms of the source one can look for pinned soliton solutions of (15) by looking for stationary solutions in a frame where the source travels at the same speed as the soliton. Taking the normalised frame speed to be M and going to the frame defined by $\zeta = \xi - M\tau$ one can convert (15) to,

$$-Ma_1\frac{\partial b_{z1}}{\partial \zeta} + a_2 b_{z1}\frac{\partial b_{z1}}{\partial \zeta} + a_3\frac{\partial^3 b_{z1}}{\partial \zeta^3} = a_4\frac{\partial S_2}{\partial \zeta} \tag{16}$$

DISTRIBUTION A: Distribution approved for public release. Distribution unlimited

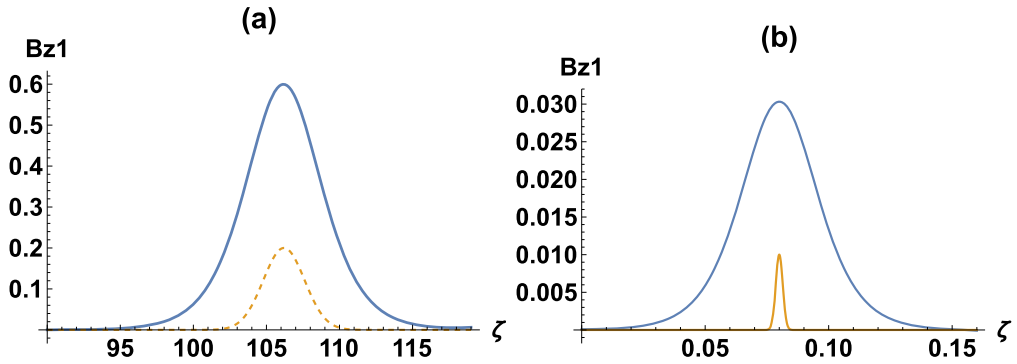


FIG. 2: (a)Pinned soliton of (17) for M=0.25, $\beta = 1.6$, $A_0 = 0.001$, $\Delta = 2.0$, propagating at an angle $\theta = 15^0$. In the plot the amplitude of the source has been multiplied by a factor of 200 to make it visible in the chosen scale and is given by a dashed orange line. (b)Pinned soliton of (17) for M=0.01, $\beta = 0$, $A_0 = 1. * 10^{-7}$,$\Delta = 0.002$ and $\theta = 2.59$. The amplitude of the source has been multiplied by a factor of 10^5 to make it visible in the chosen scale of the plot and is given by a solid orange line.

This equation can be integrated once to give,

$$a_3 \frac{\partial^2 b_{z1}}{\partial \zeta^2} + a_2 \frac{b_{z1}^2}{2} - M a_1 b_{z1} = a_4 S_2 \tag{17}$$

where we have used the condition that b_{z1} and its derivatives vanish at infinity for soliton solutions. Eqn.(17) can be solved numerically for arbitrary functional forms of S_2. Fig.2 shows some typical soliton solutions for a Gaussian current source,

$$S_2 = A_0 e^{\frac{(\zeta-\zeta_0)^2}{\Delta^2}}$$

with amplitude A_0 and width Δ. The plot in Fig. 2 (a) shows a slow magneto-sonic soliton with $\beta = 1.6$ and $M = 0.25$. Fig. 2(b) shows a much slower ion inertial wave soliton with $\beta = 0$ and $M = 0.01$. As we will discuss later these ion inertial wave solitons are more relevant for the LEO region. In both the figures it can be seen that the source is enveloped by a soliton that is several times larger in amplitude.

IV. NONLINEAR STATIONARY SOLUTIONS FOR ARBITRARY AMPLITUDES

For arbitrary amplitude solitons we look for stationary solutions of the full set of nonlinear equations given by (8-13). To get an idea of the basic nature and spectrum of the solitons

DISTRIBUTION A: Distribution approved for public release. Distribution unlimited

we first turn off the source term ($S = 0$) and also take $\beta = 0$ to look for the existence of nonlinear stationary solutions for the above equations.

A. Alfvenic and Ion Inertial Wave Solitons ($S = 0$,$\beta = 0$)

As in the KdV case, we convert the partial differential equations (8-13) to ordinary differential equations by transforming to the frame $\zeta = x - Mt$ where M is the normalized velocity of the soliton.

$$-M\frac{\partial n}{\partial \zeta} + \frac{\partial}{\partial \zeta}\left(n v_x\right) = 0 \tag{18}$$

$$(-M + v_x)\frac{\partial v_x}{\partial \zeta} = -\frac{1}{2n}\frac{\partial}{\partial \zeta}\left((\cos(\theta) + b_z)^2 + b_y^2\right) \tag{19}$$

$$(-M + v_x)\frac{\partial v_y}{\partial \zeta} = \frac{1}{n}\sin(\theta)\frac{\partial b_y}{\partial \zeta} \tag{20}$$

$$(-M + v_x)\frac{\partial v_z}{\partial \zeta} = \frac{1}{n}\sin(\theta)\frac{\partial b_z}{\partial \zeta} \tag{21}$$

$$-M\frac{\partial b_y}{\partial \zeta} = -\frac{\partial}{\partial \zeta}(v_x b_y - v_y \sin(\theta)) + \frac{\partial}{\partial \zeta}(\frac{1}{n}\sin(\theta)\frac{\partial b_z}{\partial \zeta}) \tag{22}$$

$$-M\frac{\partial b_z}{\partial \zeta} = \frac{\partial}{\partial \zeta}\left(v_z \sin(\theta) - v_x(\cos(\theta) + b_z)\right)) - \frac{\partial}{\partial \zeta}(\frac{1}{n}\sin(\theta)\frac{\partial b_y}{\partial \zeta}) \tag{23}$$

Integrating (18) once and using the asymptotic condition $n \to 1$; $v_x \to 0$ as $\zeta \to \infty$ we get

$$n(M - v_x) = M \tag{24}$$

Using (24) in (19) we can get,

$$M v_x = \frac{1}{2}\left(b^2 + 2\cos(\theta) b_z\right) \tag{25}$$

where we have used the conditions $b_y \to 0$ as $\zeta \to \infty$. Also $b^2 = b_y^2 + b_z^2$. In like fashion, from (38) and (39), we can get,

$$M v_y = -\sin(\theta) b_y \tag{26}$$

$$M v_z = -\sin(\theta) b_z \tag{27}$$

From (22) and (23) we get,

$$-M b_y = \sin(\theta)(n v_y + \frac{\partial b_z}{\partial \zeta}) \tag{28}$$

DISTRIBUTION A: Distribution approved for public release. Distribution unlimited

$$-Mb_z = \sin(\theta)(nv_z - \frac{\partial b_y}{\partial \zeta}) - nv_x \cos(\theta) \tag{29}$$

Substituting for v_y, v_z and v_x in (28) and (29) we get,

$$\sin(\theta)\frac{\partial b_z}{\partial \zeta} + \left(M - n\frac{\sin^2(\theta)}{M}\right) b_y = 0 \tag{30}$$

$$\sin(\theta)\frac{\partial b_y}{\partial \zeta} - \left(M - n\frac{\sin^2(\theta)}{M}\right) b_z + \frac{n\cos\theta(b^2 + 2\cos(\theta)b_z)}{2M} = 0 \tag{31}$$

From (24) and (25) we can get,

$$n = \frac{2M^2}{2M^2 - b^2 - 2\cos(\theta)b_z} \tag{32}$$

Substituting for n in (30) and (31) we get the following two coupled equations for b_y and b_z.

$$M\sin(\theta)\frac{\partial b_z}{\partial \zeta} + \left(M^2 - \frac{2M^2\sin^2(\theta)}{2M^2 - b^2 - 2\cos(\theta)b_z}\right) b_y = 0 \tag{33}$$

$$M\sin(\theta)\frac{\partial b_y}{\partial \zeta} - \left(M^2 - \frac{2M^2\sin^2(\theta)}{2M^2 - b^2 - 2\cos(\theta)b_z}\right) b_z + \frac{M^2\cos(\theta)(b^2 + 2\cos(\theta)b_z)}{2M^2 - b^2 - 2\cos(\theta)b_z} = 0 \tag{34}$$

Similar equations have been derived and discussed earlier[22,23] in the context of low frequency nonlinear stationary waves in a magnetised plasma. Some typical solitonic solutions of the above equations for different values of M and a chosen θ are shown in Fig. 3.

A characteristic feature of these solitons, which are pure Alfvenic solitons (since $\beta = 0$), is that they only exist for $M < 1$. As $M \to 1$, their amplitude decreases very rapidly and then they cease to exist. One requires a finite β to have soliton solutions for $M > 1$. These are discussed in the next subsection IV B.

To test whether the arbitrary amplitude stationary solutions are also solutions of the full set of fluid Eqs. (8-13) one can use them as initial conditions and see whether they propagate. In Fig.3 we show the time evolution of the soliton obtained for $M = 0.35$ at $\theta = 15^\circ$. As can be seen, the solution evolves in time without distortion suggesting that these exact time stationary numerical solutions are indeed also solutions of the full plasma system. They can thus be excited by an external driving term such as a charged debris to form a pinned soliton.

As one approaches the small M limit the existence region of ion inertial wave solitons is strongly influenced by the angle of propagation θ[22,23]. For a given angle of propagation, soliton solutions cease to exist below a certain value of M. Solitons with very low values of

DISTRIBUTION A: Distribution approved for public release. Distribution unlimited

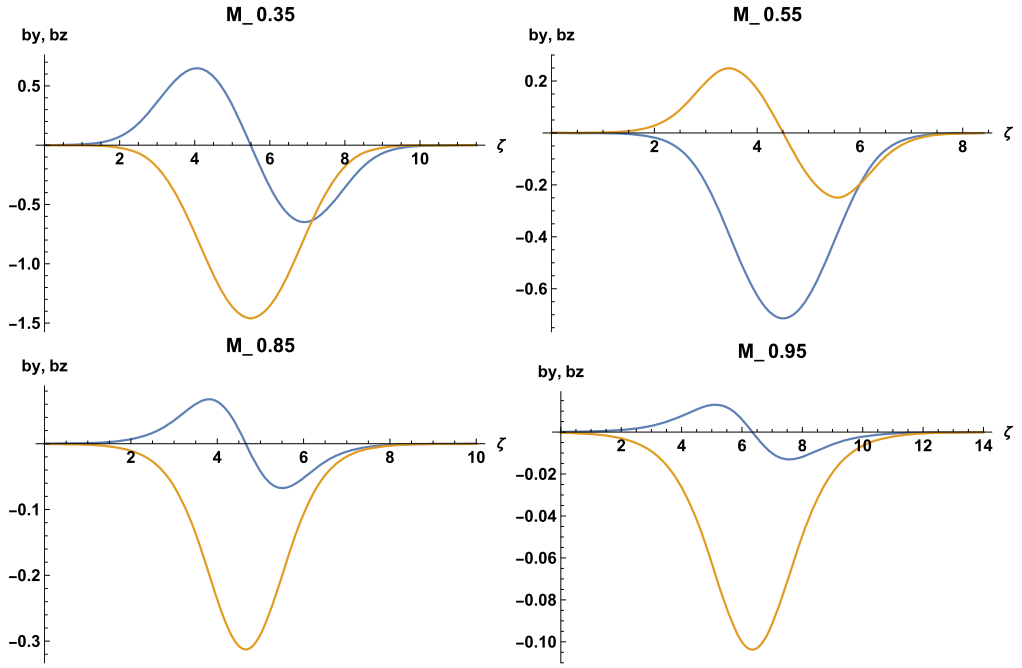


FIG. 3: Alfvenic solitons for different values of $M < 1$ and $\theta = 15^0$. The unipolar curves (orange) are of b_z and the dipolar curves (blue) are of b_y.

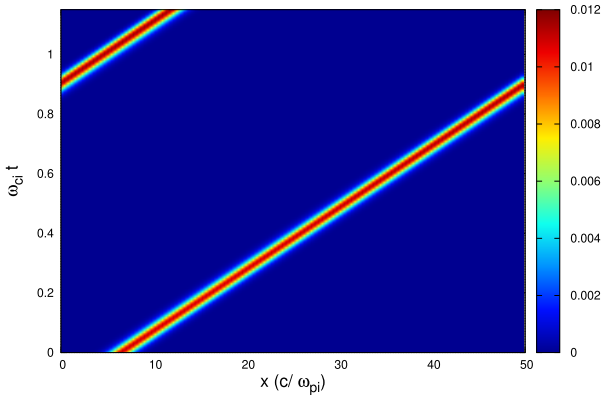


FIG. 4: Plot showing the time evolution of the soliton solution with M=0.95 obtained by simultaneously solving eqns. (8-13) using the solution of eqns. (33) and (34) as an initial condition. The intensity plot shows the profile of B_z^2. As can be seen the soliton propagates without distortion.

M exist for very small values of θ.[22,23]. Fig. 5 shows some of these typical low M solitons.

DISTRIBUTION A: Distribution approved for public release. Distribution unlimited

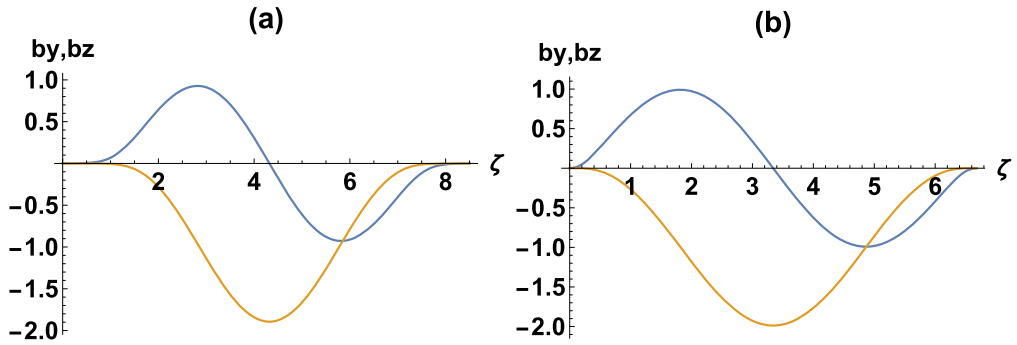


FIG. 5: Ion inertial wave solitons for (a) $M = 0.1$, $\beta = 0$, $\theta = 5^0$ and (b) $M = 0.0185$, $\beta = 0$ and $\theta = 1^0$. The unipolar curves (orange) are of b_z and the dipolar curves (blue) are of b_y.

B. Magnetosonic Solitons ($S = 0$, β finite)

We now consider finite β effects that allow for the existence of magnetosonic waves. With finite β, eqn(19) becomes,

$$(-M + v_x)\frac{\partial v_x}{\partial \zeta} = -\frac{1}{2n}\frac{\partial}{\partial \zeta}\left((\cos(\theta) + b_z)^2 + b_y^2\right) - \frac{\beta}{n}\frac{\partial n}{\partial \zeta} \tag{35}$$

Integrating once we get,

$$Mv_x = \frac{(b^2 + 2\cos(\theta)b_z)}{2} + \beta(n-1) \tag{36}$$

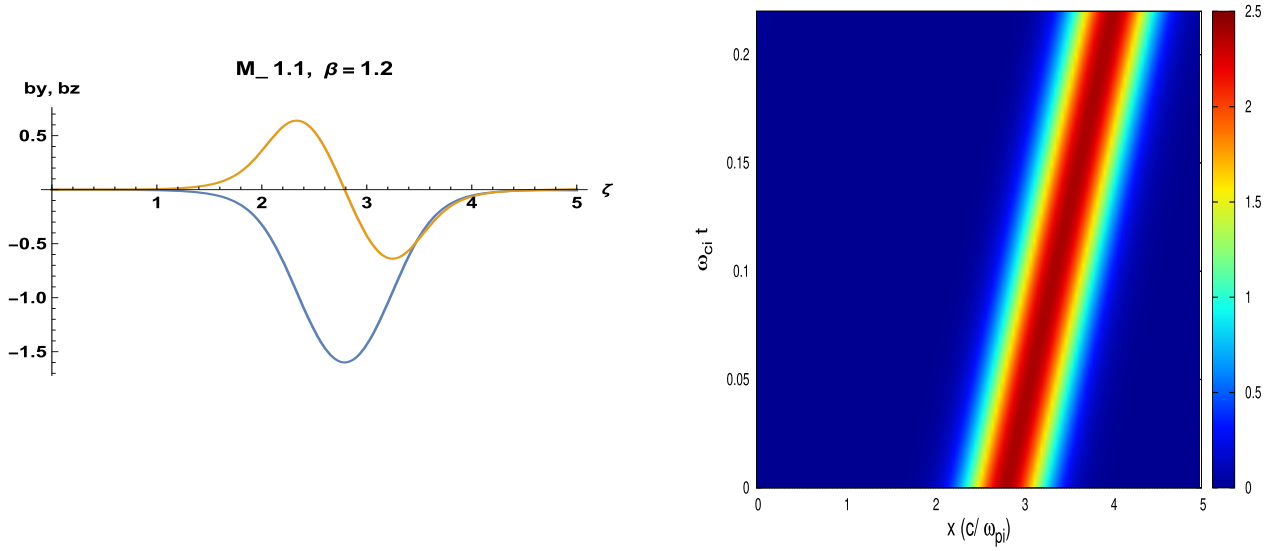
Eliminating v_x between (24) and (36) one gets a quadratic equation for n whose solutions are,

$$n_\pm = \frac{2M^2 + 2\beta - C \pm \sqrt{(2\beta + 2M^2 - C)^2 - 16M^2\beta}}{2\beta} \tag{37}$$

where $C = (b^2 + 2\cos(\theta)b_z)$. Note that the limit of $\beta \to 0$ is singular in the above expression for the density. We can arrive at a proper expression for n in that limit by applying L'Hospital's rule, namely, taking the limit of the ratio of the derivative of the numerator and the derivative of the denominator w.r.t β and then taking the limit of $\beta \to 0$. The choice of n_+ gives the correct expression for n for $\beta = 0$, namely, eqn.(32).

In Fig.6(a) we show a magnetosonic soliton solution for $M = 1.1$, $\beta = 1.2$ by solving eqns.(30) and (31) with the expression for n_+ given in (37). The time evolution of such a soliton when used as an initial condition in the full set of equations is shown Fig.6(b).

DISTRIBUTION A: Distribution approved for public release. Distribution unlimited



(a) (b)

FIG. 6: (a) Magnetosonic soliton at $M = 1.1$, $\beta = 1.2$. The unipolar curve (blue) is of b_z and the dipolar curve (orange) is of b_y. (b) Time evolution of this soliton shown in terms of b_z^2. This is obtained by simultaneously solving eqns. (8-13), with the initial condition taken from the solution of eqns. (30, 31) and eqn. (37)

C. Pinned Solitons of Ion Inertial Waves (S finite, $\beta = 0$

Our ultimate aim is to excite pinned solitons that envelope a driving current source. For this we need to look for stationary solutions that travel with the same speed as the source. In such a case we can assume that the source term S is also a function of $\zeta = x - Mt$ (in other words $v_d = M$, where v_d is the debris velocity).

Then, taking $\beta = 0$, eqns.(10), (11), (12) and (13) can be transformed to,

$$M\frac{\partial v_y}{\partial \zeta} = -\sin(\theta)\frac{\partial b_y}{\partial \zeta} - S(\cos(\theta) + b_z) \tag{38}$$

$$M\frac{\partial v_z}{\partial \zeta} = -\sin(\theta)\frac{\partial b_z}{\partial \zeta} + Sb_y \tag{39}$$

$$-M\frac{\partial b_y}{\partial \zeta} = -\frac{\partial}{\partial \zeta}(v_x b_y - v_y \sin(\theta)) + \frac{\partial}{\partial \zeta}(\frac{1}{n}\sin(\theta)\frac{\partial b_z}{\partial \zeta}) + \frac{\partial}{\partial \zeta}\left(\frac{Sb_y}{n}\right) \tag{40}$$

$$-M\frac{\partial b_z}{\partial \zeta} = \frac{\partial}{\partial \zeta}(v_z \sin(\theta) - v_x(\cos(\theta) + b_z)) - \frac{\partial}{\partial \zeta}(\frac{1}{n}\sin(\theta)\frac{\partial b_y}{\partial \zeta}) + \frac{\partial}{\partial \zeta}\left(\frac{S(\cos(\theta) + b_z}{n}\right) \tag{41}$$

DISTRIBUTION A: Distribution approved for public release. Distribution unlimited

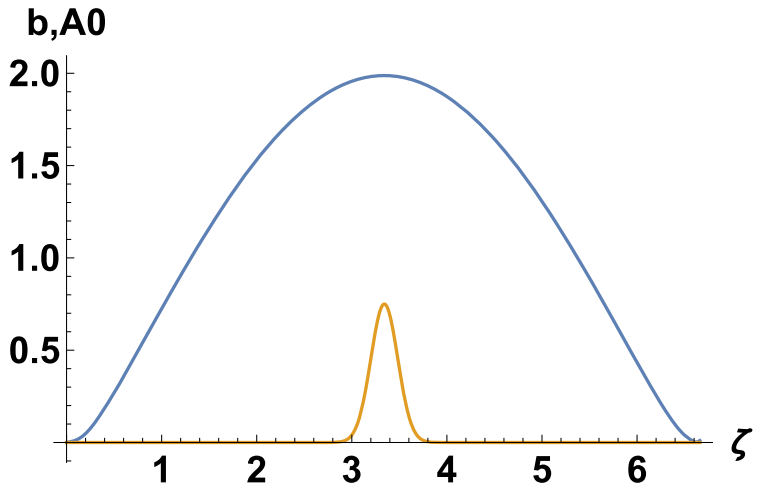


FIG. 7: Pinned Ion inertial wave soliton with $M = 0.0185$, $\beta = 0$, $\theta = 1^0$, $A0 = 1.5 \times 10^{-6}$ and $\Delta = 0.2$. The source term (orange) is multiplied by 4×10^4 to make it visible on plot.

Equations (40) and (41 can be integrated once to get,

$$\sin(\theta)\frac{\partial b_z}{\partial \zeta} + Mb_y + nv_y \sin(\theta) - S)b_y = 0 \tag{42}$$

$$\sin(\theta)\frac{\partial b_y}{\partial \zeta} - Mb_z - nv_z \sin(\theta) + nv_x \cos(\theta) - S(\cos(\theta) + b_z) = 0 \tag{43}$$

where we have used eqn.(24). The expression of n is given by eqn.(32).

We have numerically solved the coupled equations (38), (39), (42) and (43) with a source term of the form $S = A_0 e^{-\zeta^2/\Delta^2}$ where A_0 and Δ are constants. A plot of a typical pinned soliton at $M = 0.0185$ in the presence of a weak source term, with $A_0 = 1.5 \times 10^{-6}$ and $\Delta = 0.2$ is shown in Fig.7. The amplitude of the source term is multiplied by a factor of 5×10^4 to display it on the same plot. The nature of the pinned soliton is quite similar to the one that was obtained with the reduced model equation, namely, the fKdV equation (15) with $\beta = 0$. This can be understood from the linear dispersion relation given by eq.(14). Putting $\beta = 0$ and taking the limit of small θ it can be easily shown that the linear ion inertial wave solution takes the form,

$$M_1 = \frac{\omega}{kV_A} = 1 + k^2\delta^2\theta^2$$

which has the same form as the dispersion relation for an ion acoustic wave. The dispersion in this case is provided by the ion inertial contribution $k^2\delta^2$ instead of the thermal pressure

DISTRIBUTION A: Distribution approved for public release. Distribution unlimited

term. Thus in the small propagation angle limit, the region where these small M solitons exist, the fKdV equation provides a good model description.

V. DISCUSSION AND CONCLUSIONS

To summarize, we have investigated the existence and nature of electromagnetic solitons that can be excited by an external moving current source term. We have done this in the framework of an inertial magneto-hydrodynamic model. Our numerical and analytic solutions in special limits, reveal a rich variety of soliton solutions that can arise from the nonlinear evolution of Alfvén waves, magneto-sonic waves or the low frequency inertial ion waves. These can have a wide variety of applications in situations where a current beam traverses through a magnetised plasma. Our particular motivation for studying these nonlinear structures was to exploit them for the identification and tracking of small sized space debris objects that are difficult to track optically. In an earlier study, carried out for electrostatic ion acoustic waves, it was suggested that detection of precursor ion acoustic solitons emitted by the charged debris object, could provide an indirect means of tracking the trajectory of the debris objects. Our present work extends this concept in two directions. Firstly, we propose that a class of solitons, called pinned solitons, which can also be excited by the moving source, can provide a more direct means of detecting the debris objects as they travel with the same speed as the object and remain pinned to the object. Secondly, as electromagnetic nonlinear structures, their spatial widths are typically of the order of a few ion skin depths, that are much larger than the Debye length envelopes provided by the electrostatic solitons. Thus these electromagntic solitons would be easier to detect by radar scattering techniques.

We now discuss our results in the context of debris tracking in the LEO region. The typical plasma parameters in this region at an altitude of around of around 600 kms are, $n_{0e} \sim n_{0i} \sim 10^6 cm^{-3}; T_e \sim 2200K; T_i \sim 600K; \mu = \frac{m_i}{m_p} = \frac{1}{16}$ where $m_i = 16 m_p$ is the mass of the ion and m_p is the mass of the proton. The ion species is predominantly O^+ in this region. n_{0e}, n_{0i} denote the number densities of the electrons and ions respectively while T_e and T_i are the electron and ion temperatures. The electron Debye length for these parameters is about 0.3 cms whereas the ion skin depth is around 10^2 cms. As our

DISTRIBUTION A: Distribution approved for public release. Distribution unlimited

numerical solutions show, the typical width of the electromagnetic solitons is of the order of a few ion skin depths.Thus the electromagnetic solitons will have a much larger footprint compared to the electrostatic ones which typically have an extent of a few Debye lengths. The typical magnetic field in this region is of the order of 0.3 to 0.6 Gauss. The Alfven velocity is then in the range of $160km/s$ to $320km/s$. The debris velocity in this region is about $8km/s$. Hence in order for the debris to latch on to a pinned soliton traveling at its own velocity we need to consider solitons that have a Mach number that is less than ~ 0.05. Thus the pinned soliton solutions that are relevant for this region are the low Mach number ion inertial wave solitons. At higher altitudes, for example in the GEO region, where the magnetic field is weaker, the higher Mach number solitons could play a similar role. Note that the plasma β in this region is of the order of 10^{-4} and hence has a negligible effect on the dynamics. Our cold plasma approximation and use of the ion inertial MHD framework is therefore appropriate for the LEO region. Finally, it may be mentioned, that as our numerical results show, the pinned solitons create magnetic field perturbations that are comparable in magnitude to the ambient magnetic field. Similar perturbations created by magneto-sonic solitons in the magnetosheath region have been detected by the Cluster satellites[24,25]. Compared to the magnetosheath region the ambient magnetic field is larger in the LEO region and so in principle magnetic perturbations that are of that magnitude should be detectable even from ground based radar scattering measurements. It would also be interesting to carry out controlled laboratory experiments to detect such electromagnetic pinned solitons surrounding a charged object that is immersed in a flowing plasma -analogous to what has been successfully demonstrated for electrostatic pinned solitons[16].

Appendix A: Derivation of the fKdV equation

We briefly outline here the derivation of the fKdV equation (15), by applying a reduction perturbation analysis to the set of equations (8 - 13). We adopt the following expansion for the physical quantities, $f = \{n, v_x, v_y, v_z, B_x, B_y, B_z\}$,

$$f = f_0 + \epsilon f_1 + \epsilon^2 f_2 + \epsilon^3 f_3 + O(\epsilon^4)$$

where $f_0 = \{1, 0, 0, 0, sin(\theta), 0, cos(\theta)\}$ and $f_j = \{n_j, v_{xj}, v_{yj}, v_{zj}, 0, b_{yj}, b_{zj}\}$ with $j = 1, 2, 3, ...$ We also take

$$S = \epsilon^2 S_2$$

DISTRIBUTION A: Distribution approved for public release. Distribution unlimited

and define the following set of stretched variables,

$$\xi = \epsilon^{1/2}(x - Mt) \;\; ; \;\; \tau = \epsilon^{3/2}t$$

where M is the normalized wave velocity. Expressing the differential operators in terms of these stretched variable gives us,

$$\frac{\partial}{\partial x} = \epsilon^{1/2}\frac{\partial}{\partial \xi} \;\; ; \;\; \frac{\partial}{\partial t} = -M\epsilon^{1/2}\frac{\partial}{\partial \xi} + \epsilon^{3/2}\frac{\partial}{\partial \tau} \; ; \; \frac{\partial^2}{\partial x^2} = \epsilon\frac{\partial^2}{\partial \xi^2}$$

Using the expansions in the above equations and following the standard procedure of collecting terms of the same order of ϵ, we can obtain the following from each of the equations,

$$\epsilon^{3/2}: \quad -M\frac{\partial n_1}{\partial \xi} + \frac{\partial v_{x1}}{\partial \xi} = 0 \tag{A1}$$

$$\epsilon^{5/2}: \quad -M\frac{\partial n_2}{\partial \xi} + \frac{\partial n_1}{\partial \tau} + \frac{\partial (n_1 v_{x1})}{\partial \xi} + \frac{\partial v_{x2}}{\partial \xi} = 0 \tag{A2}$$

$$\epsilon^{3/2}: \quad -M\frac{\partial v_{x1}}{\partial \xi} + cos\theta\frac{\partial b_{z1}}{\partial \xi} + \beta\frac{\partial n_1}{\partial \xi} = 0 \tag{A3}$$

$$\epsilon^{5/2}: \quad -M\frac{\partial v_{x2}}{\partial \xi} + \frac{\partial v_{x1}}{\partial \tau} + v_{x1}\frac{\partial v_{x1}}{\partial \xi} + cos\theta\frac{\partial b_{z2}}{\partial \xi} - Mn_1\frac{\partial v_{x1}}{\partial \xi} + b_{z1}\frac{\partial b_{z1}}{\partial \xi} + \beta\frac{\partial n_2}{\partial \xi} = 0 \tag{A4}$$

$$\epsilon^{3/2}: \quad -M\frac{\partial v_{y1}}{\partial \xi} - sin\theta\frac{\partial b_{y1}}{\partial \xi} = 0 \tag{A5}$$

$$\epsilon^{5/2}: \quad -M\frac{\partial v_{y2}}{\partial \xi} + \frac{\partial v_{y1}}{\partial \tau} + v_{x1}\frac{\partial v_{y1}}{\partial \xi} - sin\theta\frac{\partial b_{y2}}{\partial \xi} + sin\theta n_1\frac{\partial b_{y1}}{\partial \xi} = 0 \tag{A6}$$

$$\epsilon^{3/2}: \quad -M\frac{\partial v_{z1}}{\partial \xi} - sin\theta\frac{\partial b_{z1}}{\partial \xi} = 0 \tag{A7}$$

$$\epsilon^{5/2}: \quad -M\frac{\partial v_{z2}}{\partial \xi} + \frac{\partial v_{z1}}{\partial \tau} + v_{x1}\frac{\partial v_{z1}}{\partial \xi} - sin\theta\frac{\partial b_{z2}}{\partial \xi} - Mn_1\frac{\partial v_{z1}}{\partial \xi} = 0 \tag{A8}$$

$$\epsilon^{3/2}: \quad -M\frac{\partial b_{y1}}{\partial \xi} - sin\theta\frac{\partial v_{y1}}{\partial \xi}1 = 0 \tag{A9}$$

$$\epsilon^{5/2}: \quad -M\frac{\partial b_{y2}}{\partial \xi} + \frac{\partial b_{y1}}{\partial \tau} - sin\theta\frac{\partial v_{y2}}{\partial \xi} + \frac{\partial (v_{x1}b_{y1})}{\partial \xi} \tag{A10}$$

$$\epsilon^{3/2}: \quad -M\frac{\partial b_{z1}}{\partial \xi} - sin\theta\frac{\partial v_{z1}}{\partial \xi} + cos\theta\frac{\partial v_{x1}}{\partial \xi} = 0 \tag{A11}$$

DISTRIBUTION A: Distribution approved for public release. Distribution unlimited

$$\epsilon^{5/2}: \quad -M\frac{\partial b_{z2}}{\partial \xi} + \frac{\partial b_{z1}}{\partial \tau} - sin\theta\frac{\partial v_{z2}}{\partial \xi} + \frac{\partial (v_{x1}b_{z1})}{\partial \xi} + cos(\theta)\frac{\partial v_{x2}}{\partial \xi} - M\frac{\partial^2 v_{y1}}{\partial \xi^2} - cos(\theta)\frac{\partial S_2}{\partial \xi} = 0 \tag{A12}$$

Integrating (A1),(A3), (A7) and (A11) we get,

$$\begin{aligned} -Mn_1 + v_{x1} &= 0 \\ -Mv_{x1} + cos\theta b_{z1} + \beta n_1 &= 0 \\ -Mv_{z1} - sin\theta b_{z1} &= 0 \\ -MB_{z1} - sin\theta v_{z1} + cos\theta v_{x1} &= 0 \end{aligned} \tag{A13}$$

From (A13) we get a dispersion relation,

$$M^2(M^2-1) + \beta(sin^2\theta - M^2) = 0 \tag{A14}$$

This is the dispersion relation for magneto-sonic waves. Next we consider eqns. (A2), (A4), (A8), (A12) and rewrite them as follows,

$$\begin{aligned} -M\frac{\partial n_2}{\partial \xi} + \frac{\partial v_{x2}}{\partial \xi} &= -T_1 \\ \beta\frac{\partial n_2}{\partial \xi} - M\frac{\partial v_{x2}}{\partial \xi} + cos\theta\frac{\partial b_{z2}}{\partial \xi} &= -T_2 \\ -M\frac{\partial v_{z2}}{\partial \xi} - sin\theta\frac{\partial b_{z2}}{\partial \xi} &= -T_3 \\ -M\frac{\partial b_{z2}}{\partial \xi} - sin\theta\frac{\partial v_{z2}}{\partial \xi} + cos(\theta)\frac{\partial v_{x2}}{\partial \xi} &= -T_4 \end{aligned} \tag{A15}$$

where,

$$\begin{aligned} T_1 &= \frac{\partial n_1}{\partial \tau} + v_{x1}\frac{\partial n_1}{\partial \xi} + n_1\frac{\partial v_{x1}}{\partial \xi} \\ T_2 &= \frac{\partial v_{x1}}{\partial \tau} + v_{x1}\frac{\partial v_{x1}}{\partial \xi} - Mn_1\frac{\partial v_{x1}}{\partial \xi} + b_{z1}\frac{\partial b_{z1}}{\partial \xi} \\ T_3 &= \frac{\partial v_{z1}}{\partial \tau} + v_{x1}\frac{\partial v_{z1}}{\partial \xi} - Mn_1\frac{\partial v_{z1}}{\partial \xi} \\ T_4 &= \frac{\partial b_{z1}}{\partial \tau} + \frac{\partial (v_{x1}b_{z1})}{\partial \xi} - M\frac{\partial^2 v_{y1}}{\partial \xi^2} - cos(\theta)\frac{\partial S_2}{\partial \xi} \end{aligned} \tag{A16}$$

The set of equations (A15) can be expressed in the form,

$$\begin{pmatrix} -M & 1 & 0 & 0 \\ \beta & -M & 0 & cos\theta \\ 0 & 0 & -M & -sin\theta \\ 0 & cos\theta & -sin\theta & -M \end{pmatrix} \begin{pmatrix} \partial n_2/\partial \xi \\ \partial v_{x2}/\partial \xi \\ \partial v_{z2}/\partial \xi \\ \partial b_{z2}/\partial \xi \end{pmatrix} = \begin{pmatrix} -T_1 \\ -T_2 \\ -T_3 \\ -T_4 \end{pmatrix} \tag{A17}$$

DISTRIBUTION A: Distribution approved for public release. Distribution unlimited

To obtain the solvability condition for (A17) one can start by constructing an extended matrix,

$$E = \begin{pmatrix} -M & 1 & 0 & 0 & | & T_1 \\ \beta & -M & 0 & cos\theta & | & T_2 \\ 0 & 0 & -M & -sin\theta & | & T_3 \\ 0 & cos\theta & -sin\theta & -M & | & T_4 \end{pmatrix} \tag{A18}$$

which by a few simple matrix operations, (A17) can be converted to the following form,

$$\tilde{\tilde{E}}_2 = \begin{pmatrix} 1 & -1/M & 0 & 0 & | & -T_1/M \\ 0 & 1 & 0 & -\frac{cos\theta/M}{(1-\beta/M^2)} & | & -\frac{(\beta T_1/M^2+T_2/M)}{(1-\beta/M^2)} \\ 0 & 0 & 1 & sin\theta/M & | & -T_3/M \\ 0 & 0 & 0 & D_1 & | & D_2 \end{pmatrix} \tag{A19}$$

where $D_1 = M^2(1+\beta) - M^4 - \beta sin^2\theta$ and $D_2 = T_1 \times M \times cos\theta \times \beta + T_2 \times cos\theta \times M^2 + T_3 \times sin\theta \times (\beta - M^2) + T_4 \times M \times (M^2 - \beta)$. For (A17) to have solutions the entries in the bottom row of $\tilde{\tilde{E}}_2$ should all be zero. Now $D_1 = 0$ by virtue of the dispersion relation (A14). So the solvability condition is $D_2 = 0$ Substituting for T_1, T_2, T_3 and T_4 in D_2 we get,

$$\begin{aligned} &\beta cos\theta \left[\frac{\partial n_1}{\partial \tau} + v_{x1}\frac{\partial n_1}{\partial \xi} + n_1\frac{\partial v_{x1}}{\partial \xi}\right] + M^2 cos\theta \left[\frac{\partial v_{x1}}{\partial \tau} + v_{x1}\frac{\partial v_{x1}}{\partial \xi} - Mn_1\frac{\partial v_{x1}}{\partial \xi} + b_{z1}\frac{\partial b_{z1}}{\partial \xi}\right] \\ &+ (\beta - M^2) sin\theta \left[\frac{\partial v_{z1}}{\partial \tau} + v_{x1}\frac{\partial v_{z1}}{\partial \xi} - Mn_1\frac{\partial v_{z1}}{\partial \xi}\right] \\ &+ M(M^2 - \beta)\left[\frac{\partial b_{z1}}{\partial \tau} + \frac{\partial (v_{x1}b_{z1})}{\partial \xi} - M\frac{\partial^2 v_{y1}}{\partial \xi^2} - cos(\theta)\frac{\partial S_2}{\partial \xi}\right] = 0 \end{aligned} \tag{A20}$$

From (A9) and (A13) we can get,

$$n_1 = v_{x1}\ ;\ b_{z1} = \frac{M-\beta}{cos\theta}v_{x1}\ ;\ v_{z1} = -tan\theta\frac{M-\beta}{M}v_{x1}\ ;\ v_{y1} = \frac{Msin^2\theta}{M^2 - sin^2\theta}\frac{(M-\beta)}{Mcos\theta}\frac{\partial v_{x1}}{\partial \xi}$$

Using the above relations we can express (A20) in terms of a single variable, namely, b_{z1}. The final equation is,

$$a_1\frac{\partial b_{z1}}{\partial \tau} + a_2 b_{z1}\frac{\partial b_{z1}}{\partial \xi} + a_3\frac{\partial^3 b_{z1}}{\partial \xi^3} = cos(\theta)\frac{\partial S_2}{\partial \xi} \tag{A21}$$

where,

$$a_1 = (\beta + M^2)cos(\theta) - \frac{(\beta - M^2)((M-\beta)}{M}sin(\theta)tan(\theta) + \frac{M(M^2-\beta)(M-\beta)}{cos(\theta)}$$

$$a_2 = 2\frac{\beta}{M-\beta}cos^2(\theta) + \left(1 - M + \frac{(M-\beta)^2}{cos^2(\theta)}\right)\frac{M^2}{M-\beta}cos^2(\theta) + \frac{(M^2-\beta)(1-M)}{M}sin^2(\theta)$$

DISTRIBUTION A: Distribution approved for public release. Distribution unlimited

$$+2M(M^2-\beta)$$
$$a_3 = -\frac{(M^2-\beta)(M-\beta)M^2 tan(\theta) sin(\theta)}{(M^2-sin^2(\theta))}$$

Acknowledgement

A.S. acknowledges AOARD for their research grant FA2386-18-1-4022 and is grateful to the Indian National Science Academy for the Honorary Scientist position. Work at NRL is supported by NRL Base Funds.

DATA AVAILABILITY

The data that support the findings of this study are available from the corresponding author upon reasonable request.

REFERENCES

[1] "Low earth orbit visualization," `https://platform.leolabs.space/visualization`.

[2] L. Perek, Space Debris **2**, 123 (2000).

[3] A. Horstmann, C. Kebschull, S. Müller, E. Gamper, S. Hesselbach, K. Soggeberg, M. K. Ben Larbi, M. Becker, J. Lorenz, C. Wiedemann, and E. Stoll, Aerospace **5** (2018), 10.3390/aerospace5020037.

[4] A. Murtaza, S. J. H. Pirzada, T. Xu, and L. Jianwei, IEEE Access **8**, 61000 (2020).

[5] E. Christiansen, J. Hyde, and R. Bernhard, Advances in Space Research **34**, 1097 (2004), space Debris.

[6] J.-C. Liou, 28th International Symposium on Space Technology and Science, Okinawa, Japan, June 5-12 (2011).

[7] W. Flury, A. Massart, T. Schildknecht, U. Hugentobler, J. Kuusela, and Z. Sodnik, ESA bulletin **104**, 92–100 (2000).

[8] D. Mehrholz, L. Leushacke, W. Flury, R. Jehn, H. Klinkrad, and M. Landgraf, ESA bulletin **109**, 128 (2002).

[9] A. Juhasz and M. Horanyi, Journal of Geophysical Research **102**, 7237 (1997).

[10] A. Sen, S. Tiwari, S. Mishra, and P. Kaw, Advances in Space Research **56**, 429 (2015).

[11] S. Jaiswal, P. Bandyopadhyay, and A. Sen, Phys. Rev. E **93**, 041201(R) (2016).

[12] S. K. Tiwari and A. Sen, Physics of Plasmas **23**, 022301 (2016).

DISTRIBUTION A: Distribution approved for public release. Distribution unlimited

[13]S. K. Tiwari and A. Sen, Physics of Plasmas **23**, 100705 (2016), https://doi.org/10.1063/1.4964908.

[14]G. Arora, P. Bandyopadhyay, M. G. Hariprasad, and A. Sen, Physics of Plasmas **26**, 093701 (2019), https://doi.org/10.1063/1.5115313.

[15]A. S. Truitt and C. M. Hartzell, Journal of Spacecraft and Rockets **57**, 876 (2020), https://doi.org/10.2514/1.A34652.

[16]G. Arora, P. Bandyopadhyay, M. G. Hariprasad, and A. Sen, Phys. Rev. E **103**, 013201 (2021).

[17]V. V. Gavrishchaka, S. B. Ganguli, and G. I. Ganguli, Phys. Rev. Lett. **80**, 728 (1998).

[18]A. Kumar and A. Sen, New Journal of Physics **22**, 073057 (2020).

[19]A. Sen, S. Yadav, G. Ganguli, and C. Crabtree, 2019 International Conference on Electromagnetics in Advanced Applications (ICEAA), Granada, Spain, 9-13 September 2019 , 156 (2019).

[20]A. Sen, A. Kumar, S. Yadav, G. Ganguli, and C. Crabtree, 2021 International Conference on Electromagnetics in Advanced Applications (ICEAA), Honolulu, Hawaii, U.S.A. , 09 - 13 August 2021 , 32 (2021).

[21]Y. A. Berezin and V. Karpman, Soviet Physics JETP **19**, 1265 (1964).

[22]K. Stasiewicz, Journal of Geophysical Research: Space Physics **110** (2005).

[23]M. Gedalin, Physics of Plasmas **5**, 127 (1998).

[24]K. Stasiewicz, P. K. Shukla, G. Gustafsson, S. Buchert, B. Lavraud, B. Thidé, and Z. Klos, Phys. Rev. Lett. **90**, 085002 (2003).

[25]K. Stasiewicz, Phys. Rev. Lett. **93**, 125004 (2004).

DISTRIBUTION A: Distribution approved for public release. Distribution unlimited